Applied Clay Science 136 (2017) 112–141

Contents lists available at ScienceDirect

Applied Clay Science

journal homepage: www.elsevier.com/locate/clay

Review article

Recent development of layered double hydroxide-derived catalysts — Rehydration, reconstitution, and supporting, aiming at commercial application —

Katsuomi Takehira

Hiroshima University, Japan

ARTICLE INFO

Article history:
Received 16 March 2016
Received in revised form 17 October 2016
Accepted 13 November 2016
Available online 22 November 2016

Keywords:
Layered double hydroxide
Catalysis
"Memory effect"
Rehydration
Reconstitution, supporting

ABSTRACT

Layered double hydroxide (LDH) has a unique feature, i.e., reconstitution of layered structure from the calcined oxides. The application of LDH as the heterogeneous catalysts by adopting reconstitution phenomenon and supporting on appropriate carrier were reviewed aiming at their commercial uses. After a short explanation on fundamental properties of LDH, such as phase transition by calcination and rehydration of calcined LDH (reconstitution of LDH by "memory effect"), their applications in the catalyst preparations were discussed.

By adopting "memory effect", the surface of LDH-derived mixed oxide was rehydrated or reconstituted as well as decorated with various metals and anions, resulting in an enhanced catalytic activity and selectivity via base sites activation and high dispersion of active metal species. Active OH^- species, as Brønsted base, was produced on calcined Mg-Al LDH after the rehydration and exhibited high activity in various reactions. Catalytically active transition metals such as Ni, Fe and Mn were highly dispersed on Mg(Al)O via reconstitution, resulting in the high catalytic activity in dehydrogenation and oxidation reactions.

Pt-Sn/Mg(Al)O catalysts prepared by adopting reconstitution phenomenon exhibited an excellent activity in the dehydrogenation of propane to propene. This is owing to the formation of highly dispersed and stable Pt-Sn bimetallic species on the catalyst surface. By supporting LDH on magnetic carriers such as ferrite, the catalyst became magnetically separable and could be utilized recyclably in the fine chemicals synthesis. Paper structured catalyst prepared from LDH by utilizing paper making technology opened new type usage of LDH materials which can be applied in the reforming catalysts for fuel cells.

Moreover the reconstitution phenomena donate several beneficial properties to the LDH-derived mixed oxides in their uses as the heterogeneous catalysts. Reconstitution of LDH kinetically accelerated the conversion of anions such as toxic NO_3^- and refractory $(COO)^{2-}$ in aqueous solution by entrapping the anions in the interlayer space of rehydrated LDH as observed on Pd-Cu/Mg(Al)O and Cu/Mg(Al)O catalysts, respectively. In the reforming of hydrocarbons for H_2 production, self-regenerative activity appeared on trace amount of Pt doped Ni/Mg(Al)O catalyst by reversible oxidation-reduction between Ni^0 and Ni^{2+} on/in Mg(Ni,Al)O periclase assisted by reversible change between periclase and LDH structure of the support.

Both Pt-Ni/Mg(Al)O and Pt-Sn/Mg(Al)O catalysts exhibited excellent activities almost closing to the commercial uses.

1. Introduction

Layered double hydroxide (LDH) belongs to the anionic clay family. The structure of most of them corresponds to that of Mg-Al LDH, a natural magnesium-aluminum hydroxycarbonate, $Mg_6Al_2(OH)_{16}CO_3 \cdot 4H_2O$. This mineral in turn is similar to brucite $[Mg(OH)_2]$, where Mg^{2+} ions occupy octahedral positions and form infinite layers connected by hydrogen bonds. In Mg-Al LDH, some Mg^{2+} ions were substituted by Al^{3+} ions, and produced an excess positive charge which is compensated by carbonate anions present in the interlayer space (Cavani et al., 1991 and references cited therein). Moreover, both Mg^{2+} and Al^{3+} can also be substituted by other divalent caions and even trivalent ones and the interlayer ion can differ in nature. The general formula of LDH is $[M^{2+}_{1-x}M^{3+}_x(OH)_2]^{x+}[A_{x/n}]^{n-} \cdot mH_2O$, where M^{2+} is a divalent cation, such as Mg^{2+}, Mn^{2+}, Fe^{2+}, Co^{2+}, Cu^{2+}, Ni^{2+}, Zn^{2+}, or Ca^{2+}; M^{3+} is a trivalent cation, such as Al^{3+}, Cr^{3+}, Mn^{3+}, Fe^{3+}, Co^{3+}, or La^{3+}, and A^{n-} is the anion (Cavani et al., 1991 and references cited therein).

LDH can be obtained by precipitation from soluble salt precursors or by ion-exchange. Thermal decomposition of LDH leads to the formation of mixed oxides. The mixed oxides exhibited an interesting property: "memory effect" (Miyata, 1980; Sato et al., 1986, 1988; Cavani et al.,

E-mail addresses: takehira@hiroshima.u.ac.jp, satomit@ebony.plala.or.jp.

http://dx.doi.org/10.1016/j.clay.2016.11.012
0169-1317/

1991; Marchi and Apesteguía, 1998; Rives and Ulibarri, 1999; Allada et al., 2005), by which original layered structure was reconstituted when the mixed oxides were contacted with aqueous solution containing many different anions or even with vaporized water (Fig. 1).

Interest in LDH and derived materials arises from their use in various fields: catalysts or catalyst supports, processing of selective chemical nanoreactors, separation and membrane technology, filtration, scavenging and controlled release of anions, electroactive and photoactive materials, electrodes, sensor, etc. (Cavani et al., 1991; Therias and Mousty, 1995; Monneyron et al., 1995; Guth et al., 1996; Ulibarri et al., 2001; Wang et al., 2012). Most of the applications correspond to the field of heterogeneous catalysis (Meyn et al., 1990; Cavani et al., 1991; Pinnavaia et al., 1995; Tichit and Vaccari, 1998; Vaccari, 1999; Stoica et al., 2010; Nagendrappa, 2011; Xu et al., 2011; Zhou, 2011a,b), where the choice of different metal cations make these materials rather suitable for a fine modulation of chemical composition leading to good catalytic properties. LDH has been also prepared containing two or more different M^{2+} or M^{3+} cations in the brucite-like layers. As the cations in LDH are homogeneously dispersed, heterogeneous catalysts obtained upon thermal decomposition usually show a high dispersion of the metal sites (Cavani et al., 1991; Corma, 1997).

LDH-derived mixed oxides possess high surface area, phase purity, basic surface properties, and structural stability (Cavani et al., 1991; Tichit and Coq, 2003). Moreover, LDH-derived oxides containing various metal cations exhibit not only their original acid-basic properties of Mg-Al system but also reduction-oxidation properties as catalysts depending on the other metal species incorporated (Vaccari, 1999). LDH and LDH-derived oxides thus catalyze various types of reactions in both liquid and gaseous phase as heterogeneous catalysts. However, no commercial use of LDH-derived materials as the catalysts was reported, since LDH itself is not mechanically strong enough for recyclable or continuous use due to its easy pulverization or exfoliation during the reaction. Therefore, in most cases except some researches (Nishimura et al., 2013), LDH-derived oxides after calcination have been used for aiming at practical application. In gaseous phase reaction at high temperature, LDH is inevitably used as mixed oxides after calcination. Even in liquid phase reaction, usage as mixed oxides after the calcination is recommended. Moreover, even after the calcination, enough mechanical strength cannot be attained and, therefore, utilization as the supported form is desirable.

In recent years, a few good reviews have been published from scientific viewpoints. LDH have also been used to obtain discrete brucite-like layers by exfoliation (Wang and O'Hare, 2012). However, isolation of nanosheets from the exfoliated solution is still difficult due to a use of highly polar solvent (Liu et al., 2008), and a further development is now anticipated for their effective usages. Supporting of the exfoliated LDH on a certain carrier is one of the solutions, but this still meets with serious difficulty. Moreover, oxidation and hydrogenation on LDH-supported catalysts were recently reviewed (Feng et al., 2015), but LDH or LDH-derived mixed oxides may not be enough tolerable as the catalyst support in the use in commercial process due to the lack of mechanical strength. Another recent review reported that various LDH materials prepared using different metals and intercalating ions were tested as the catalyst itself or as the catalyst supports in various reactions (Baskaran et al., 2015), but these systems possess a similar drawback.

In this paper, the uses of LDH-derived mixed oxides as heterogeneous catalyst and the effect of catalyst preparation by rehydration (or reconstitution) or supporting on an appropriate carrier were discussed aiming at their commercial uses. After a short explanation on fundamental properties of LDH, such as phase transition by calcination and rehydration (reconstitution of LDH by "memory effect"), the discussions were focused on their utilizations for catalyst preparations.

By utilizing "memory effect", the surface of LDH-derived mixed oxide was rehydrated as well as decorated with various metals and anions. Rehydration donate active Brønsted base, OH^-, species on the mixed oxide and accelerated various base catalyzed reactions. Various transition metals can be supported in highly dispersed state and exhibited high activity. Supported Pt-Sn bimetallic catalyst on calcined Mg-Al LDH showed an excellent activity in the dehydrogenation of propane after the catalyst preparation via rehydration. Magnetic carrier supported LDH catalysts was magnetically separable and could be utilized recyclably. Another type of supported LDH catalysts, paper structured catalyst exhibited high activity as well as high durability in the H_2 production for fuel cells. Moreover reconstitution phenomena donate beneficial properties, i.e., kinetic acceleration of nitrate and oxalate removal by entrapping the anions in the interlayer of LDH reconstituted from Mg(Al)O and self-regenerative activity in reforming of hydrocarbons to Pt doped Ni/Mg(Al)O.

In the commercial use of the catalysts, the activity and the long term stability as well were required. Among these catalysts, both Pt-Ni/Mg(Al)O and Pt-Sn/Mg(Al)O catalysts exhibited high and sustainable activities almost closing to the level of their commercial uses.

2. Calcination of LDH and rehydration of calcined LDH

2.1. Calcination (dehydration, dehydroxylation and phase transition) of LDH

The most common method applied to prepare LDH compounds is coprecipitation, which is based on the reaction of a solution containing M^{2+} and M^{3+} metal cations in adequate proportions with an alkaline

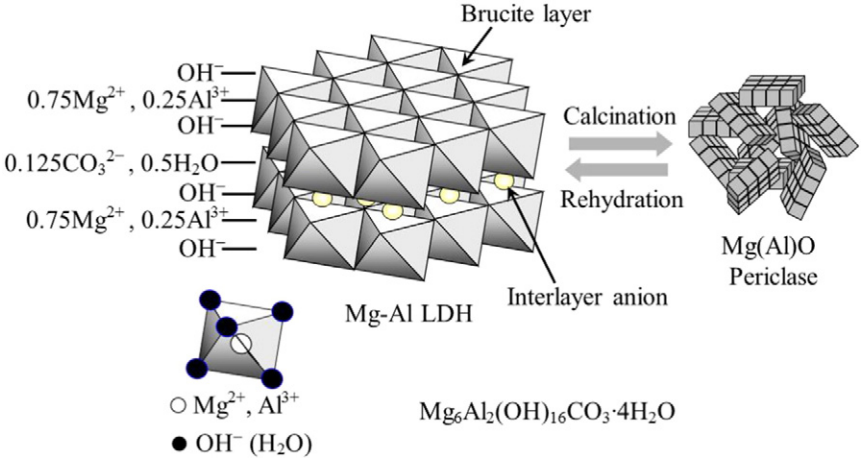

Fig. 1. Crystal structure, calcination of Mg-Al LDH and rehydration of the calcined LDH.

solution. However, the product crystallinity may be affected by various experimental parameters such as reaction pH and temperature, concentration of used solutions, flow rate during addition of reactants, hydrodynamic conditions in the reactor and/or post synthesis operations; e.g., hydrothermal treatment substantially affected the crystallite size and strain of synthetic Mg-Al LDH compounds with various Mg/Al molar ratios was studied (Miyata, 1980).

In spite of the numerous investigations on the processes of thermal decomposition of Mg-Al LDH by various modern methods, many inexplicable and contradictory problems remain. Stanimirova et al. (1999) reported that, when synthetic $Mg_6Al_2(OH)_{16}CO_3 \cdot 4H_2O$ was calcined at the temperature interval 120–260 °C, two types of metaphases were obtained as structural models: one is $Mg_6Al_2(OH)_{16}CO_3$ formed at 140–180 °C by the reversible dehydration of the interlayer, and another is $Mg_6Al_2(OH)_{12}O_2CO_3$ formed at temperatures 240–260 °C as a result of the dehydroxylation of a part of OH groups of the brucite-like layer and inclusion of two oxygens from the CO_3-group in the same layer. Pérez-Ramírez et al. (2007) reported that, in the presence of water vapor (2 vol.% H_2O in N_2), the Mg-Al LDH was decomposed to the mixed oxide via formation of an intermediate phase, consisting of a highly disordered, dehydrated, layered structure, at 150–200 °C. The dehydration of Mg-Al LDH can be quantified by determination of the interlayer space from the value of d-spacing of the first basal diffraction line (003 or 002, dependently on polytype). The interlayer space in as-synthesized Mg-Al LDH (Mg/Al = 3/1) is defined as the distance between two hydroxyl groups in adjacent layers, and can be calculated as the difference between the basal d spacing from the XRD pattern (0.77 nm) and the thickness of the brucite sheet (0.48 nm) (Cavani et al., 1991). The latter evolves by removal of interlayer water on heating, causing a shrinking of the interlayer space (it is up to 45% smaller than that of as-synthesized LDH). Upon heating up to 200 °C Mg-Al LDH are dehydrated, the product still retaining a layered structure. A significant rearrangement of the octahedral brucite-type layer occurs with migration of Al^{3+} ions out of the layer to tetrahedral sites in the interlayer. Upon heating up to 400 °C the anions in the interlayer are decomposed, and the material is completely dehydroxylated. Mokhtar et al. (2010) reported that thermal decomposition of Mg-Al LDH led to the formation of a dehydrated intermediate phase at 200 °C, followed by crystalline MgO formation at 450 °C. Finally the products were converted to an MgO-like structure where Al^{3+} ions are dissolved in the lattice to form a solid solution. Thus, the activation of the as-synthesized Mg-Al LDH is initiated by its thermal decomposition, leading to a high-surface-area Mg(Al)O mixed oxide with strong O^{2-} Lewis basic sites. This material displays high activity in base-catalyzed reactions. Further calcination at high temperatures (up to 1000 °C) yields a mixture of well-crystallized phases corresponding to MgO and $MgAl_2O_4$ (spinel) (Millange et al., 2000).

The nature, density, and strength of surface basic sites of Mg-Al mixed oxide obtained by calcination of Mg-Al LDH largely depends on the Al content (Mg/Al = 0.5 ~ 9.0). On pure MgO, strong basic sites consisted predominantly of O^{2-} anions. Calcined LDH contained surface sites of weak (OH^- groups), medium (Mg-O pairs), and strong (O^{2-} anions) basicity (Di Cosimo et al., 1998a). The relative abundance of weak and medium strength basic sites increased with the Al content. The addition of small amounts of Al to MgO diminished drastically the density of surface basic sites because of a significant Al surface enrichment. Formation of surface amorphous AlO_y structures in samples with low Al content (Mg/Al > 5) partially covered the Mg-O pairs and decreased the concentration of surface O^{2-} anions. At higher Al contents (5 > Mg/Al > 1), the basic site density increased because the Al^{3+} cations within the MgO lattice created a defect in order to compensate the positive charge generated, and the adjacent oxygen anions became coordinately unsaturated. In samples with Mg/Al < 1, segregation of bulk $MgAl_2O_4$ spinels occurred and caused the basic site density to diminish (Di Cosimo et al., 1998a).

2.2. Rehydration of calcined LDH (Reconstitution of LDH)

It was first reported that hydration of the calcined product resulted in the reconstitution of the original Mg-Al LDH structure (Fig. 1) (Miyata, 1980). This phenomenon was later named as "memory effect", for which two mechanisms, retro-topotactic mechanism and dissolution-recrystallization mechanism, were proposed. Sato et al. (1988) reported that, on the basis of SEM data, the lamellar structure of natural LDH is preserved unchanged at heating up to 500 °C as well as after regenerating in 0.2 M aqueous solution of Na_2CO_3 at 80 °C for 5 days. The results indicate that the formation of NaCl-type oxide and the reconstitution of Mg-Al LDH proceeds topotactically without dissolution of the sample. The "memory effect" was reduced by increasing the calcination temperature of the parent Mg-Al LDH. It is proposed that the reconstitution of the Mg-Al LDH phase occurs via a retro-topotactic transformation from the Al^{3+} and Mg^{2+} ions located both in the octahedral sites of the oxide matrix (Marchi and Apesteguía, 1998). The increase in the calcination temperature causes the solid-state diffusion of octahedral Mg^{2+} ions into tetrahedral sites and the unstable inverse spinel is progressively transformed to a stable normal structure.

Reconstitution of Mg-Al LDH structure from the oxide with water vapor or by immersion in decarbonated water leads to formation of meixnerite ($Mg_6Al_2(OH)_{18} \cdot 4H_2O$), an Mg-Al LDH analogue with OH^- groups as compensating anions in the interlayer instead of the original carbonates (Pérez-Ramírez et al., 2007). They studied on reconstitution of Mg-Al LDH phase for Mg(Al)O oxide with the periclase structure: reversion of the intermediate dehydrated structure to Mg-Al LDH upon contact with water vapor is complete and very fast at room temperature. Recovery of LDH from the Mg(Al)O oxide calcined at 450 °C is two orders of magnitude slower than rehydration of the intermediate layered structure and one order of magnitude slower than the typically practiced liquid-phase reconstitution. The gas-phase rehydration and reconstitution was interrupted above 30 °C. This is attributed to the poor wetting of the surface of the decomposed materials induced by hampered H_2O adsorption above room temperature at the water vapor pressure applied. These data indicate that surface wetting, i.e., surface steam concentration to form liquid water, was important for the reconstitution of Mg-Al LDH layered structure, suggesting dissolution-recrystallization mechanism. Moreover, interlayer anions affected the rehydration by insertion of water; I^- and ClO_4^- exhibited the second staging phase - alternate stacking of hydrated and non-hydrated interlayers - in the intermediate humidity region (Iyi et al., 2007).

In the case of Zn-Al system, morphology change was significant when the LDH aggregates was prepared by reconstitution in water, but the details were not discussed (Kooli et al., 1997). After thermal treatment of Co-Al LDH at 200 °C, the original layered structure was not reconstituted even after 30 days in contact with a wet gas flow (5 vol% H_2O in N_2) or after 12 h in an aqueous solution of 0.5 M Na_2CO_3 (Pérez-Ramírez et al., 2001), which deviates from the typical behavior observed for Mg-based LDH and other layered compounds. The presence of oxidizable Co^{2+} cations in the octahedral sheets and their diffusion to the interlayer space in the dehydrated layered structure, and the stability of the homogeneous crystalline solid solution of cobalt spinels, already identified at 150 °C, are responsible for this behavior.

Stanimirova et al. (2001) reported that XRD patterns of the reconstituted Mg-Al LDH differ substantially from these of the initial samples, and further carried out SEM study of the so called "memory effect" using both synthetic samples of various composition and crystallinity as well as natural samples of different polytypes. In contrast to the report (Sato et al., 1988) for the topotactical reconstitution, the results indicate unambiguously that the reconstitution proceeds through dissolution of Mg(Al)O and subsequent Mg-Al LDH recrystallization. The reconstitution of the high-temperature metaphase in Mg-Al LDH takes place through crystallization from solution. Actually, this is a method for synthesis of Mg-Al LDH with rhombohedral crystal structure

with a highly developed surface, a typical structure of crystalline aggregates and interlayer anion composition. The only observed indication for "memory effect" is the preservation of the Mg/Al ratio of the initial sample in the reconstituted samples. Moreover, the reconstitution phenomena of the $Mg_4Al_2(OH)_{12}CO_3{\cdot}3H_2O$ LDH after a moderate thermal treatment is a very fast process, as it is already completed after 5 min of soaking in a 0.1 M Na_2CO_3 solution (Delorme et al., 2006). Powder XRD patterns are also similar for all the reconstituted samples without significant FWHM variations. SEM and TEM observations coupled with granulometric and BET measurements show that all the samples, both mixed oxides and reconstituted Mg-Al LDH, are composed by aggregates of small plate-like particles (>100 nm) with a sub-hexagonal morphology but with different porosities. Kinetic data for the reaction have been determined and modelled using the Avrami-Erofeev nucleation-growth model, consistent with the process taking place by dissolution of the starting material and crystallization of the LDH from the solution (Millange et al., 2000; Pérez-Ramírez et al., 2007).

When Mg(Al)O periclase, obtained by calcination of Mg-Al-CO_3 LDH (Mg/Al = 2, 3 and 3.7) at 600 °C for 2 h, was dipped in aqueous solutions of divalent (Mg, Zn, Co, Ni, Cu) or trivalent (Al, Fe) cations for 48 h, the Mg-Al LDH structure was restored (Stanimirova and Kirov, 2003). The presence of Mg^{2+}, Zn^{2+}, Ni^{2+}, Co^{2+}, Cu^{2+} salts or of low soluble hydromagnesite increased the M^{2+}/Al ratio, reaching a maximum value of 3.8. An incorporation of Zn^{2+}, Ni^{2+}, Co^{2+} and Cu^{2+} cations in the newly formed Mg-Al LDH was detected, while Mg^{2+} remained in solution. In the presence of soluble Al salts or freshly precipitated $Al(OH)_3$, the M^{2+}/Al ratio approximated the minimal possible value of 2. The results obtained support the conception of the dissolution-recrystallization mechanism of Mg-Al LDH regeneration from mixed (Mg,Al) oxides contrary to the concept of topotactic processes.

The recent work reported a comparative study for Mg(Al)O periclase after thermal decomposition between the gas phase hydration in the presence of water vapor at 30 °C and the liquid phase reconstitution in Na_2CO_3 aqueous solution at 25 and 70 °C (Mokhtar et al., 2010). Thermal decomposition of Mg-Al LDH led to the formation of a dehydrated intermediate phase at 200 °C, followed by crystalline Mg(Al)O formation at 450 °C. Hydration of Mg(Al)O in H_2O/N_2 mixed gas resulted in the formation of broad patterns of the meixnerite phase after 2 h, which retained its structure even after 52 h exposure to water vapor. Reconstitution of Mg(Al)O in carbonated water at 25 and 70 °C resulted in intensified patterns of the Mg-Al LDH phase. It is concluded that liquid phase treatment completed the reconstitution of Mg-Al LDH phase by dissolution-recrystallization mechanism, whereas gas phase treatment just hydrated Mg(Al)O to form poorly crystallized meixnerite by retro-topotactic mechanism.

3. Activation of base sites on Mg(Al)O.

The Brønsted (OH^-) basic sites formed by reconstitution method are briefly reported to be more active than Lewis (O^{2-}) basic sites for aldol condensation reactions (Tichit et al., 2002, 2003), however no clear result was obtained as for the effect of reconstitution. Although effect of reconstitution time on the structural properties of LDH is well documented in the literature (Pérez-Ramírez et al., 2007), limited literature is available for the effect of reconstitution time on catalytic activity of reconstituted LDH. Calcination of Mg-Al LDH materials produces a mixed magnesium and aluminum oxide phase. In contact with liquid water or a flow of inert gas saturated with water, the oxide phase can be transformed into the layered structure. The reconstituted material possesses a meixnerite-like structure, mainly containing OH^- as compensating ions in the interlayer space. These hydroxyl groups exhibit a basic character.

The basic properties of LDH have led to them being widely used in several base-catalyzed reactions such as self- and cross-aldol condensation of aldehydes and ketones, Knoevenagel condensation, and Claisen–Schmidt condensation, etc. (Cavani et al., 1991; Di Cosimo et al., 1998b). All of these are important processes in the pharmaceutical and fragrance industries, where LDH are increasingly replacing traditional homogeneous catalysts such as NaOH and KOH (Abelló et al., 2005a). One of the solutions to enhance catalytic performance of LDH-derived oxides is the rehydration (Table. 1).

3.1. Aldol condensation

Aldol condensation of acetaldehyde with calcined Mg-Al LDH (Table 1, Entry 1) as base catalyst exhibited low yield of crotonaldehyde together with various by-products (Kagunya and Jones, 1995). In the aldol condensation of benzaldehyde and acetone at 0 °C on Mg-Al LDH, no activity was observed on the pure LDH (carbonated) or on the solid just decarbonated at 450 °C. The activity was the maximum after calcination at 450 °C, followed by rehydration by water vapor at room temperature. Such high activity of the rehydrated sample (alcohol yield > 85 mol%) suggests that aldolisation is specifically catalyzed by OH^- ions (Table 1, Entry 2) (Rao et al., 1998).

In the aldol condensation of acetone at 0 °C with Mg-Al LDH with Cl^- and/or CO_3^{2-} as compensating anions, the main products were diacetone alcohol (DAA) and mesityl oxide (MO) (Tichit et al., 1998). The catalytic activity of Mg(Al)O mixed oxides after calcination of the LDH at 450 °C increased with the Al content to reach a conversion of ca. 20%. The nature and the amount of the compensating anion in the LDH greatly influenced the catalytic activity, particularly traces amount of Cl^- was very detrimental. By contrast, the addition of controlled amounts of H_2O in acetone enhanced the conversion with a higher selectivity to DAA and caused the reconstitution at the same time (Table 1, Entry 3). The degree of reconstitution of the lamellar structure was estimated by the $I_{003}/(I_{003} + I_{004})$ intensity ratio of the (003) and (004) lines of respectively the LDH and the Mg(Al)O periclase phases (Fig. 2) (Tichit et al., 1998). The rehydration was carried out in vapor or in liquid phases for the Mg(Al)O mixed oxides, previously decarbonated by calcination at 450 °C. The rehydration of the mixed oxide into the meixnerite structure modifies the strength and the concentration of the active OH^- sites, which well correlated with the initial reaction rate, V_0. This reconstitution with the unique OH^- in an atmosphere free of CO_3^{2-} leads to the meixnerite structure.

The activities of the rehydrated LDH (Table 1, Entry 4) in the aldol condensation of acetone showed a linear increase with the amount of accessible Brønsted basic sites as determined by CO_2 adsorption (Roelofs et al., 2001). The number of accessible sites, based on the CO_2/Al ratio, was below 5%. Both results support the model in which only basic sites near edges of LDH platelets are partaking in aldol condensations. In contrast to this, LDH with interlayer OH^- prepared via ion exchange lacked the high catalytic activity. The results show an enhanced activity of interlayer OH^- close to disordered edges, obtained via rehydration, in contrast to interlayer OH^- in a regular LDH structure (Roelofs et al., 2002).

Activated Mg-Al LDH by rehydration (Table 1, Entry 5) was also efficient catalyst in the aldol condensation of campholenic aldehyde (**1**) and methyl ethyl ketone (**2**) (Scheme 1) (Abelló et al., 2007). Mg-Al LDH rehydrated in liquid water exhibited 91 % conversion of campholenic aldehyde and ca. 50 % selectivity to each **3** and **4** at 60 °C and 1 h of reaction time. Using ultrasounds during rehydration originated a higher initial reaction rate due to the higher surface area and thinner platelets of the sample. This effect was also observed in the aldol reaction of citral and acetone and attributed to a larger number of OH^- groups located at the edges of the platelet.

Abelló et al. (2007) reported that the elemental analysis of the solid LDHas (as prepared) revealed the following chemical formula: $Mg_{0.78}Al_{0.22}(OH)_2(CO_3)_{0.113-0.575}$. The XRD pattern is characteristic of a well-crystallized LDH-type layered material. The detailed XRD data are shown in Table 2 together with the data obtained by adsorption. Calcination of as-synthesized LDH (LDHas) at 450 °C gives an Mg(Al)O mixed oxide with a periclase-like structure (LDHc). Rehydration of

Table 1
Mg-Al LDH catalyst activated by rehydration (Y: Yield; S: Selectivity).

Entry	Mg/Al	Rehydration	Reaction	Products	Activity	References
1	2.0	Calcination alone	Acetaldehyde self-condensation	Croton-aldehyde	low Y ~ 5.3% + by-products	Kagunya and Jones, 1995
2	3.0	By H_2O vapor	Acetone + Benzaldehyde	Benzal-acetone	Y > 85%	Rao et al., 1998
3	~3.0	In situ H_2O	Acetone self-condensation	DAA + MO	Y ~ 23% thermo-dynamic eq.	Tichit et al., 1998
4	2.0	By H_2O vapor	Acetone self-condensation	DAA + MO	OH^- active species	Roelofs et al., 2001
5	3.0	In liquid H_2O sonication	**1** + **2**	**3** + **4**	Conv. = 91% S = 50%	Abelló et al., 2007
6	3.0	By H_2O vapor	Furfural + acetone	FAc + F_2Ac in Scheme 2	Y = 23% (FAc) and 11% (F_2Ac)	Hora et al., 2014
7	3.0	By H_2O vapor	Acetophenone + benzaldehyde	*trans*-Chalcone	Y > 80%	Climent et al., 2004b
8	3.0	By H_2O vapor	2,4-Dimethoxy-acetophenone + 4-Methoxybenz-aldehyde	2′,4,4′-Tri-methoxy-chalcone (Vesidryl)	Y = 57% S = 99%	Climent et al., 2004b
9	4.0	In liquid H_2O	Styrene + H_2O_2	Styrene oxide	OH^- by many defects	Chimentão et al., 2007
10	3.0	In liquid H_2O	Ethanol + acrylonitrile	β-Ethoxy-propionitrile	OH^-/CO_3^{2-} ratio	Pavel et al., 2008
11	3.0	Multiple Calcination-Rehydration	Ethanol + acrylonitrile	β-Ethoxy-propionitrile	S > 99%	Teodorescu et al., 2013
12	3.5	In liquid H_2O	1-Heptanal + benzaldehyde	Jasmin-aldehyde	Y = 84% S = 88%	Sharma et al., 2010
13	4.0	In liquid H_2O sonication	Glycerol + DEC	GC + GDC	Y = 65% Y = 35%	Álvarez et al., 2010
14	3.0	In liquid H_2O mechanical stirring	D-glucose	D-fructose	Y = 30%	Yu et al., 2012
15	3.0	In liquid H_2O sonication	D-glucose	D-fructose	Y = 37% S = 88%	Lee et al., 2014
16	3.0	In situ H_2O	Citral + acetone	Pseudo-ionone	Y = 96% S = 99%	Climent et al., 2004a

LDHc in the liquid phase at high stirring speed (LDHrl-ms) or using ultrasounds (LDHrl-us) regenerates the layered structure (Álvarez et al., 2013a). The rehydrated samples consist of thin nanoplatelets, resulting in an increased number of accessible basic sites, which are active in aldol condensations. These results further confirm the higher activity of Brønsted OH^- groups in aldol condensation as compared to Lewis O^{2-} groups.

Aldol condensation of furfural and acetone catalyzed by Mg-Al LDH was studied in order to convert fufural obtained from biomass to compounds of higher molecular weight as fuel components (Scheme 2) (Table 1, Entry 6) (Hora et al., 2014). Catalytic activity of LDH was tested in the form of mixed oxides (after calcination) and ex situ or in situ rehydrated samples. A significant effect of reaction temperature on the product distribution was observed. While C_8 alcohol formation was prevailing at the lower temperatures, higher temperatures supported C_8 alcohol dehydration and the formation of the desired FAc and F_2Ac products. The optimum Mg/Al molar ratio was found to be around 3. The best results were achieved with this catalyst at 100 °C (>95% furfural conversion and only a minor selectivity to C_8 alcohol). Selectivity to the main by-product diacetone alcohol did not exceed 5% (Hora et al., 2014).

The activity of laboratory-prepared and commercial Mg-Al LDH with Mg/Al = 2 ~ 4 were compared in the liquid phase aldol condensation of furfural and acetone at 20 ~ 60 °C (Hora et al., 2015). Labo.-LDH was phase-pure crystalline sample with LDH structure while commercial LDH was a mixture of LDH and MgO phases. The labo.-LDH possesses larger BET surface area and mesopore volume in comparison with the commercial LDH. However, no substantial difference between labo.-LDH and commercial LDH was observed in basic properties obtained by CO_2-TPD and the chemical compositions. Catalytic experiments showed that both samples exhibited good catalytic activity, among which the both catalysts with Mg/Al = 3/1 were the most active for labo.-LDH and commercial LDH. Nevertheless, labo.-LDH exhibited better properties in aldol condensation when comparing the samples of the same chemical composition. The observed difference could be attributed to the increased mesoporosity of the labo.-LDH as well as the increased susceptibility to reconstitution of mixed oxide phase back to LDH structure.

3.2. Claisen–Schmidt condensation

The Claisen–Schmidt condensation between acetophenone and benzaldehyde was studied on rehydrated Mg-Al LDH in vaporized water flow (Table 1, Entry 7) (Climent et al., 2004b). The LDH (Mg/Al = 3/1) with a water content of 35 wt% exhibited an excellent activity for this condensation and was successfully applied to the synthesis of several chalcones with excellent activities and selectivities to the corresponding chalcones. The chalcone yield increased with increasing the time of water treatment and reached the maximum value at the 35 wt% of water content (18 h of rehydration). After this maximum, the activity decreased due to the excess of water on the catalyst surface that negatively affects the active sites and the reaction equilibrium.

Moreover, this catalyst was applied in the synthesis of Vesidryl (2′,4,4′-trimethoxychalcone) (Table 1, Entry 8), which is a chalcone with a pharmaceutical interest owing to its choleretic and diuretic properties. Vesidryl is obtained by Claisen–Schmidt condensation between 2,4-dimethoxy- acetophenone and 4-methoxybenzaldehyde under base catalysis and more specifically using KOH as catalyst. The present reaction was performed in the absence of solvent, using 12 wt% of the catalyst and 80 °C, where Vesidryl was produced with 57% yield and 99% selectivity. This rehydrated Mg-Al LDH can compete with the conventional KOH when the reaction is performed at higher reaction temperatures. The accessible active sites (OH^-) were located closely to disordered edges obtained via rehydration, resulting in the small concentration. It becomes evident that exfoliated LDH or LDH with smaller crystallites is preferably prepared in which the number of accessible active sites is larger.

3.3. Epoxidation

Use of mechanical stirring or ultrasound during the reconstitution leads to an enhancement in the catalytic activity, due to modifications

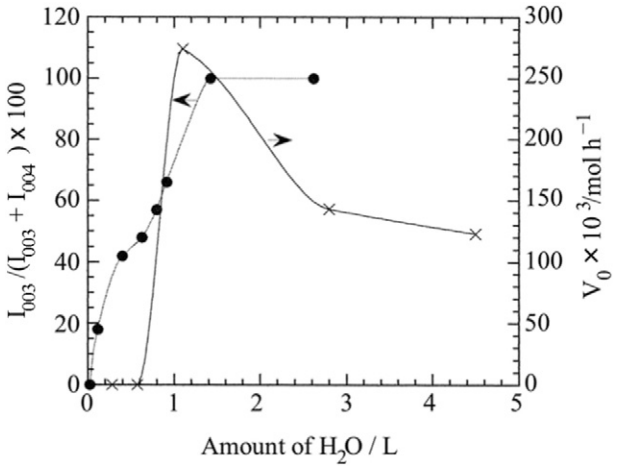

Fig. 2. Degree of reconstitution of the meixnerite-like structure and initial reaction rates as a function of the amount of H_2O contacted with the catalyst. (Tichit et al., 1998, Elsevier).

Table 2
Characterization data of the samples (Abelló et al., 2007, Elsevier).

Phase	LDHas LDH	LDHc periclase	LDHrl-ms meixnerite	LDHrl-us meixnerite
a/Å	3.07	–	3.058	3.055
c/Å	23.36	–	23.58	23.39
S_{BET}[a]/m^2 g^{-1}	57	210	270	440
Pore volume[b]/cm^3 g^{-1}	0.4	0.8	0.7	0.93
Average pore diameter[c]/Å	205.6	78.5	56.4	84.7
Crystallite size (001)[d]/Å	49.5	–	71	49

[a] BET method.
[b] Volume at $p/p_0 = 0.99$.
[c] BJH method applied in the adsorption branch.
[d] Using the Scherrer equation.

in the structure and basicity of the resulting materials, together with an increased surface area and improved accessibility to the active sites. An amount of defects in the lamellar structure of the small LDH nanoplatelets are likely responsible of the presence of stronger and more accessible active basic sites in the epoxidation of styrene with H_2O_2 (Table 1, Entry 9) (Chimentão et al., 2007). The greater performance of these materials has been disclosed for the epoxidation of styrene. The linear defects produced by sonication are also depicted in Fig. 3, with the main irregularities clearly indicated by arrows. The formation of defects or distortions in the LDH nanoplatelets on longer ultrasound treatment is a powerful method for creating stronger and more active basic sites for base-catalyzed reactions.

3.4. Cyanoethylation

The activity of rehydrated Mg-Al LDH in cyanoethylation of ethanol with acrylonitrile, where the β-ethoxypropionitrile is the prevailing reaction product, was evaluated compared with that of the as prepared LDH (Pavel et al., 2008) (Table 1, Entry 10). Full reconstitution of the LDH lamellar structure was attained by the rehydration of mixed oxides obtained from LDH calcined at 460 °C. Increasing the OH^-/CO_3^{2-} interlayer anions ratio and, modifying the accessibility and the amount of basic active sites, enhanced the catalytic activity in the reaction of cyanoethylation of ethanol with acrylonitrile. The rehydration took place for all Mg-Al LDH samples in water, whereas the hydration with alkaline solution leads to an extraction of Al from LDH resulting in brucite-type structure. During the preparation, LDH precipitated were usually aged in the mother liquor after the coprecipitation. The non-"aged" samples possess a higher catalytic activity for the cyanoethylation compared to the corresponding "aged" samples both after the rehydration. The crystallite size after the rehydration was smaller in the non-aged samples than the aged samples, suggesting higher number of active OH^- sites was produced on the surface of non-aged samples after the rehydration. (Pavel et al., 2011).

However, MMgAlO mixed oxide catalysts (M = Mn, Fe, Co, Ni, Cu and Zn) prepared by thermal decomposition of the corresponding LDH precursors showed different tendency in cyanoethylation of methanol with acrylonitrile (Pavel et al., 2012). Mixed oxides were much more active than their LDH precursors, while both were quite selective for β-metoxypropionitrile. A straight correlation between the number of basic sites of the mixed oxides and their catalytic activity was evidenced. However, the equilibrium between the acid and basic sites is a key factor determining the catalytic activity. In this cyanoethylation, the mixed oxides which have strongly superficial O^{2-} ions showed a higher activity than that of LDH which has superficial OH^- ions with lower basic character (Table 1, Entry 11) (Teodorescu et al., 2013). This result was not consistent to that persisting OH^- as the active species. More careful study will be required to clarify the real active species.

3.5. Jasminaldehyde synthesis

The effect of activation of as-synthesized Mg-Al LDH of varied Mg/Al molar ratio on its catalytic activity for the synthesis of jasminaldehyde by solvent free condensation of 1-heptanal with benzaldehyde was correlated with their basicity (Sharma et al., 2008). Reconstitution of Mg-Al LDH (Mg/Al = 3.5) was carried out by stirring calcined LDH in de-carbonated water under inert atmosphere which results in the restoration of original layered structure containing OH^- anions as major compensating anions in the interlayer space. Reconstitution of Mg-Al LDH yielded a highly active solid base catalyst (Table 1, Entry 12), for synthesis of jasminaldehyde. LDH after 8 h of the reconstitution showed 96% conversion of 1-heptanal within 120 min as compared to 51 and 60% conversion using as-synthesized LDH and calcined LDH, respectively, under identical reaction conditions. 88% selectivity to jasminaldehyde was obtained in 4 h reaction time using 12 mg LDH after the reconstitution as a catalyst at 8.05 mmol 1-heptanal and 40.25 mmol benzaldehyde concentrations (Sharma et al., 2010). The calcined LDH showed poor selectivity to jasminaldehyde (56%) due to presence of Lewis basic sites (O^{2-}), which assist faster self-condensation of 1-heptanal

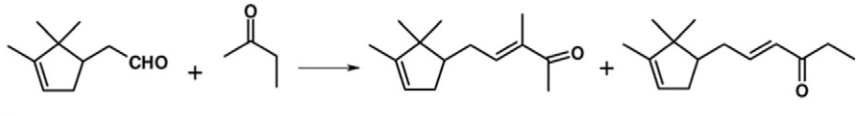

Campholenic aldehyde — 1
Methyl ethyl ketone — 2
3-Methyl-5-(2,2,3-trimethylcyclopent-3-enyl) pent-3-en-2-one — 3
6-(2,2,3-Trimetyl-cyclopent-3-enyl) hex-4-en-3-one — 4

Scheme 1.

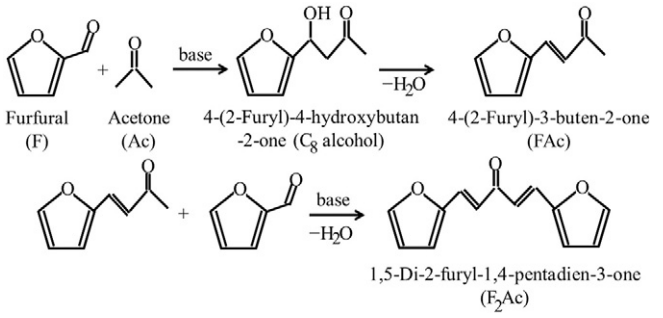

Scheme 2.

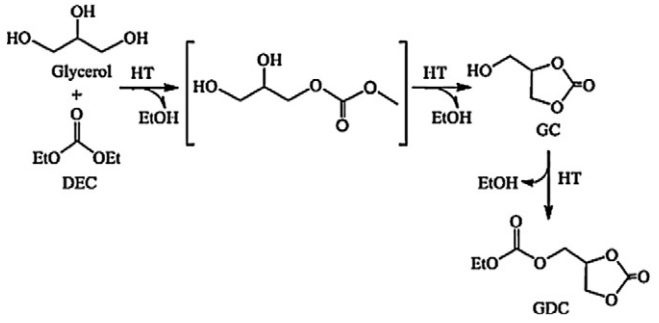

Scheme 3.

to 2-*n*-pentyl-2-nonenal. Kinetic data showed that the initial rate of reaction increased linearly up to 45 mg catalyst amount, thereafter, slow increase in the rate of reaction was observed up to 90 mg catalyst amount. Higher reaction temperature and catalyst amount favored the faster self-condensation of 1-heptanal which results into lower selectivity to jasminaldehyde. The activation energy was calculated by Arrhenius plot and found to be 37.6 kJ/mol.

3.6. Glycerol carbonate synthesis

The increase in bio-diesel production is generating high quantities of glycerol as by-product. Glycerol carbonate and its esters are key multifunctional compounds employed as chemical intermediates, monomers, solvents, additives and fuel contents. Glycerol carbonate (GC) and glycerol dicarbonate (GDC) were synthesized as glycerol value-added products via a transesterification reaction using diethyl carbonate (DEC) as co-substrate (Scheme 3) (Álvarez et al., 2010). The experimental results show that the type of basic center has a large influence on the activity in the heterogeneous glycolysis reaction. In addition, the absorption capacity of the Brønsted heterogeneous catalyst favors the subsequent transesterification of the GC (Table 1, Entry 13). Various Mg-Al LDH (Mg/Al = 2−4) were activated by calcination followed by rehydration under ultrasound or by anion exchange (F^-, Cl^-, CO_3^{2-}). Large amounts of water lead to a certain deactivation provoking an induction period as observed with catalyst Mg-Al LDH (Mg/Al = 2) after the rehydration (Álvarez et al., 2012a). Among the catalysts tested before and after the rehydration, Mg-Al LDH (Mg/Al = 3) after the rehydration was the best catalyst and could be recycled a few times.

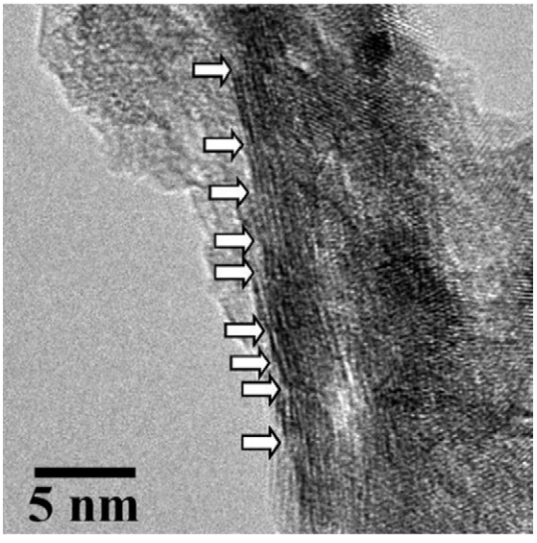

Fig. 3. HRTEM image corresponding to the rehydrated sample under ultrasounds [LDHrus (50 min)]. Several structural defects are marked by arrows (Chimentão et al., 2007, Elsevier).

Structure changes during the calcination of Mg-Al LDH (Mg/Al = 3) as-synthesized as well as the rehydration of calcined Mg-Al LDH (Mg/Al = 3) can be clearly seen in their XRD patterns.

The basicity of the catalysts can also be tuned by anion exchange; the catalyst Mg-Al LDH (Mg/Al = 4) exchanged by F^- was also one of the most active in the transesterification of glycerol. Moreover, it has been demonstrated that transesterification does not require a great basicity, since a non-activated LDH behaving as a Brønsted base such as Mg-Al LDH (Mg/Al = 4) exchanged by CO_3^{2-} has a catalytic activity comparable to that found in the calcined Mg-Al LDH. Thus it is concluded that rehydrated Mg-Al mixed oxide catalysts are promising candidates for the transesterification reaction and would be able to replace homogeneous catalysts that have similar activity. It is however observed that the meixnerite active phase showed a poor mechanical-strength, since the solid changes with every consecutive run due to the strong affinity between the surface of the catalyst and the products of the reaction (Álvarez et al., 2012b).

3.7. Isomerization

Mg-Al LDH (Mg/Al = 3/1) catalyst was successfully rehydrated using two methods (mechanical stirring method and sonication assisted method). "Memory effect" of LDH through the calcination and rehydration process was well confirmed by XRD and SEM analyses. Rehydrated LDH showed a better catalytic activity than mother LDH in the isomerization of D-glucose to D-fructose, indicating that rehydration is an efficient method to improve catalytic activity of LDH in this reaction (Table 1, Entry 14) (Yu et al., 2012). Particularly, all rehydrated LDH with a sonication assisted method showed better catalytic activities than rehydrated LDH with a vigorous mechanical stirring. When considering catalytic activity and rehydration time, sonication was a good way for rehydration of LDH to improving its catalytic activity in this reaction. Yield for fructose over the LDH rehydrated with a sonication showed a volcano-shaped curve with respect to sonication time. Glucose isomerization reaction was facilitated by weak base site of the catalyst at low temperature, while glucose degradation reaction was accelerated by strong base site of the catalyst at high temperature. Therefore, the weak basicity of the rehydrated LDH catalyst must be considered as a key factor in this reaction. Among the catalysts tested, the LDH rehydrated with sonication for 10 h showed the highest yield for fructose (Lee et al., 2014). (Table 1, Entry 15). The enhanced catalytic activity of this LDH catalyst was attributed to its abundant surface weak base sites formed by a facile vertical breaking and exfoliation of LDH layers during the sonication assisted rehydration process.

3.8. Pseudoquinone synthesis

Mg-Al LDH prepared under sonication at 25 °C were dispersed as particles of 80 nm average particle size and calcined to the mixed oxides with the large surface area (~300 $m^2\ g^{-1}$). This method of preparation increased not only the surface area but also the number of defects in the solid, leading to sites of higher basicity. The LDH were calcined at 450 °C

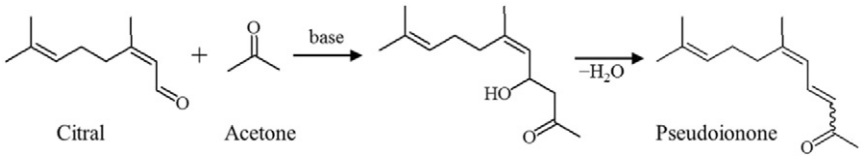

Scheme 4.

for 6 h in a N_2 flow, and then rehydrated at room temperature by direct decarbonated water (MilliQ) addition just before their use as catalysts. Samples originally prepared by sonication present smaller crystallite size and have a larger number of accessible active sites. The samples were tested for the aldol condensation between citral and acetone to pseudoionone (Scheme 4) (Climent et al., 2004a). LDH were regenerated from mixed oxides by hydration while giving Brønsted basic sites. The calcined LDH was less active than the rehydrated samples and a maximum of activity was found when the condensation was carried out using freshly calcined LDH with 36% (wt/wt) of water added (Table 1, Entry 16). It is very interesting to note, that the optimized rehydrated sample reached yields of pseudoionone of 96% with 99% of selectivity in 15 min of reaction time, working at a very low acetone/citral molar ratio. This result is superior to any reported up to now for this condensation in a homogeneous and heterogeneous phase.

Two different rehydration procedures in the liquid or gas phase have been applied to reconstitute mixed oxides derived from calcined LDH (Abelló et al., 2005b,c). Compared to the Mg-Al mixed oxide rehydrated in the gas phase (LDHrg), that rehydrated in the liquid phase (LDHrl) exhibited a superior catalytic performance in the aldol condensation of citral with acetone to yield pseudoionones. As seen in SEM images of the samples (Fig. 4) (Abelló et al., 2008), the as-synthesized LDH (LDHas) shows a well-developed layered structure. The mixed oxide obtained upon calcination at 450 °C (LDHc) maintains the lamellar structure and the morphology seems to be similar to that of LDHas. When rehydration was performed in the liquid phase, a sample with a high degree of exfoliation was obtained, as mentioned above (LDHrl). The shape is preserved with respect to the as-synthesized material, and the smaller particles generated by mechanical stirring in the rehydration procedure formed very thin platelets. Contrarily, LDHrg is built of complex aggregates of LDH platelets that are significantly thicker than those in LDHrl. This is in agreement with the higher crystallinity and markedly lower surface area of LDHrg. The higher degree of reconstitution of the lamellar structure was attained when the mixed oxide was rehydrated in the gas phase rather than in the liquid phase. CO_2-TPD shows that the number of OH^- groups and their nature are very similar in LDHrg and LDHrl, and cannot explain the markedly different catalytic behavior. Accordingly, only a small fraction of the available basic sites in the rehydrated samples is active in liquid-phase aldol condensations. These results support the model in which only basic sites near the edges of the LDH platelets are partaking in aldol reactions. Based on this, reconstituted materials with small crystallites (produced by exfoliation during mechanical stirring), that is, possessing a high external surface area, are beneficial in the reactions compared to larger crystals with a high degree of intraplatelet porosity.

It is concluded that the strong difference in surface areas for the two different types of rehydrated samples, the number of basic sites and their accessibility are the main factors for enhancing the catalytic activity of these reactions. Therefore, this provides an approach for the preparation of active catalysts for aldol condensation reactions and, in general, for enhancing the catalytic activity of LDH by controlling the rehydration process.

The catalytic performance of gas-phase reconstituted Mg-Al LDH in the citral/acetone condensation was modified by the presence of alkaline metals. To avoid the presence of alkaline retained during the preparation of LDH, a large amount of deionized water (around 10 L of water per 20 g of sample) is needed during the washing step. However, the Na-free gas-phase rehydrated sample hardly shows any activity in the reaction. The activity is significantly improved in the presence of alkaline metals, depending on the nature and amount of these metals (Abelló et al., 2005b). Alkaline can be incorporated into the material by impregnation or it can be retained in the solid during preparation. Unfortunately, from the practical point of view, alkaline-promoted LDH show an important leaching of the alkaline to the reaction medium upon consecutive runs.

3.9. Deactivation

It seems still difficult to widely use LDH-type bases in commercial scale as alternative to conventional inorganic bases, such as NaOH. The

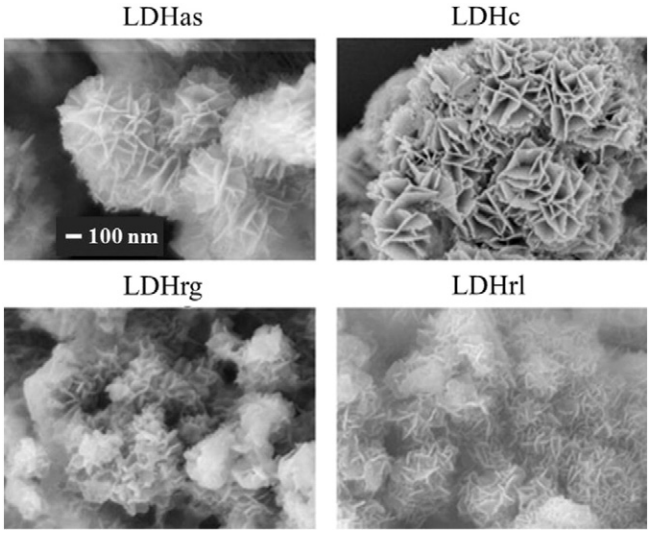

Fig. 4. Scanning electron micrographs of the as-synthesized and rehydrated LDHs. LDH as-synthesized (LDHas); LDH after calcination at 450 °C (LDHc); LDH, rehydrated in the gas phase (LDHrg); LDH, rehydrated in the liquid phase (LDHrl) (Álvarez et al., 2010, Elsevier).

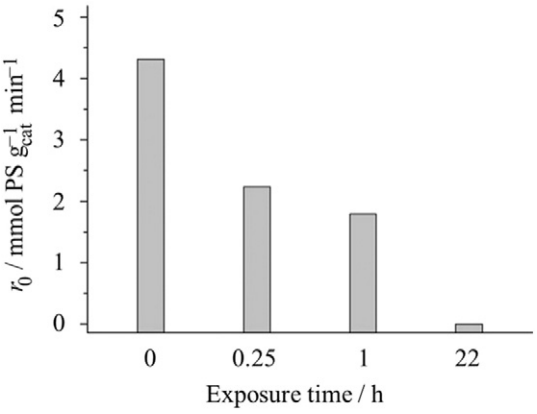

Fig. 5. Initial rate of pseudoionone (PS) formation over rehydrated LDH after different exposure times to air. Conditions: $T = 60$ °C, Acetone/Citral = 3, $W_{cat}/W_{citral} = 16\%$ (Abelló et al., 2008, Elsevier).

technical reasons explaining this disadvantage was discussed by taking the intensively researched citral/acetone condensation over activated LDH as case study. In fact, fresh rehydrated Mg-Al LDH shows excellent yields to pseudoionone compared to NaOH solutions and upscaling catalyst synthesis and reactor have been successfully accomplished. However, technical barriers making activated LDH less attractive in the fine chemical industry derive from the extremely fast poisoning of the active OH^- centers in contact with air (Fig. 5), unfeasible reusability, and time-consuming regeneration steps (Abelló et al., 2008). This can be likely extrapolated to other aldolizations and C—C bond formation reactions where OH^- centers are required. These technical adversities of solid bases, the low cost of alkaline solutions, and the lack of environmental policies associated with their use, motivate the conservatism of chemical industry to use the traditional process. In one opinion, moving forward in the topic of base catalysis requires radically new fundamental directions. Calcined LDH with Lewis basicity are more stable but much lower catalytic activity compared to the rehydrated counterpart is often attained. We should endeavor new strategies to design solid bases, which involves finding the optimal compromise between activity, selectivity, and stability.

4. Preparation of supported catalysts

4.1. LDH-derived oxide supported metal catalysts

4.1.1. Monometallic catalysts

Metal supported catalysts are frequently used in various liquid phase reactions not only for fine chemicals synthesis but also for ecofriendly processes. Mg(Al)O obtained from LDH possesses acid-base character, on which reduction-oxidation character can be added by the doping of transition metals.

4.1.1.1. Ni/Mg(Al)O catalyst. It is well known that Ni-Al combination forms LDH structure; Ni impregnation on γ-Al_2O_3 can produce Ni-Al LDH on the surface of γ-Al_2O_3 at pH close to isoelectric point of alumina (Merlen et al., 1995). Moreover, Mg^{2+} in Mg-Al LDH can be easily replaced by Ni^{2+}, etc. A series of transition metal (M) doped LDH [M/Mg(Al)O] were prepared by using reconstitution of Mg-Al LDH. Further calcination yields mixed oxides with more open structure and tunable basicity. The basicity of the calcined M/Mg(Al)O strongly depends on the type of transition metal and calcination temperature. The resulting M/Mg(Al)O materials were used as solid base catalysts and evaluated in the transesterification between glycerol and dimethyl carbonate (DMC) (Liu et al., 2014b). The base strength distribution of the M/Mg(Al)O catalysts varied depending on the doped transition metal, with Ni, Co and Mn doping showing more medium- as well as more high-strength basic sites than the transition-metal-free Mg(Al)O catalyst. The catalytic activity increased in the order Cr/Mg(Al)O < Fe/Mg(Al)O < Cu/Mg(Al)O < Zn/Mg(Al)O < Mg(Al)O < Mn/Mg(Al)O < Co/Mg(Al)O < Ni/Mg(Al)O, which is in good agreement with the trend of surface basic site density. Thus, the Ni/Mg(Al)O calcined at 500 °C exhibited maximum activity, ca. 50% yield of which is about 10 times higher than uncalcined Mg(Al)O precursor for the transesterification reaction. The promotional effect of Ni^{2+} doping could be attributed to the enhancement of the base strength of all three types of basic sites of the calcined Mg(Al)O. Although no comment was found on the deactivation of active OH^- species by CO_2, the active Ni/Mg(Al)O catalyst possessed a wide range of basic sites and, therefore, seems more reliable than simply rehydrated catalyst from the view point of sustainability.

4.1.1.2. Mn/Mg(Al)O catalyst. Although benzylic ketones is produced by the oxidation of alkylbenzenes with molecular oxygen using cobalt acetate as catalyst in acetic acid (Maeda, et al., 1995), this method suffers from a homogeneous feature of the catalyst as well as the corrosive nature of the solvent. The use of heterogeneous catalysts and particularly of neat substrate is recommended, because of easiness of separation of product and catalyst. Mn/Mg(Al)O prepared by adopting reconstitution showed very high catalytic activity, stability, and reusability in the selective oxidation of alkylaromatics to the corresponding benzylic ketones with molecular O_2 under solvent-free reaction conditions (Scheme 5) (Jana et al., 2007). Mn was successfully incorporated onto the surface of Mg(Al)O via reconstitution under CO_2 atmosphere. Mn/Mg(Al)O, surface-enriched with Mn, thus prepared exhibited much higher activity than Mn-Al oxide or MnO_4^- exchanged Mg(Al)O catalysts. The Mn/Mg(Al)O catalyst showed good catalytic performance also for the oxidation of a wide range of alkylaromatics to their corresponding benzylic ketones. In most cases, alkylbenzene conversion was high, and the —CH_2— group was selectively converted to the –CO– group, indicating high chemoselectivity in the oxidation. Alkylbenzenes with different alkyl chain lengths of C_2 and C_4 were transformed into the corresponding benzylic ketones at moderate yield (abve 50%) and conversion is not affected significantly with the chain length of substrate. The ethylbenzene derivatives possessing an electron donating substituent such as —CH_3 or —NH_2 at the 4-position afford the corresponding acetophenones in good yield (62–65%), but the presence of the electron-withdrawing substituent —NO_2 group adversely affects the corresponding acetophenone yield. Bulky alkylarenes, such as diphenylmethane and 4-ethylbiphenyl, were also oxidized to give the corresponding oxygenated products in very high yield (70–79%). In all cases, only the benzylic C—H bonds of alkylaromatics were oxidized selectively to their corresponding ketones. It was confirmed that the Mn/Mg-Al LDH is stable and reusable in the reaction.

LDH derived oxide supported metal catalysts were also used in various gaseous phase reactions.

4.1.1.3. Fe/Mg(Al)O catalyst. Styrene is produced commercially by the dehydrogenation of ethylbenzene using a Fe-K oxide catalyst in the presence of a large excess amount of superheated steam at 600–700 °C. Mg-Fe LDH is also known as pyroaurite, $[Mg_{(8-x)}Fe^{3+}{}_x(OH)_{16}]^{x+}[(CO_3)_{x/2}\cdot yH_2O]^{x-}$ (x = 1.45 ~ 3.07), and was synthesized by oxidation of Fe^{2+} with air in Mg^{2+} nitrate solutions (Hansen and Koch, 1995). Al was proved to be an excellent promoter, preventing sintering in iron-oxide catalysts (De Souza Ramos et al., 2008). MgO had especially good characteristics as an additive to a K-promoted iron oxide catalyst. Mg^{2+} ions possess a small ionic radii leading to a high electrostatic potential due to the stable valence state, resulting in an effective suppression of Fe sintering due to the reduction of Fe^{2+} to Fe^0 (Stobbe et al., 1991).

The supported iron catalyst prepared from Mg-Fe-Al LDH was applied for the ethylbenzene dehydrogenation to styrene (Ohishi et al., 2005). The Mg-Fe-Al LDH was calcined to mixed oxides with a high surface area as well as a mesoporous character, composed of periclase Mg(Fe,Al)O. The $Mg_2Fe_xAl_{1-x}$ catalysts showed that the styrene conversion increased with increasing the iron content up to x = 0.75 and then decreased, while the selectivity was the highest at x = 0.25. The optimum temperature for the reaction was 550 °C, which was lower than that used in the commercial process. The ethylbenzene conversion of 60% and the styrene selectivity of 95% were kept for 3 h over $Fe_{0.5}/Mg_3(Al_{0.5})O$ catalyst at 550 °C. The high catalytic performance can probably be attributed to the formation of partially reduced iron oxides of the valence state between Fe^{2+} and Fe^{3+} on the surface of catalyst

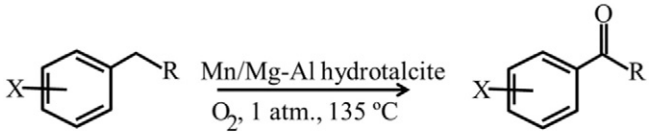

[where X = CH_3, C_6H_5, NH_2 or NO_2 and R = CH_3, C_3H_7 or C_6H_5]

Scheme 5.

and to the high surface area along with the porous structure, which originated from the Mg-Fe-Al LDH structure in the precursors. Moreover this Mg-Fe-Al catalyst was modified by replacing a part of Fe with various metals, Cu, Zn, Cr, Mn, Fe, Co and Ni (Balasamy et al., 2010), among which Co was effective, followed by Ni (Atanda et al., 2011). Essential role of $Mg^{2+}O^{2-}$ basic sites and Fe^{3+}/Fe^{2+} redox sites was clarified on Fe-Zn/Mg(Al)O (Balasamy et al., 2011) and finally the best system was found to be Fe-Co/Mg(Al)O catalyst (Tope et al., 2011). Co species exists as a mixture of Co^{3+}/Co^{2+} on the Fe–Co/Mg(Al)O and was partially isolated from the regular sites in the structures with increasing the Co content. Co addition enhanced Lewis acidity of Fe^{3+} active sites by forming Fe^{3+}—O—$Co^{3+/2+}$(1/1) bond, resulting in an increase in the activity. Reaction mechanism was proposed by in situ FT-IR measurements as follows: ethylbenzene was first adsorbed on the Fe-Co/Mg(Al)O by forming C—O bond and π-adsorbed aromatic ring. Ethylbenzene was strongly adsorbed on the Fe^{3+} Lewis acid sites via π-bonding and the dehydrogenation was initiated by α-H abstraction from ethyl group on Mg^{2+}-O^{2-} basic sites, followed by C—O—Mg bond formation. The α-H abstraction by O^{2-}(—Mg^{2+}) was likely followed by β-H abstraction, leading to the formations of styrene and H_2. Such catalytic mechanism by the Fe^{3+} acid—O^{2-}(—Mg^{2+}) base couple and the Fe^{3+}/Fe^{2+} reduction–oxidation cycle was further assisted by Co^{3+}/Co^{2+}, leading to a good catalytic activity for the dehydrogenation of ethylbenzene (Tope et al., 2011).

FeO_x/Mg(Fe,Al)O and VO_x/Mg(Fe,Al)O catalysts were prepared by adopting reconstitution as follows (Carja et al., 2008): iron containing Mg(Fe)-Al LDH was first synthesized by the coprecipitation of Mg^{2+} nitrate, Fe^{2+} sulfate and Al^{3+} nitrate in aqueous solution, and calcined in air at 450 °C. Then, the calcined Mg(Fe,Al)O was added to the aqueous solutions of Fe^{2+} sulfate or VO^{2+} sulfate, at a constant pH of 8.7 with stirring, under nitrogen atmosphere. The obtained samples were aged at 65 °C and denoted as FeO_x/Mg(Fe,Al)O and VO_x/Mg(Fe,Al)O respectively. These catalysts were used in the ethylbenzene dehydrogenation after pretreated under N_2 from room temperature to 450 °C. The reaction was carried out with ethylbenzene/N_2 mixed gas. The ethylbenzene conversion increased with temperature up to 580 °C, at which a maximum value of 74% was reached for FeO_x/Mg(Fe,Al)O, whereas the corresponding value decreases by nearly 8% for Mg(Fe,Al)O. For the both catalysts the styrene selectivity was above 90% up to 550 °C, while it showed steep decrease with further increase in the temperature. For the VO_x/Mg(Fe,Al)O, the conversion was lower than that of Mg(Fe,Al)O, but was improved in the co-presence of CO_2 in the feed gas.

4.1.1.4. Eggshell-type loaded Ni/Mg(Al)O catalyst. Ni/Mg(Al)O catalysts prepared by calcination of Mg(Ni)-Al LDH, followed by reduction, showed high and stable activity in steam reforming (Takehira et al., 2003), oxidative reforming (Shishido et al., 2002a) and dry reforming (Tsyganok et al., 2003) of CH_4 to syngas. All these catalysts were prepared starting from Mg(Ni)-Al LDH carbonates, where Ni^{2+} was homogeneously included in the particles of Mg(Ni,Al)O periclase after the calcination. A part of Ni^{2+} species were reduced and appeared as finely dispersed Ni metal particles on the catalyst surface after the reduction. More effective usage of Ni metal can be realized by preparing the eggshell-type loaded Ni catalyst. Eggshell-type Ni loaded catalysts, eggshell-Ni/Mg(Al)O, was prepared by adopting reconstitution of Mg-Al LDH and successfully used in the steam reforming of CH_4 (Takehira et al., 2004a, 2005a).

Mg-Al(3/1) mixed oxide particles prepared by the thermal decomposition of Mg-Al LDH ($Mg_6Al_2(OH)_{16}CO_3 \cdot 4H_2O$) were dipped in aqueous solution of Ni^{2+} nitrate. Mg-Al LDH was reconstituted in the surface layer of the particles, and simultaneously Ni^{2+} substituted for the Mg^{2+} sites, leading to the formation of eggshell-type Ni loading. The conditions of preparation of Mg-Al(3/1) mixed oxide and dipping in Ni^{2+} nitrate solution affected substantially eggshell-type Ni loading as well as catalytic activity. The slow heating, the lower final calcination temperature, and a dipping in the aqueous solution at the lower pH were preferable for the Ni loading in eggshell-type. Under the mild heating conditions, Mg(Al)O periclase structure was formed, on which the reconstitution of Mg-Al LDH was preferentially provoked in the surface layer of the particle by reconstitution during the dipping at the lower pH.

A typical result of SEM-EDS analyses of cross section of the catalyst particle is shown in Fig. 6 (Takehira et al., 2004a). The Mg-Al LDH powders were calcined at 650 °C, dipped in 1.0 M Ni^{2+} nitrate aqueous solution of pH = 4.7 for 45 min, washed and dried at 105 °C. Al showed an almost constant value across the diameter of the particle. Ni increased, while Mg decreased, ongoing to the surface layer from the center of catalyst particle. This suggests that Ni^{2+} substitutes for the Mg^{2+} sites during the dipping treatment, since the ionic radii of Ni^{2+} (0.069 nm) is close to that of Mg^{2+} (0.072 nm) (Shannon, 1976). It is likely that the eggshell-type Ni loading was realized by the reconstitution of Mg(Ni)-Al LDH layered structure, accompanied by Ni^{2+} incorporation (Takehira et al., 2005a). The condition of calcination of Mg-Al LDH powders significantly affected the eggshell loading. A slow heating

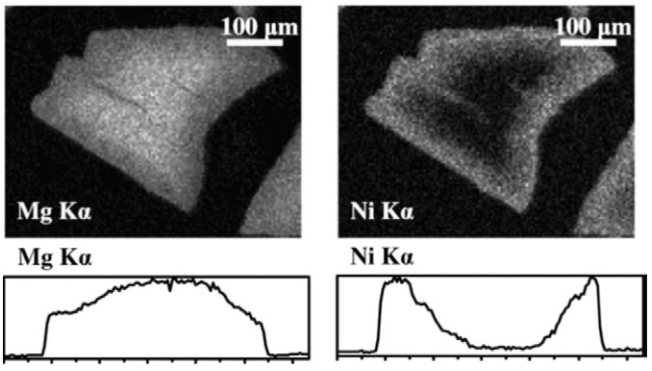

Fig. 6. SEM/EDS analyses of cross section of eggshell loaded $Ni_{0.50}/Mg_{2.63}Al$ catalyst particle (Takehira et al., 2004a, Elsevier).

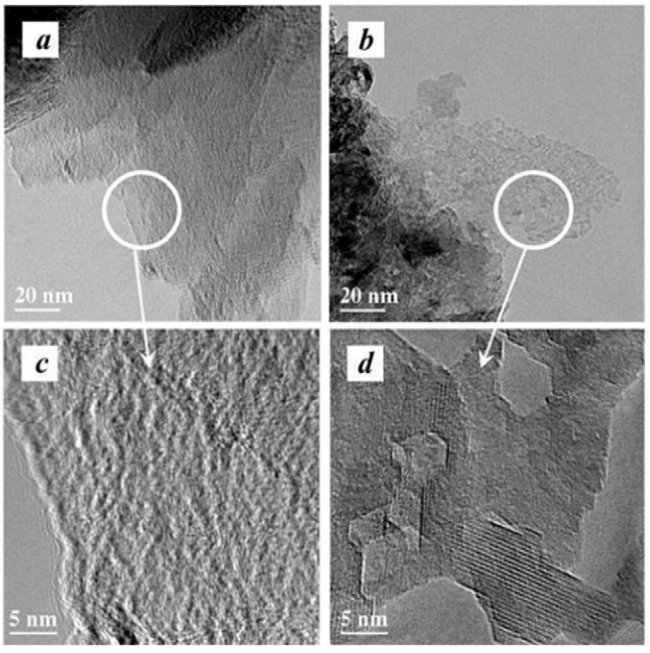

Fig. 7. TEM images of outer edges of Mg-Al (Mg/Al = 3/1) mixed oxide particles calcined at 650 (*a* and *c*) and 950 °C (*b* and *d*). (*a* and *b*) after dipping in 0.5 M Ni^{2+} nitrate aqueous solution for 1 h; (*c* and *d*) high magnification image of a part in the circle in *a* and *b*, respectively (Takehira et al., 2005a, Elsevier).

(0.8 ~ 1.5 °C min^{-1}) and a lower calcination temperature (550 ~ 650 °C) was preferable for provoking eggshell-type Ni loading (Takehira et al., 2004a, 2005b).

The mechanism of reconstitution of LDH from Mg(Al)O periclase, leading to eggshell-type Ni loading on Mg-Al mixed oxide, was carefully studied (Takehira et al., 2005a). The pore distribution, surface morphology, and crystal and coordination structure of the mixed oxides were studied by XRD, MAS ^{27}Al NMR, TG-DTA, SEM, TEM, ICP, and N_2 and H_2 adsorption methods. When Mg(Al)O periclase particles were dipped in an aqueous solution of Ni^{2+} nitrate, the reconstitution of Mg-Al LDH took place in the surface layer of the particles, and simultaneously Ni^{2+} replaced a part of the Mg^{2+} sites of the LDH structure. The reconstitution proceeded by a dissolution- recrystallization mechanism on the microporous phase and formed "worm-like" structures, which finally constructed a dense layer and covered the surface of the particles. The dense layer hindered the further penetration of Ni^{2+} nitrate solution into the cores of the particles, resulting in eggshell-type Ni loading.

TEM observations of Mg-Al mixed oxide obtained by calcination of Mg-Al(3/1) LDH at 650 and 950 °C, respectively, showed that the surface of mixed oxide particles were covered by aggregates of many small crystallites, in which pore structures were observed, and the crystallite size increased with increasing calcination temperature (Takehira et al., 2005a). The average crystal size was obtained as 7.6 and 13.4 nm after calcination at 650 and 950 °C, respectively, from the line width of the reflection (200) in the XRD. In the TEM images of the outer edges of the mixed oxide particles after dipping in 1.0 M Ni^{2+} nitrate aqueous solution and drying at 85 °C (Fig. 7), the surface layer calcined at 650 °C was changed to a densely packed structure (Fig. 7a), whereas that at 950 °C still kept its porous structure (Fig. 7b). TEM images under high magnification clearly showed that a dense and amorphous film formed on the particles calcined at 650 °C (Fig. 7c), whereas the crystalline and porous structure was still preserved on the particles calcined at 950 °C (Fig. 7d). It is concluded that, after the oxide was dipped in Ni^{2+} nitrate aqueous solution, the low calcination temperature bestowed the particles with a thick and dense outer phase consisting of reconstituted Mg(Ni)-Al LDH, and the high temperature afforded a porous phase. These are consistent with the observations by SEM (Takehira et al., 2005a). The research (Rocha et al., 1999) on the reconstitution of Mg-Al LDH from Mg-Al mixed oxides in the presence of water vapor by XRD and MAS ^{27}Al NMR showed that the reconstitution was complete when the sample was calcined at or below 550 °C, whereas only partial reconstitution was observed after calcination at 1000 °C. The dense layer formed by Mg(Ni)-Al LDH hindered the further penetration of Ni^{2+} nitrate solution into the cores of the particles, resulting in eggshell-type Ni loading. A balance between the rate of reconstitution of Mg-Al LDH and the rate of penetration of the aqueous solution of nickel nitrate determined the loading type of Ni.

The activity of eggshell-type loaded Ni/Mg(Al)O catalysts was evaluated by TOF (Turnover frequency), together with the values of other Ni/Mg(Al)O catalysts (Takehira et al., 2005a,b). Product distribution always followed the thermodynamic equilibrium of the reaction. TOF values were calculated based on the rate of CH_4 consumption at 700 °C and at a GHSV of 9.0×10^5 mL h^{-1} g_{cat}^{-1}, and the total amount of Ni atom in the catalyst. The rate of reaction was calculated at CH_4 conversion below 50%. The TOF was higher on *eggshell*-Ni/Mg(Al)O (0.86 s^{-1}) than on Ni/Mg(Al)O (0.81 s^{-1}) catalysts, indicating clearly an enhanced activity per unit amount of Ni due to the surface enrichment of active Ni species. A measurement of the effectiveness factor of the catalyst showed that the intraparticle mass transfer limitation exists in steam reforming of CH_4 over the catalyst at 800 °C (Takehira et al., 2005a).

4.1.2. Bimetallic catalysts

4.1.2.1. Pt or Mg-Cu/Zn(Al)O catalysts. Trace amounts of noble metal were supported on Cu/Zn(Al)O catalysts by adopting reconstitution of Zn(Cu)-Al LDH. Ternary Cu/Zn(Al)O (molar ratio Cu/Zn = 1/1, Al content 0–25 mol%) catalysts prepared by co-precipitation (*cp*) was mainly composed of aurichalcite $(Cu,Zn)_5(CO_3)_2(OH)_6$ and small amount of LDH $(Cu,Zn)_6Al_2(OH)_{16}CO_3 \cdot 4H_2O$. When the *cp*-Cu/Zn(Al)O (Cu/Zn/Al = 45/45/10) was dipped in aqueous solution of noble metal nitrates (Nishida et al., 2008), LDH was reconstituted and simultaneously noble metals were incorporated. The noble metal-doped samples were calcined at 300 °C and tested for the water-gas shift (WGS) reaction (3). Among the noble

$$CO + H_2O \rightarrow H_2 + CO_2 \Delta H^0_{298K} = -41.1 kJmol^{-1} \quad (3)$$

metals, Pt, Rh and Ru, tested, Pt was the most effective for stabilizing the catalytic activity although some deactivation due to Cu sintering took place. An intrinsic promoting effect of Pt was clearly observed by evaluating the TOF of the catalyst. TOF calculated based on CO conversions at 150 °C increased from 2.85×10^{-3} s^{-1} for non-doping to 5.41×10^{-3}. 4.66×10^{-3} and 5.19×10^{-3} s^{-1} for 0.05, 0.1 and 0.5 wt% Pt doping, respectively. Surface areas of Cu metal significantly decreased by the Pt-doping, indicating that Cu metal particles sintered on *cp*-Cu/Zn(Al)O (45/45/10) catalysts. The Cu/Zn(Al)O mixed oxide calcined at 300 °C contained carbonate anions and possibly assisted the reconstitution of LDH structure during the Pt-doping step. A small amount of LDH was effective for improving the sustainability of the catalyst by the surface reconstitution. By 0.5 wt% Pt-doping, active and sustainable catalysts were obtained. It is likely that trace Pt enhanced both intrinsic activity and sustainability of the catalyst by accelerating the reduction-oxidation between Cu^0 and Cu^+ as well as by suppressing the oxidative sintering of active Cu metal species by hydrogen-spillover from Pt metal to Cu metal particles (Nishida et al., 2008).

The effect of Mg doping on Cu/Zn(Al)O catalysts in WGS reaction was further studied by comparing *cp*-Mg-Cu/Zn(Al)O and *m*-Mg-Cu/Zn(Al)O catalyst. The former catalyst was prepared by Mg^{2+}, Cu^{2+}, Zn^{2+} and Al^{3+} coprecipitation, whereas the latter was by utilizing reconstitution, i.e., "memory effect" by Mg doping on *cp*- Cu/Zn(Al)O (Nishida et al., 2009). Mg^{2+} ions were enriched in the surface layer of *m*-Mg-Cu/Zn(Al)O, whereas Mg^{2+} ions were homogeneously distributed in the particles of *cp*-Mg-Cu/Zn(Al)O. CuO particles were significantly sintered on the *m*-catalyst, whereas CuO particles were highly dispersed on the *cp*-catalyst. However, TOF values per exposed copper calculated from the CO conversion at 150 °C were higher on the *m*-catalyst than on the *cp*-catalyst. The highest TOF was attained at 0.193×10^{-3} mol% Mg doping of *m*-Mg-Cu/Zn(Al)O, where MgO was effectively incorporated in the surface layer of the catalyst particles and assisted the WGS reaction over the Cu species. Moreover, the *m*-catalyst was more sustainable against sintering than the *cp*-catalyst. It is concluded that the trace amounts of MgO stabilized Cu^0 (or Cu^+) species against oxidative sintering to Cu^{2+} and simultaneously enhanced the activity by accelerating catalytic reduction-oxidation cycles between Cu^0 and Cu^+.

4.1.2.2. Pt-Sn/Mg(Al)O catalysts. Light alkenes, propene and ethene, are important base chemicals for the chemical industry. Catalytic dehydrogenation of light alkanes is believed to be a potentially important route to selective production of high purity alkenes. Two types of catalysts are used in commercial dehydrogenation processes, supported Pt-Sn catalysts and CrO_x supported on Al_2O_3 (Moulijn et al., 2001). The alkane dehydrogenation reaction is strongly endothermic. In Cr-based processes, heat is supplied by burning off coke deposits from the catalyst in either a fixed bed rector with alternate feed (Catofin) or in a continuously regenerated fluid bed reactor (FBD-4). On the other hand, in Pt-based processes, heat is supplied by external heating of either a tubular fixed bed (STAR) or an adiabatic moving-bed reactor (Oleflex) (Moulijn et al., 2001). Cr-based catalysts are not suited for such direct heating methods, due to their intolerance toward heat and steam (Thomas, 1970; Weckhuysen and Schoonheydt, 1999). Pt-based catalysts have several advantages compared to Cr-based catalysts: First, they may be used in

steam-containing atmospheres, such as under autothermal dehydrogenation conditions. Second, they are fairly stable even at temperatures ≥ 600 °C, which are necessary to overcome the limit of thermodynamic equilibrium of the ethane dehydrogenation reaction. For many years, growth in the propene market has been higher than that for ethene. Propane dehydrogenation is believed to have a great potential as a propene booster in the future. The reaction is carried out catalytically because of cracking losses under thermal dehydrogenation conditions. UOP has commercialized a catalytic dehydrogenation process based on such a catalyst (Abrevaya and Imai, 1986; Imai, 1987, 1988a, Imai et al., 1988b). In this section, Mg(Al)O supported Pt-Sn bimetallic catalyst is introduced as a prominent catalyst for the propane dehydrogenation together with the important role of rehydration phenomenon in the preparation procedure of the catalyst.

Pt-Sn supported on Al_2O_3 and SiO_2 have been believed to be the promising catalysts in the dehydrogenation process and extensively investigated (Bariås et al., 1996). Sn is believed to inhibit hydrocracking, isomerization and coke formation; addition of Sn improves Pt dispersion due to favorable size ensemble formation based on geometric effects (Meitzner et al., 1988). Most of the dehydrogenation catalysts are Pt-Sn supported on Al_2O_3. Owing to the strong interaction between the metals and Al_2O_3 support, that affects the reduction behaviors and stability of the catalysts (Cortright and Dumesic, 1994). However acidic properties of Al_2O_3 frequently caused some disadvantages such as coking, etc. A few works have been focused on the use of some solid spinels such as $MgAl_2O_4$ to suppress the acidity (Aguilar-Ríos et al., 1999; Armendáriz et al., 2001). Pt-Sn/$MgAl_2O_4$ catalysts were prepared by the impregnation, coprecipitation-impregnation and sol-gel methods and used for propane dehydrogenation (Salmones et al., 2002).

Mg-Al LDH was used as the support of Pt-Sn catalyst in the form of Mg(Al)O after the calcination. Mg(Al)O, regarded as a defect-rich, aluminum-containing magnesium oxide, has a high surface area (typically 160–220 $m^2\ g^{-1}$) and shows a much higher resistance to sintering under steam-rich conditions than pure MgO. These properties combined with a basic character make Mg(Al)O an interesting material for applications as a catalyst carrier. Mg(Al)O possesses excellent properties as support material for metal-based catalysts. Davis and Derouane, 1991 reported a catalyst for the aromatization of *n*-hexane that utilizes Mg(Al)O as the carrier material. The support material is particularly suited for applications in an intermediate temperature range (≤600 °C), where it has been shown to maintain a high surface area (above 100 m^2/g) even after 14 days in a steam-rich atmosphere (Olsbye et al., 2002). Propane dehydrogenation to propene is one reaction for which the intermediate temperature range is particularly suited, and Pt,Sn/Mg(Al)O has been shown to possess superior activity and stability for this reaction compared to conventional Pt,Sn/Al_2O_3 catalysts (Akporiaye et al., 2000; Rytter et al., 2000; Olsbye et al., 2002).

4.1.2.3. Pt-Sn/Mg(Al)O catalyst for propane dehydrogenation. Pt and Sn deposited on Mg(Al)O constituted a new and highly efficient catalyst for the dehydrogenation of propane (Akporiaye et al., 2000; Rytter et al., 2000). The catalyst was superior to conventional alumina-supported systems in terms of life-time stability, activity, and propene selectivity (Akporiaye et al., 2001).

The catalysts were prepared in a two-step manner. First, the Mg-Al LDH was prepared by coprecipitation from Mg^{2+} and Al^{3+} nitrate in a basic solution at the pH ≈ 8 and at 60 °C. In a second step, the active metals were deposited onto the LDH or calcined LDH by impregnation from solution. Pt and Sn were deposited onto the support by impregnation techniques using ethanol or water as the solvent. The importance of Sn in supported Pt-Sn catalysts is well described in the literature (Passos et al., 1996; Humblot et al., 1998). It is known that the two metal precursors, $SnCl_2$ and H_2PtCl_6, form various colored anionic complexes, for example, the red-colored $PtCl_2(SnCl_3)^{2-}$ species (Jin, 1991). These complexes can be obtained in aqueous solution as well as in polar organic solvents such as ethanol. These mixed Pt-Sn complexes are ideal species for the metal impregnation. Ethanol was first chosen because the calcined LDH maintains its structure in this solvent. In water, on the other hand, LDH phase is reconstituted (Cavani et al., 1991; Hibino and Tsunashima, 1998; Akporiaye et al., 2001). It was noted in the literature that this water induced reconstitution of LDH was considered disadvantageous because of the lower surface area compared to that of the calcined material (Hibino and Tsunashima, 1998; Takehira et al., 2005a). Another argument in favor of ethanol was the possible decomposition of the LDH material in an acidified aqueous solution. However, water was finally preferred to ethanol for the industrial scale production of a catalyst because of the health and safety hazards associated with organic solvents. Moreover, the impregnation in water afforded well dispersed metal particles as well as high surface area after the calcination (Takehira et al., 2005a). Therefore, a detailed study was launched into aqueous impregnation of the carrier material. Thus, LDH reconstitution caused by using aqueous solution resulted in enhanced surface dispersion of active Pt and Sn species as observed in the Pt-Ni/Mg(Al)O catalyst (Li et al., 2008) and finally result in enough surface area after the calcination.

To assess the performance of the LDH-based catalysts, a comparison with conventional Al_2O_3-based catalysts was carried out. A reference catalyst was prepared according to a UOP patent (Imai, 1988a, Imai et al., 1988b, Imai and Jan, 1988c). This catalyst contained Pt, Sn, and Cs supported on θ-Al_2O_3 and was compared to several Mg(Al)O-supported catalysts. Pt, Sn, and in some cases Cs were deposited onto the support by impregnation in ethanol solution. Two Mg(Al)O support samples were used: Mg(Al)O-1 was precipitated using $NaOH/Na_2CO_3$ as the basic agent, whereas $(NH_4)_2(CO_3)_2/NH_3$ was used for the preparation of Mg(Al)O-2. The use of the stronger base $NaOH/Na_2CO_3$ presumably results in the higher Mg/Al ratio of Mg(Al)O-1. These θ-Al_2O_3- and Mg(Al)O-supported Pt-Sn catalysts were tested for propane dehydrogenation in a fixed-bed reactor. The catalysts were screened at 600 °C, 1 bar pressure, and 690 h^{-1} space velocity based on propane (NTP). The feed was propane (33%), H_2 (4.5%), N_2 (24%), and steam (38.5%). The catalysts were activated prior to the testing by an in situ reduction (R) or reduction-oxidation-reduction (ROR) sequence carried out at 600 °C. The ROR pretreatment involved heating the sample (35 °C min^{-1}) to 600 °C under a H_2 flow (20 mL min^{-1}). After keeping at the final temperature for 120 min, the sample was oxidized under a 5% O_2/He flow (50 mL min^{-1}) at 600 °C for 60 min and under an air flow (50 mL min^{-1}) at 600 °C for another 60 min. Then, the catalyst was again reduced under a H_2 flow (20 mL min^{-1}) at 600 °C for another 120 min and flushed with Ar (20 mL min^{-1}) at 600 °C for 60 min. Finally, the sample was cooled to 35 °C under an Ar flow.

Conversion and selectivity data from the screening test results are also given in Table 3 (Akporiaye et al., 2000). All catalysts show a higher initial activity after a ROR treatment compared to R treatment, i.e., only one initial reduction. However, this effect is much more pronounced for the Mg(Al)O-, specifically Mg(Al)O-2-based catalysts. Comparing the performance of the catalysts, the Mg(Al)O-2-based catalysts are clearly superior in terms of activity and stability compared to the Al_2O_3-based catalysts containing 2.5 times much amount of Pt as well as Cs accelerator. The Mg(Al)O-based catalysts showed small deactivation after 25 h on stream. The Mg(Al)O-based catalysts exhibited higher conversion than the Al_2O_3-based catalysts with the comparable or even better propene selectivity. This effect became more evident after 25 h on stream, at which point almost all of the Mg(Al)O-based catalysts show higher propene selectivity than the Al_2O_3-based samples after ROR treatment.

4.1.2.4. Effect of preparation procedure. The Pt-Sn/Mg(Al)O catalysts, cat-A ~ cat-D, were prepared from the same metal precursors by various impregnation procedures (Table 4) (Akporiaye et al., 2001). The BET surface areas reported were measured using pelletized samples and the values were some 50 $m^2\ g^{-1}$ higher on the powders. $SnCl_2$ is only soluble in acidified aqueous solution; therefore, HCl was used in most cases.

Table 3
Propane dehydrogenation over Pt-Sn/Mg(Al)O catalyst in a fixed bed reactor[a] (Akporiaye et al., 2001, American Chemical Society).

Catalyst[b]	Mg/Al/atomic ratio	Pt/wt%	Sn/wt%	Cs/wt%	Conversion/% at TOS[c] of		Selectivity/% at TOS[c] of		Yield/% at TOS[c] of
					5 h	25 h	5 h	25 h	25 h
Pt-Sn/Mg(Al)O-1^{ROR}	4.0	0.3	0.6	0	58.7	53.0	93.3	97.3	51.6
Pt-Sn/Mg(Al)O-2^{ROR}	2.1	0.3	0.6	0	58.8	57.5	93.0	95.9	55.1
Pt-Sn/Mg(Al)O-2^{ROR}	2.1	0.3	0.9	0	58.0	57.8	93.9	96.1	55.5
Pt-Sn/Mg(Al)O-2^{ROR}	2.1	0.3	1.2	0	58.6	57.5	94.9	95.9	55.1
Pt-Sn/θ-$Al_2O_3^{R}$	0	0.7	0.5	3.9	38.0	27.0	97.0	95.0	25.7
Pt-Sn/θ-$Al_2O_3^{ROR}$	0	0.7	0.5	3.9	41.4	31.0	96.4	95.9	29.7

[a] Test conditions: $T = 600$ °C; $P = 1$ bar; GHSV = 690 h^{-1} (NTP, based on propane); feed = C_3H_8 (33%), H_2 (4.5%), N_2 (24%), and steam (38.5%).
[b] Catalyst was pretreated by R (reduction) or ROR (reduction-oxidation-reduction) treatment at 600 °C.
[c] Time on stream.

However, chlorine may increase the acidity of the support, possibly leading to increased coking and, in turn, render the catalyst more difficult to regenerate. Therefore, the reduction of chlorine content of the catalysts after impregnation is important. In this case, however, calcination under steam-rich conditions (wet calcination) did not give satisfying results: the chlorine content of one Pt-Sn/Mg (Al) O catalyst was only reduced from 1.7 to 1.1 wt%. Finally, repeated washing with water proved to be very efficient: the chlorine content of cat-B was reduced from 5.4 wt% before washing to 0.25 wt% after washing. Thereafter, repeated washing with water was used as the standard procedure for chlorine removal. Use of water as the solvent during impregnation has important consequences for the structure of the carrier material. After calcination of LDH obtained by coprecipitation, the XRD patterns shows Mg(Al)O as the only crystalline phase, but the diffuse peaks indicate that the material has a relatively high defect density. The cat-B sample after aqueous impregnation showed the patterns of LDH reconstituted, whereas the cat-A sample impregnated in ethanol solution showed no LDH patterns, and Mg(Al)O pattern is retained. After the final calcination step, both cat-A and cat-B exhibit Mg(Al)O as the only crystalline phase.

The catalytic performances of cat-A ~ cat-D were compared in propane dehydrogenation. Although water induced reconstitution is said to be disadvantageous (vide supra), testing results reveal that aqueous impregnation, in fact, improves the catalytic performance compared to the initial procedure using ethanol. Moreover, the low surface area was drastically improved after the calcination. This was confirmed in cat-B and cat-C in Table 4. The results from the catalytic tests for cat-A, cat-B, cat-C and cat-D are shown in Table 5 (Akporiaye et al., 2001). All catalysts showed deactivation within each cycle mainly as a result of coke formation. As the propane conversion decreases, the selectivity to propene increased. A comparison of samples cat-A and cat-B showed that aqueous impregnation with subsequent chlorine removal yields a catalyst with improved stability compared to ethanol impregnation (cat-A). After each regeneration cycle, the initial activity of the former reaction cycle was nearly fully restored for cat-B. The ethanol sample (cat-A), on the other hand, deactivated more significantly from one cycle to the next. This may be due to the structure change of the support during impregnation, i.e., rehydration of Mg(Al)O leading to LDH reconstitution. Such importance of LDH structure was partly supported by the results obtained over cat-D prepared from uncalcined LDH: cat-B and cat-D were comparable in their stabilities, which are clearly superior to cat-A. A comparison between catalysts cat-B and cat-C indicates the importance of chlorine removal. The chlorine-rich catalyst deactivates significantly, presumably because of increased coking on acidic sites. Hence, the higher chlorine content clearly reduces the lifetime stability of the catalyst.

Thus, the Pt-Sn/Mg(Al)O catalyst showed substantially higher propane conversion than the commercial Pt-Sn/Al_2O_3 catalyst, while at the same time maintaining high propene selectivity near the thermodynamic limit. The preparation procedure used in the metal deposition step proved to be important for the performance of the catalyst. Impregnation of Mg(Al)O in HCl-acidified aqueous solution with subsequent chlorine removal enhances regenerability and long term stability of the catalyst compared to impregnation in ethanol. This is most likely due to a water-induced phase transition, i.e., rehydration of Mg(Al)O to Mg-Al LDH reconstitution on the catalyst particles, leading to the higher dispersion of active metal species. This was clearly verified by CO adsorption measurements, indicating that catalytic activity was well correlated with platinum dispersion.

4.1.2.5. Pt-Sn/Mg(Al)O catalyst for ethane dehydrogenation. The Pt-Sn/Mg(Al)O and Pt/Mg(Al)O catalysts were tested for ethane dehydrogenation at 450-650 °C. An Mg(Al)O support material, a high-loading Pt-Sn/Mg(Al)O catalyst, and for comparison, a high-loading Pt/Mg(Al)O catalyst were studied. The study has been extended to a semi-commercial low-loading Pt-Sn/Mg(Al)O catalyst characterization (Table 6) (Virnovskaia et al., 2007a). The carrier material Mg(Al)O with an Mg/Al ratio of 4.8 was synthesized via the corresponding LDH phase, using a standard coprecipitation method (Olsbye et al., 2002). Prior to characterization, the obtained $Mg_{9.6}Al_2(OH)_{19.2}CO_3 \cdot xH_2O$ phase was calcined at 600 °C in air for approximately 15 h to yield the final Mg(Al)O phase. The active metals in the high-loading Pt/Mg(Al)O and Pt-Sn/Mg(Al)O were deposited onto the calcined LDH by impregnation from aqueous solution. $SnCl_2 \cdot 2H_2O$ was dissolved in concentrated HCl; $H_2PtCl_6 \cdot 6H_2O$ was dissolved in distilled water. For coimpregnation of Pt and Sn, the two solutions were mixed, yielding a red solution due to Pt-Sn complex formation (Jin, 1991). It is known that $SnCl_2$ and H_2PtCl_6 metal precursors form various colored anionic complexes in HCl acidic solution, such as the red-colored $PtCl_2(SnCl_3)^{2-}$. The solid material was dried at 100 °C and calcined at 800 °C in air for 5 h. The semi-commercial Pt-Sn/Mg(Al)O catalyst was "Statoil C440-139".

Table 4
List of the LDH-supported catalysts (Akporiaye et al., 2001, American Chemical Society).

Material code	Mg/Al/atomic ratio	Pt/wt%	Sn/wt%	S_{BET}[a]/$m^2\ g^{-1}$	Impregnation method
cat-A	3	0.3	1.2	150	Ethanol onto calcined LDH
cat-B	3	0.3	1.2	162	Aqueous solution onto calcined LDH; chlorine removal
cat-C	3	0.3	1.2	130	Aqueous solution onto calcined LDH; no chlorine removal
cat-D	5	0.3	1.2	156	Ethanol onto uncalcined LDH

[a] The BET surface area was measured on the pelletized catalysts.

Table 5
Propane conversion obtained from catalytic testing in a fixed-bed reactor (Akporiaye et al., 2001, American Chemical Society).

	Conversion/%[a]							
	cycle 1		cycle 3		cycle 5		cycle 10	
Catalyst	Initial	Final	Initial	Final	Initial	Final	Initial	Final
cat-A	n.m.[b]	n.m.[b]	62	38	54	33	n.m.[b]	n.m.[b]
cat-B	59	48	57	45	55	38	55	39
cat-C	68	47	59	43	46	32	n.m.[b]	n.m.[b]
cat-D	52	48	53	45	n.m.[b]	n.m.[b]	49	40

[a] Test conditions: 600 °C; GHSV 1000 h^{-1}; 4.5% H_2, 32% propane, remainder steam.
[b] n.m. = not measured.

The catalytic properties of Pt-Sn/Mg(Al)O and Pt/Mg(Al)O toward the ethane dehydrogenation reaction were investigated during an activation sequence. Activation energies at 550–650 °C and product selectivities at 600 °C and at 9% ethane conversion are shown in Table 6 (Virnovskaia et al., 2007b) for samples Pt/Mg(Al)O, Pt-Sn/Mg(Al)O, and semi-commercial Pt-Sn/Mg(Al)O, all after three activation cycles. Holding time variation experiments using sample Pt/Mg(Al)O (not shown) indicated that ethene is a primary product, while methane and CO are secondary products from ethane. When product selectivities are compared, it is interesting to note that over Pt/Mg(Al)O, CO was the main C-containing product (80% CO selectivity) from ethane at 600 °C, even at only 9% ethane conversion. Over Pt-Sn/Mg(Al)O, ethene was the main C-containing product, and the CO selectivity was 18%, whereas over semi-commercial Pt-Sn/Mg(Al)O ethane selectivity was very high and only traces of CO was observed under the same conditions. Only trace amount of the other C_2 and C_3 compounds such as acetylene, propene and propane were observed.

It is well known from the literature that the ethane hydrogenolysis reaction, which bears strong resemblances to the ethane reforming reaction to syngas (CO and H_2), is strongly surface sensitive (Chen and Goodwin, 1995; Cortright and Watwe, 2000b). The high selectivity to CO over Pt/Mg(Al)O compared to Pt-Sn/Mg(Al)O and semi-commercial Pt-Sn/Mg(Al)O suggested that, while Pt/Mg(Al)O contains low-coordinated Pt sites, those sites are covered by Sn on Pt-Sn/Mg(Al)O and semi-commercial Pt-Sn/Mg(Al)O. Several groups have previously reported an increase in alkene selectivity and a corresponding decrease in cracking or reforming to syngas when Sn is added to Pt-based catalysts for alkane (ethane, propane, butane) dehydrogenation (Cortright et al., 2000a). As for the apparent activation energies for ethane conversion, they increase in the order semi-commercial Pt-Sn/Mg(Al)O ≈ Pt-Sn/Mg(Al)O < Pt/Mg(Al)O (Table 6). It would be expected that the activation energy of reaction is lower on low-coordinated Pt sites. However, while C—H bond scission has been reported as the rate-determining step in alkane dehydrogenation reactions (Cortright and Dumesic, 1995), C—C bond scission is reported to be rate determining for ethane hydrogenolysis (Sinfelt, 1972). If ethane reforming to synthesis gas is rate-limited by the same step as ethane hydrogenolysis, the trend in apparent activation energy for the three catalysts is well correlated with the selectivities observed for the three catalysts. The faster deactivation of Pt/Mg(Al)O compared to Pt-Sn/Mg(Al)O and semi-commercial Pt-Sn/Mg(Al)O further suggests that adsorption of reaction intermediates, subsequently leading to coke formation, is favored on the former catalyst.

The semi-commercial Pt-Sn/Mg(Al)O catalyst used here consists of a pure (nonsegregated) Mg(Al)O phase (Virnovskaia et al., 2007a, b), in which Mg and Al are homogeneously distributed. Further, while Pt/Mg(Al)O catalyst contained both low coordinated (steps, edges, corners, or defects) Pt sites and Pt terrace sites, in Pt-Sn/Mg(Al)O catalyst the low-coordinated Pt sites were found to be covered by Sn. This means that the accessible Pt sites in the semi-commercial Pt-Sn/Mg(Al)O consist mainly of terraces (Virnovskaia et al., 2007b), leading to high selectivity of ethene.

This Pt-Sn/Mg(Al)O catalyst has been developed under the collaboration between Oslo University, Statoil, Linde and BASF, and its processing was discussed by them.

4.2. LDH catalysts supported on various carriers

LDH-derived mixed oxides possess excellent catalytic ability, such as high surface area, phase purity, basic surface properties, and structural stability. Moreover, LDH-derived oxides exhibit not only their original acid-basic properties of Mg-Al system but also reduction-oxidation properties as catalysts depending on the metal species introduced in the structure. Although LDH-derived oxides work as heterogeneous catalysts for various reactions in both liquid and gaseous phase, they are not mechanically strong enough for recyclable or continuous use due to its easy pulverization or exfoliation during the reaction.

Roelofs et al. (2000, 2001) proposed that the active sites participating in catalysis are located at the edge of the platelets. Thus, the number of accessible edge active sites is limited by the lateral size of the LDH crystallites and increases with decreasing particle size. Consequently, several studies have been conducted to maximize the number of active sites by minimizing the lateral size of the activated LDH (Winter et al., 2004; Abelló et al., 2005a). This was achieved by using ultrasound during reconstitution (Climent et al., 2004a; Abelló et al., 2005b) or by preparing small LDH platelets (≈20 nm). The resulting catalysts showed a significant increase in catalytic activity in reactions such as self-condensation of acetone and in the transesterification of glycerol by diethyl carbonate (DEC). However, for commercial applications, such LDH has the inconvenience to be obtained in very small particle sizes, which can be used in batch reactors but not in continuous flow reactors due to the severe pressure drop. It is highly urged to use the LDH-derived oxide as a

Table 6
Properties of Pt-Sn/Mg(Al)O catalysts and their catalytic activities (Virnovskaia et al., 2007b, American Chemical Society).

Sample	Mg/Al/atomic ratio	Pt/wt%	Sn/wt%	$S_{BET}/m^2\ g^{-1}$	$E_A/kJ\ mol^{-1}$	selectivity at 9% ethane conversion[a]/%		
						C_2H_4	CO	CH_4
Pt/Mg(Al)O	4.8	1.2	0	172	135 ± 5	43	55	2
Pt-Sn/Mg(Al)O	4.8	2.3	5.4	186	117 ± 5	80	18	1
Pt-Sn/Mg(Al)O[b]	4.8	0.5	1.2	130	116 ± 10	99	t	1

[a] Selectivity determined after full activation for all catalysts. Conditions: 600 °C, $C_2H_6/H_2/CO_2/N_2/Ar$ = 1/0.2/0.7/0.6/7.5, WHSV = 1.6 h^{-1} for samples Pt/Mg(Al)O and Pt-Sn/Mg(Al)O and 18.5 h^{-1} for semi-commercial Pt-Sn/Mg(Al)O catalyst. t = traces.
[b] Semi-commercial Pt-Sn/Mg(Al)O catalyst "Statoil C440–139".

supported form on an appropriate carrier, which may be also convenient for enhancing the mechanical strength. Several carriers have been tested to support the LDH-derived oxides for their sustainable use as the effective catalysts.

4.2.1. Carbon nanofibers supported Mg-Al LDH catalysts

First, Winter et al. (2004) used a mixture of activated Mg-Al LDH as solid base and Pd on carbon nanofibers (CNF) as a catalyst for single-stage liquid-phase synthesis of methyl isobutyl ketone (MIBK) from acetone and H_2 at 40 °C and H_2 pressures of 1–20 bar. Under the presented conditions the dehydration reaction of diacetone alcohol (DAA) to mesityl oxide (MO) is rate limiting in the production of MIBK. Then, they prepared Pd supported on rehydrated LDH (LDHr) as bi-functional catalyst and compared its activity with that of physical mixture of LDHr and Pd/CNF (Winter et al., 2006). However the activity for MIBK production was rather lower on the Pd/LDHr catalysts compared with the physical mixture. Actually the conversion of MO to MIBK in the single-stage experiments turned out to be dependent on the Pd loading, which was not observed with the physical mixtures. Deposition of Pd on activated LDHr resulted in agglomerates of irregular stacks of LDH platelets that cause inclusion of a large part of the Pd particles. The low activities and TOF in the hydrogenation of MO were obtained with the Pd/LDHr catalysts compared to the other hydrogenation catalysts, which was ascribed to entrapment of Pd particles in the LDH agglomerates making them less accessible for the organic reactants.

Then, CNF supported Mg-Al LDH catalysts were prepared starting from Ni/SiO_2 catalyst (Winter et al., 2005). Mechanically strong CNF spheres of millimeter size were grown from CH_4 over a spherically preshaped Ni/SiO_2 catalyst. After reduction of the Ni catalyst, CH_4 gas was passed over the Ni catalyst at 570 °C to afford CNF on it. The CNF samples were refluxed in a 1 M KOH solution to remove the silica support, washed, and then refluxed in concentrated nitric acid to remove exposed Ni and to introduce oxygen-containing groups on CNF (denoted as CNFox). Supported Mg-Al LDH (Mg/Al = 2) were prepared by impregnation of both Mg^{2+} and Al^{3+} nitrates on CNFox, then with an aqueous solution of NaOH and Na_2CO_3, followed by aging in an autoclave. The samples were heated at 60 or 150 °C for 20 h in a water-saturated atmosphere, and then dried. The spherical Mg-Al LDH/CNF samples were activated by rehydration, and were stored under N_2 atmosphere.

Mg-Al LDH loadings as high as 16 wt% were obtained. LDH as platelets with a lateral size of ~20 nm supported on the CNF. After activation by rehydration, a high number of accessible Brønsted base sites were formed (0.7–0.9 mmol g_{LDH}^{-1}), resulting in high specific activity in the self-condensation of acetone, more than four times higher than that of unsupported catalysts. The greatly improved efficiency of the supported LDH was ascribed to the high number of active edge sites (Abelló et al., 2005a; Chimentão et al., 2007). An efficient and mechanically strong catalyst for the single-stage liquid-phase synthesis of MIBK from acetone and H_2 at 58 °C was obtained with the deposition of Pd and LDH on the same support.

Finally CNF supported Mg-Al LDH were tested as solid base catalysts for the synthesis of glycerol carbonate (GC) and dicarbonate (GDC) by transesterification (Scheme 3) (Alvarez et al., 2013b). The supported materials exhibited a 300 times higher activity compared to bulk activated LDH for the transesterification. The materials could be reused while maintaining a high yield of GC. In contrast in the acetone self-condensation reaction the rehydrated samples were more active in this reaction. This indicates that the polarity of the catalyst related to the reactant properties has a huge impact on the performance of a solid base catalyst.

In transesterification of glycerol, CNF itself did not show any catalytic activity. A high activity was found for the supported catalysts, especially the calcined sample (LDH/CNFc) showed superior activities (Alvarez et al., 2013b). If comparing the initial rate expressed per mol LDH of calcined supported LDH sample, LDH/CNFc (53 mmol $Gly \cdot g_{LDH}^{-1} \cdot h^{-1}$), with the bulk, LDHc (0.18 mmol $Gly \cdot g_{LDH}^{-1} \cdot h^{-1}$), the supported material is almost a factor 300 better than the bulk. Furthermore, this sample showed significant higher catalytic activity than traditional transesterification catalysts such as K_2CO_3 which first achieves full conversion (97%) of glycerol conversion after 6 h under the same reaction conditions (Álvarez et al., 2012b), while the LDH/CNFc reached this level within 90 min. The high activity in combination with the fact that LDH/CNFc could be reused in three consecutive runs without significant loss of activity make it a promising candidate as a solid catalyst for the transesterification reaction. The catalyst rehydrated in gas phase revealed a catalytic activity higher than the catalyst rehydrated in liquid phase, probably due to relocation/migration of the active phase in the latter. Thus, the reconstitution method of the LDH has a great influence on the catalytic behavior of the final catalyst. The low-hydration degree of the mixed oxide together with the hydrophobicity of the CNF support led to the enhanced activity of the transesterification reaction for the LDH/CNFc compared to the rehydrated samples. The opposite trend was observed in the acetone self-condensation reaction where the rehydrated sample was considerably better than the oxide. This indicates that polarity of the catalyst and polarity of different reactants is very important to consider in the optimization of solid base catalysts for a given reaction. Insight in these matters might make it possible to design more efficient catalysts in the future.

4.2.2. Al_2O_3 supported Mg-Al LDH catalysts

Álvarez et al. (2012b) prepared Al_2O_3 supported Mg-Al LDH catalyst and tested in transesterification of glycerol by DEC to GC and GDC (Scheme 3). Mg-Al LDH was grown onto α- and γ-Al_2O_3. In the XRD patterns, the peaks of corundum were observed for α-Al_2O_3, together with the reflections of (003) and (006) planes of meixnerite phase on the sample LDH2r/α-Al_2O_3 (n = Mg/Al; x = r, after rehydration or o, after calcination, in LDHnx) obtained after rehydration of Mg(Al)O. Diffraction lines of boehmite (γ-AlO(OH)) and meixnerite were also clearly detected on rehydrated samples supported by γ-Al_2O_3, i.e., LDH2r/γ-Al_2O_3 indicating that at least part of the γ-Al_2O_3 support was transformed into boehmite after the rehydration treatment.

On the calcined supported materials, the thermal desorption of CO_2 evidences the presence of relatively strong basic sites which are absent on the pure supports. The samples supported by α-Al_2O_3 exhibit a higher basic strength than those supported on γ-Al_2O_3. After rehydration, the total number of basic sites changes only little, but the original basic sites, presumed to be of Lewis type are converted to stronger Brønsted sites. Catalysts were activated by calcination (LDH2o/α-Al_2O_3 or LDH2o/γ-Al_2O_3) or by rehydration of the calcined catalysts (LDH2r/α-Al_2O_3 or LDH2r/γ-Al_2O_3). Due to their better mechanical properties, these solids can be used in a continuous flow reactor. They are active for the conversion of glycerol into GC and GDC. Due to the immiscibility of glycerol and DEC, the reaction was carried out using a solvent to favor the flow of reactants through the catalytic system. The experimental results show that the type of basic center has a significant influence on the activity in the transesterification reaction. The catalysts which present Brønsted basicity (rehydrated catalysts) showed better performances than calcined samples which present mainly Lewis basic sites. In addition, the stronger adsorption at the Brønsted sites favors the consecutive transesterification of the GC. Moreover, it has been observed that the most active catalysts lead to a higher yield of GDC produced at the expenses of GC. An increase in the Mg content in the catalyst led to a higher glycerol conversion and higher yield of GDC; however catalyst LDH4r/α-Al_2O_3 showed lower stability than catalyst LDH2r/α-Al_2O_3, probably due to the presence of an extra-phase of MgO(H) in the catalyst. On the other hand, the support effect on catalytic properties is clearly evident, the catalysts supported on α-Al_2O_3 being more active. This higher activity is accounted for by the stronger basicity of LDH supported onto α-Al_2O_3 due to the weak interaction between the LDH and the support, evidenced by TPD of CO_2.

4.2.3. Magnetic materials supported catalyst.

The selective oxidation of alcohols to the corresponding carbonyl compounds is a greatly important transformation in synthesis chemistry (Corma et al., 2007). Recently, it has been disclosed that LDH-supported Au nanoparticles as environmentally benign catalysts could catalyze the oxidation of alcohol with good efficiency (Fang et al., 2011; Liu et al., 2014a). The activity of the nanometer-sized catalysts will benefit from decreasing the particle size. However, as the size of the support is decreased, separation using physical methods, such as filtration or centrifugation, becomes a difficult and time-consuming procedure. A possible solution could be the development of catalysts with magnetic properties, allowing easy separation of the catalyst by simply applying an external magnetic field (Polshettiwar et al., 2011). The importance of magnetic separation is rising along with extending the utilization and development of catalysts.

Magnetically separable Mg-Al LDH/Fe_3O_4 catalyst was first prepared by titration method in various molar ratios of (Mg + Al) to Fe, and their catalytic behavior was tested for epoxidation of 2-cyclohexen-1-one using hydrogen peroxide (Nishimura et al., 2010). Monodispersed Fe_3O_4 nanoparticles (Mono-FeNPs) were synthesized by thermal decomposition of Fe-oleate complex. Then, Mg-Al LDH was deposited on magnetic Fe_3O_4 core by coprecipitation method as follows: Mg^{2+} and Al^{3+} nitrates, and synthesized mono-FeNPs were dispersed in water, in which aqueous solution of NaOH and Na_2CO_3 was slowly added until pH reaching 10 under vigorous stirring. The resulting solution was aged at 60 °C, then filtered, washed with water, and dried at 100 °C overnight. The FeLDH100 thus obtained with the molar ratio of (Mg + Al)/Fe = 100 showed high activity and selectivity in epoxidation of 2-cyclohexen-1-one with hydrogen peroxide. After magnetic separation, FeLDH100 kept superior properties and could be reused for four reactions without loss of activity.

A novel nanostructured magnetic composite materials for solid base catalyst composed of $CoFe_2O_4$ as the magnetic core and Mg-Al LDH providing basic sites was prepared and tested in self-condensation of acetone (Xu et al., 2009). Xu et al. (2015) prepared magnetically separable Mg-Al LDH/$CoFe_2O_4$ and used in cellulose hydrolysis as base catalyst. The highest activity was obtained with the catalyst of Mg/Fe molar ratio = 3/1, a maximum yield (46.5%) of soluble reducing sugars with high glucose selectivity (84.4%) at 150 °C for 24 h. Moreover, the solid catalyst could be easily separated and possibly reused.

Recently finely tuned core-shell structured magnetic LDH catalysts have been prepared. Zhang et al. (2004) prepared Mg-Al LDH/$MgFe_2O_4$ by a method involving separate nucleation and aging steps, and subsequently calcined to give a mixed metal oxide composite Mg(Al)O/$MgFe_2O_4$ which was rehydrated to give LDH supported on a ferrite core. Li et al. (2009b) prepared Mg-Al LDH/Fe_3O_4 through a layer-by-layer assembly of exfoliated LDH nanosheets as a magnetic matrix for loading $W_7O_{24}^{6-}$ as a catalyst. These core-shell structural nanocomposites possess the magnetization of magnetic materials and multiple functionalities of the LDH materials. Nevertheless, these reported synthesis routes need multi-step and sophisticated procedures. Mi et al. (2011) designed a facile synthesis strategy for the fabrication of a novel Au/Mg-Al LDH/Fe_3O_4 nanocatalyst, consisting of Au particles supported on oriented grown Mg-Al LDH crystals over the Fe_3O_4 nanospheres, which combines the excellent catalytic properties of Au nanoparticles with the super paramagnetism of the magnetite nanoparticles. This is the first instance of direct immobilization of vertically oriented Mg-Al LDH platelet-like nanocrystals onto the Fe_3O_4 core particles by a simple coprecipitation method and the fabrication of hierarchical magnetic metal-supported nanocatalysts via further supporting metal nanoparticles.

The samples at various stages of the fabrication of the Au/Mg-Al LDH/Fe_3O_4 nanocatalyst were observed by SEM/TEM and the synthetic strategy is shown in Fig 8 (Mi et al., 2011). The Fe_3O_4 nanospheres (Fig. 8a) show a smooth surface and a mean diameter of 450 nm with a narrow size distribution. After direct coating with Mg-Al LDH carbonate (Fig. 8b), a honeycomb like morphology with many voids in the size range of 100–200 nm is clearly observed, and the LDH shell is composed of interlaced platelets of ca. 20-nm thickness. Interestingly, the Mg-Al LDH shell presents a marked preferred orientation with the *c*-axis parallel to, and the *ab*-face perpendicular to the surface of the magnetite cores. The TEM image of two separate nanospheres (Fig. 8d) undoubtedly confirms the core–shell structure of the Mg-Al LDH/Fe_3O_4 with the Fe_3O_4 cores well-coated by a layer of LDH nanocrystals. In detail, the Mg-Al LDH crystal monolayers are formed as large thin nanosheet-like particles, showing an edge-curving lamella with a thickness of ca. 20 nm and a width of ca. 100 nm, growing from the magnetite core to the outer surface and perpendicular to the Fe_3O_4 surface. The outer honeycomb like microstructure of the obtained core–shell Mg-Al LDH/Fe_3O_4 nanospheres with a surface area of 43.3 $m^2\ g^{-1}$ provides abundant accessible edge and junction sites of LDH crystals making it possible for this novel hierarchical composite to support metal nanoparticles. With such a structural morphology, interlaced perpendicularly oriented Mg-Al LDH nanocrystals can facilitate the immobilization of nano-metal particles along with avoiding the possible aggregation. Though the XRD pattern fails to show the characteristics of Au nanoparticles, it can be clearly seen by the TEM of Au/Mg-Al LDH/Fe_3O_4 (Fig. 8e) that Au nanoparticles are evenly distributed on the edge and junction sites of the interlaced Mg-Al HT nanocrystals with a mean diameter of 7.0 nm, implying their promising catalytic activity. Meanwhile, the reduced packing density (large void) and the less sharp edge of LDH platelet-like nanocrystals can be observed (Fig. 8c and e). To get more insight on structural information of Au/Mg-Al LDH/Fe_3O_4, the HRTEM image was obtained (Fig. 8f). It can be observed that both the Au and Mg-Al LDH nanophases exhibit clear crystallinity as evidenced by well-defined lattice fringes. The interplanar distances of 0.235 and 0.225 nm for two separate nanophases can be indexed to the (111) plane of cubic Au and the (015) facet of the hexagonal Mg-Al LDH phase (inset in Fig. 8f).

The catalytic oxidation of 1-phenylethanol as a probe reaction over the present novel magnetic Au/Mg-Al LDH/Fe_3O_4 (7.0 nm Au) nanocatalyst demonstrates high catalytic activity. The yield of acetophenone is 99%, with TOF of 66 h^{-1}, which is similar to that of the previously reported Au/Mg-Al LDH (TOF, 74 h^{-1}) with a Au average size of 2.7 nm at 40 °C (Mitsudome et al., 2009), implying that the catalytic activity of Au/Mg-Al LDH/Fe_3O_4 can be further enhanced as the size of Au nanoparticles is decreased as seen on LDH (Fang et al., 2011) or in dendrimer (Myers et al., 2011). Meanwhile, the high activity and selectivity of the Au/Mg-Al LDH/Fe_3O_4 can be related to the honeycomb like morphology of the support Mg-Al LDH/Fe_3O_4 being favorable to the high dispersion of Au nanoparticles and possible concerted catalysis of the basic support. Five reaction cycles have been tested for the Au nanocatalysts after easy magnetic separation by using a magnet (4500 G), and no deactivation of the catalyst has been observed (Mi et al., 2011). Moreover, no Au, Mg and Al leached into the supernatant as confirmed by ICP (detection limit: 0.01 ppm) and almost the same morphology remained as evidenced by SEM of the reclaimed catalyst.

4.2.4. Paper structured catalysts

Recently monolithic catalysts, "paper-structure catalysts (PSC)" have been prepared by paper making technique and utilized in H_2 production for fuel cell (FC) systems. The monolithic catalyst have been utilized for specific use of the catalyst in exhaust gas-cleaning for automobile and NO_x elimination for coal-fired power plant, etc. The H_2 production for FC requires high efficiency as well as high stability as mentioned in the Chapter 5.2. Utilization of monolithic form of the catalyst seems one solution. On the other hand, LDH-derived catalysts are mainly obtained as powder forms, which are inconvenient to handle in practical cases. Further developments are needed to mold or immobilize the catalyst powders. Reforming catalysts for the H_2 production have been formed into spheres, pellets and rods with a typical size of 5–10 mm, but the activity decreased seriously compared with the original powder catalysts as seen with commercial CuO-ZnO-Al_2O_3 catalyst

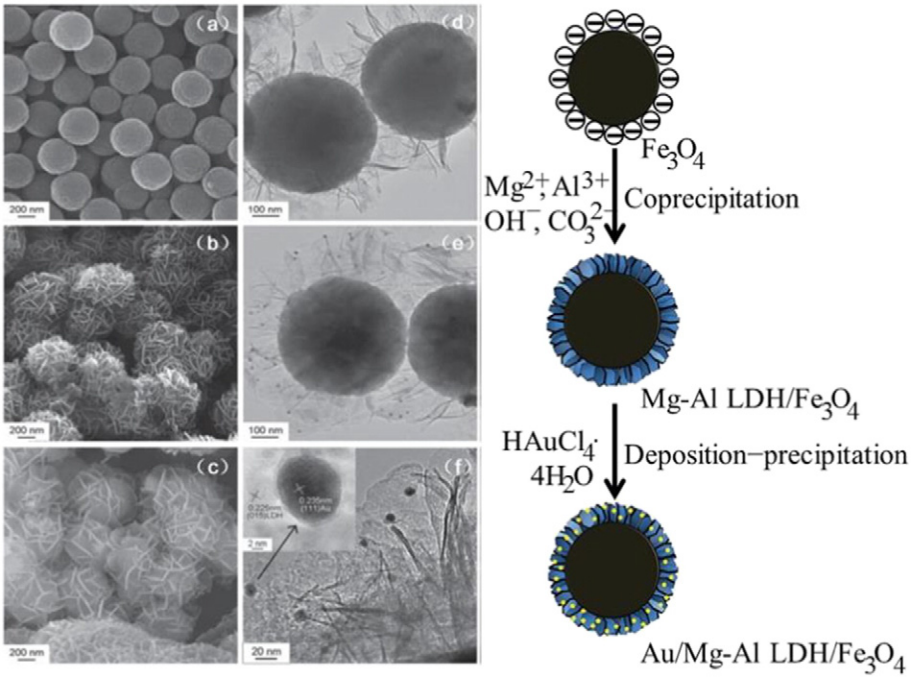

Fig. 8. Synthetic strategy and SEM (a, b and c), TEM (d and e) and HRTEM (f) images of Fe_3O_4 (a), Mg-Al LDH/Fe_3O_4 (b and d) and Au/Mg-Al LDH/Fe_3O_4 (c, e, and f) (Mi et al., 2011, the Royal Society of Chemistry).

(Purnama et al., 2004). In addition, rapid deactivation due to spot-heating during the reforming process was frequently observed. Therefore, new types of monolithic catalyst form as well as development of catalytic reforming materials are anticipated.

The monolithic catalysts were first prepared starting from "ex-LDH" materials, such as Cu-ZnO and Ni-MgO, both of which are easily converted to LDH by the addition of Al. Fukahori et al. (2006a) reported on the fabrication of Cu-Zn PSC for methanol steam reforming. Cu-Zn oxide catalyst powders were incorporated into paper-like composites, using ceramic fibers as the carrier matrix. Catalyst particles were supported on the ceramic fiber networks tailored in the PSC having various types of pores. They demonstrated a higher performance for methanol conversion and H_2 production than commercial Cu-ZnO catalyst pellets. The concentration of CO, which poisons fuel cell electrode catalysts, decreased remarkably, without any CO reduction system. These PSC showed also high activity in autothermal reforming of methanol (Koga et al., 2006). Excellent catalyst durability was shown by suppressing Cu sintering during the autothermal reforming (Koga et al., 2008). Then, ceramic fibers composed of fibrous silicon carbide (SiC) were used for making PSC containing Cu-ZnO as active species (Fukahori et al., 2006b). The high heat conductivity of the SiC fibers improved the catalytic performance, especially by suppressing the reverse water gas shift reaction. The computational fluid dynamic (CFD) analysis confirmed that the heat transfer and the heat distribution inside PSC were improved by the SiC fibers (Fukahori et al., 2008).

Ni-MgO catalyst was in situ synthesized on a microstructured inorganic paper support and tested in steam reforming of CH_4 (Miura et al., 2013). Porous paper supports were prepared beforehand using a conventional papermaking technique, and then simply impregnated with Mg^{2+} and Ni^{2+} nitrates solutions, either stepwise or at the same time. After reduction in an H_2 flow, Ni/MgO catalysts were formed in the paper composites. The as-prepared Ni/MgO paper is much like an ordinary paper product, being flexible, lightweight, and easy to handle. The Ni/MgO paper composites, especially the co-impregnated paper, exhibited excellent catalytic performances in the steam reforming of CH_4.

Then, Mg-Al LDH was dispersed in an inorganic fiber network during the preparation of PSC, and Ni was then loaded on this paper matrix via an impregnation method. $Mg_6Al_2(OH)_{16}CO_3 \cdot 4H_2O$ and pure oleic acid methyl ester (oleic FAME, $C_{19}H_{36}O_2$) was used as the LDH and biodiesel fuel, respectively. During the preparation of the inorganic fiber network, Mg-Al LDH was calcined at 800 °C to form Mg(Al)O periclase and $MgAl_2O_4$ spinel. The Mg(Al)O was rehydrated to Mg(Ni)-Al LDH during the Ni impregnation, which produced Mg(Ni,Al)O solid solution. Thus, highly dispersed and stable fine Ni particles were formed during reduction treatment. The PSC exhibited fuel conversion comparable to a pelletized catalyst material and, moreover, showed extremely high activity even with one hundredth Ni loading compared to that of the conventional Ni-zirconia cermet anode, when used in the reformer of biodiesel-fueled SOFC (Fig. 9) (Quang-Tuyen et al., 2015). Finally, a performance of electrolyte-supported cell connected with the PSC was evaluated in the feed of oleic-FAME, and stable operation was achieved. After testing for 60 h, coking was not observed in both SOFC anode and PSC.

The PSC is a flexible planar catalyst that can be well stacked on the anode of SOFC; an excellent catalytic performance was obtained in the reforming of hydrocarbon fuels at the operating temperature of the SOFC (Shiratori et al., 2015). Ni loading state in the PSC prepared, and the results of 5 ppm H_2S poisoning test for the dry reforming of CH_4 at 800 °C under GHSV = 3500 h^{-1} are shown in Table 7. The catalytic performance of PSC was considerably improved by the dispersion of Mg-Al LDH in the inorganic fiber network due to the formation of fine Ni particles by controlling Ni loading on SiO_2-Al_2O_3 ceramic fibers (Cf). The exchange of Mg^{2+} in the LDH for Ni^{2+} in aqueous solution was remarkably promoted by the lowering of the heat treatment temperature of the raw paper sheet before the Ni loading. However, the introduction of excess Ni^{2+} into the LDH structure caused an opposite effect enhancing carbon deposition. To realize actually the positive effect of LDH addition, the best conditions of the LDH/Cf ratio, the heat-treatment temperature of raw paper and the Ni^{2+} concentration in the impregnation solution must be determined.

In order to apply PSC in direct internal reforming SOFCs fueled by biogas, the tolerance of PSC to sulfur impurities (H_2S) in biogas must

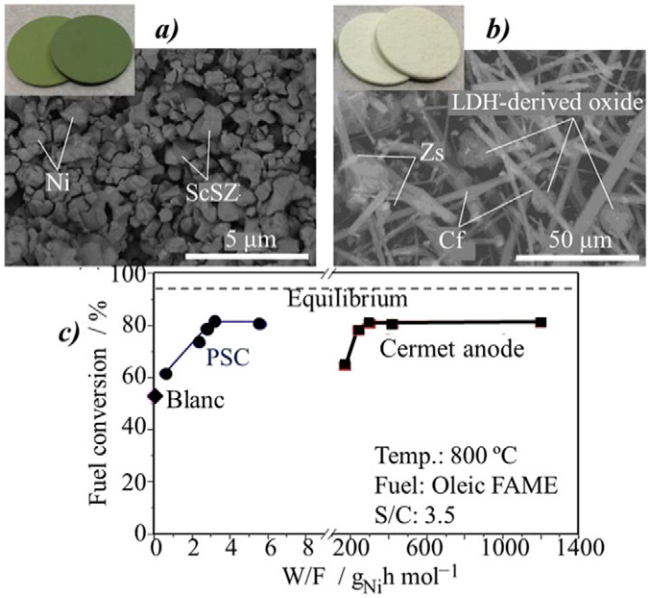

Fig. 9. FESEM images of (a) porous Ni-ScSZ cermet anode, (b) 3.2 mg Ni loaded PSC and (c) comparison of fuel conversion between PSC and porous Ni-ScSZ cermet anode for steam reforming of oleic-FAME (S/C = 3.5) at 800 °C (Quang-Tuyen et al., 2015, Elsevier).

be improved. In this work, Mg-Al LDH-dispersed inorganic fiber network was prepared by a paper-making process, and then impregnated with Ni. Thus prepared Ni-loaded Mg-Al LDH-dispersed PSC exhibited considerably higher tolerance to H_2S than that of LDH-free PSC.

5. Dynamic effects of LDH structure on catalytic behaviors

5.1. Anion entrapping effect in Mg-Al LDH interlayer

5.1.1. Pd-Cu/Mg(Al)O catalyst

It is necessary to reduce the nitrate (NO_3^-) intake of man because NO_3^- can pose a health risk. The advantage of the catalytic process is the fast and complete removal of NO_3^- and NO_2^- without any occurrence of waste water. For a commercial application of the catalytic NO_3^- reduction, the catalysts have to be optimized with regard to a high selectivity in the formation of N_2.

The Pd bimetallic catalysts, Pd-Sn, Pd-In and Pd-Cu, supported on carbon have been studied, in which NO_3^- reduction was inhibited strongly by NO_2^- (Lemaignen et al., 2002; Gauthard et al., 2003; Barrabés et al., 2006). To solve this limitation of reaction, use of Mg-Al LDH as the catalyst support was studied in the catalytic hydrogenation of NO_3^- (Palomares et al., 2003). Pd-Cu/Mg(Al)O catalyst enhanced NO_3^- removal in water; NO_3^- was incorporated into the interlayer space of Mg-Al LDH reconstituted and reduced to N_2 with H_2 catalyzed by Pd-Cu active species (Palomares et al., 2004).

Pd was impregnated on calcined Mg(Cu)-Al LDH prepared by coprecipitation (Palomares et al., 2004). The activity and selectivity of the catalyst increases, especially if the LDH is synthesized with copper in its structure. Metal composition of the catalyst was as follows: Pd 5.0 wt%, Cu 1.5 wt% and Mg/Al ratio was 4.0. The LDH structure of Pd-Cu/Mg(Al)O after coprecipitation was transferred to the ill-crystalline MgO-like structure after the calcination.

The reconstitution of the LDH phase in the material is attributed to the presence of NO_3^- located in the interlayer space compensating the positively charged layers, as was supported by measuring the nitrogen content of the reconstituted sample by elemental analysis: the value of 0.50% at the beginning gradually decreased to 0.03% at the end of the reaction for 200 min. In addition, the presence of NO_3^- in the LDH was confirmed by the intense band observed at 1384 cm^{-1} in the infrared spectrum of the material, that is typically assigned to the presence of NO_3^- groups (Xu and Zeng, 2001) and that is not observed when the calcined LDH was reconstituted with water without NO_3^-. These results can be explained by considering "memory effect" of calcined LDH structures, that when rehydrated recovers its positively charged layered structure forcing the NO_3^- anions present in the media to be located in the interlayer space compensating the positive charge.

NO_2^- appears as a primary and unstable product, which presents a maximum concentration at 85–90% of NO_3^- conversion. After this, it decreases and completely disappears after 120 min of reaction when using Pd-Cu/Mg(Al)O as catalyst. On the other hand, with Pd-Cu/Al_2O_3, the NO_2^- concentration does not go to zero. Moreover, the amount of NH_4^+ formed as a secondary product is about three times larger on Al_2O_3 than on Mg(Al)O. The results obtained here could be explained by considering the capacity of LDH to concentrate anions in the interlayer space. Although the surface area of the reconstituted LDH is very low, the NO_3^- are concentrated by ionic forces between the layers. Therefore, the NO_3^- are reduced by the neighboring Pd-Cu active sites to NO_2^-:

$$NO_3^- + H_2 \rightarrow NO_2^- + H_2O \quad (1)$$

Since this first reduction step does not involve any modification in the charge of the anions located in the interlayer space, the NO_2^- formed should remain in the interlayer space to compensate the positively charged LDH structure, and this will facilitate the reduction of NO_2^- to N_2:

$$2NO_2^- + 3H_2 \rightarrow N_2 + 2OH^- + 2H_2O \quad (2)$$

During the above reaction step, the electro-neutrality of the system is maintained by the OH^- anions produced during NO_2^- reduction. These will balance the LDH charge while the N_2 (or in less extension NH_4^+) formed will be easily released to the solution. This proposal is supported by the observed increment of the pH during the course of the reaction (from 10.6 to 11.2). The above catalytic behavior will diminish the problems related with diffusion limitations that affect the selectivity of the reaction. The OH^- ions located in between the HT layers can be exchanged in the presence of more NO_3^- anions (Cavani et al., 1991), and a new reaction cycle will start. Thus, a reaction scheme for the reduction of NO_3^- on Pd-Cu/Mg(Al)O catalysts is proposed in Scheme 6 (note that in this scheme, the position of the Pd and Cu species is only indicative that these centers are randomly distributed in the catalyst) (Palomares et al., 2004).

Table 7
Ni loading state in the PSCs prepared and the results of 5 ppm H_2S poisoning test for the dry reforming of CH_4 at 800 °C under GHSV = 3500 h^{-1} (Shiratori et al., 2015, Elsevier).

Name of PSC	Ni loading[a]/wt%	S_{BET} after reduction.[b]/m^2 g^{-1}	Ni_i specific S^c/m^2 g^{-1}	Ni particle size[c]/nm	Relative Ni S^d/—	Initial CH_4 conv./%	CH_4 conv. after 48 h H_2S poisoning/%	Relative steady-stte CH_4 conv./—
PSC-A	2.2	4.0	6.2	107	1	96	3.4	1
PSC-B	3.2	17.7	9.8	69	2.7	91	20	5.9
PSC-C	8.6	15.5	21	32	16.4	95	43	12.6

[a] Measured by ICP.
[b] S: specific surface area measured by BET method.
[c] S: specific surface area measured by CO pulse method.
[d] [S_{Ni} of a PSC]/[S_{Ni} of PSC-A].

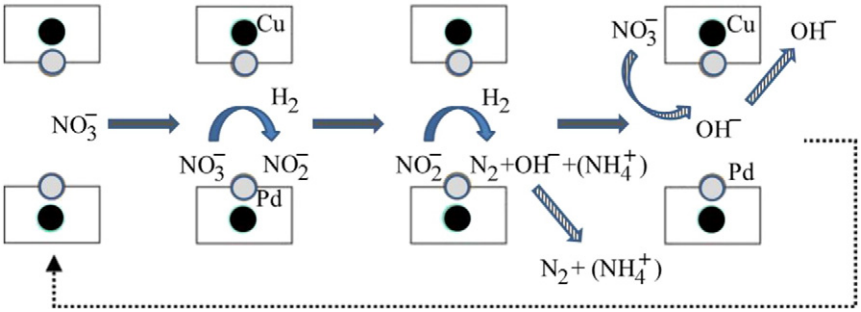

Scheme 6.

It was thus shown that the use of calcined LDH as support reduces the problems associated with mass transfer limitations observed on Pd-Cu/Al_2O_3, by introducing a new concept of active supports. In this case by taking advantage of "memory effect" of calcined LDH, the NO_3^- are forced to be located between the positively charged layers of the LDH and therefore close to the reductive active sites. The NO_3^- are reduced to NO_2^- that remain in the same position, and these are further reduced to N_2 or in a much lower extent to NH_3. These final compounds due to their inadequate charge are released to the solution, reducing the problems related with diffusion limitations that strongly affect the selectivity of the reaction.

5.1.2. Cu/Mg(Al)O catalyst

Ozone, due to its high oxidation and disinfection potential, has recently received much attention in water treatment technology (Kasprzyk-Hordern et al., 2003). Ozone is known to be a powerful oxidant, but it reacts slowly with some organic compounds such as inactivated aromatics, which results in the formation of carboxylic acids, and carbonyl compounds. Catalytic ozonation can improve the oxidation and degradation of organic contaminant compounds, especially small carboxylic acids, refractory compounds, those cannot be easily attacked by conventional oxidation processes.

Fe, Co, Ni or Cu containing Mg-Al LDH were calcined and tested for the ozonation of phenol and oxalic acid in aqueous solution, among which Cu/Mg(Al)O catalyst was the most effective (Shiraga et al., 2006). Mg(Al)O supported Cu oxide catalyst was prepared by co-precipitation of metal nitrates, followed by calcination at 400, 600, 850 and 1100 °C, and used as the catalyst. Loading amount of Cu was fixed at 8.1 wt.% after the calcination. The reaction was carried out using the catalyst and aqueous solution of phenol or oxalic acid in an O_3/O_2 mixed gas-flow at 20 °C.

In the oxidation of phenol, ozone was effective even in the absence of catalyst, but TOC removal was not completed without catalyst; the combination of ozone and Cu/Mg(Al)O catalyst was effective for the TOC removal. As by-product, oxalic acid was formed as major one together with small amount of maleic acid, hydroquinone and catechol. Considerable amount of oxalic acid was formed just after starting reaction but then was totally consumed within 120 min of the reaction with the $Cu_{0.23}/Mg_{2.77}$(Al)O (Shiraga et al., 2006). In the ozonation of oxalic acid over $Cu_{0.23}/Mg_{2.77}$(Al)O calcined at various temperatures, the highest activity was obtained over the catalyst calcined at 600 °C. Assuming that the reaction proceeds by a quasi-first order with respect to oxalic acid, the rate constant (k_1/min^{-1}) was calculated from the value of $ln(C/C_0)$ at the reaction time for 15 min and was plotted against the calcination temperature. The highest rate constant was obtained by the calcination at 600 °C (Fig. 10A).

XRD patterns of the $Cu_{0.23}/Mg_{2.77}$(Al)O catalyst clearly showed the reconstitution of LDH phase after the reaction. Intensity of the diffraction by basal plane (003) of LDH formed on $Cu_{0.23}Mg_{2.77}$(Al)O by the reconstitution was plotted against the calcination temperature and compared with the rate constant k_1 (Fig. 10A) (Shiraga et al., 2006). Both peak intensity and rate constant showed the maximum value at 600 °C; a good correlation was observed between the peak intensity and the rate constant, suggesting that the catalytic activity was enhanced by the reconstitution of LDH phase on the $Cu_{0.23}Mg_{2.77}$(Al)O catalysts.

The $Cu_{0.23}/Mg_{2.77}$(Al)O samples calcined at various temperatures were dipped in aqueous solution of oxalic acid and the quasi-first order rate constant (k_1'/min^{-1}) of Cu leaching was obtained (Fig. 10B). The values of k_1' were almost 10 times larger than those of k_1 and showed no clear peak with respect to the calcination temperature, suggesting no distinct correlation between the Cu leaching and the oxalic acid ozonation. The oxalic acid ozonation proceeded regardless of the amount of Cu dissolved, indicating the heterogeneous catalytic ozonation mechanism. It is considered that the ozonation of oxalic acid with the Cu catalyst proceeded via the formation of active oxygen species from ozone on the active Cu site, followed by the oxidative cleavage of C—C bond of oxalic acid by the active oxygen. Hydroxyl radicals were detected by ESR measurements in the catalytic ozonation and possibly worked as the active species on the catalyst surface to cleave oxidatively the C–C bond of oxalic acid to form carbon oxides (Shiraga et al., 2006).

The LDH reconstitution on the $Cu_{0.23}/Mg_{2.77}$(Al)O catalysts is possibly due to the presence of oxalate anions compensating the positively

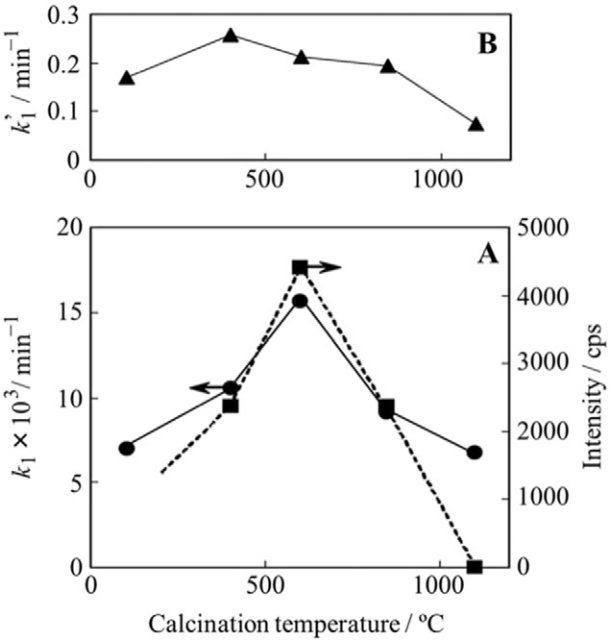

Fig. 10. Effect of the calcination temperature of $Cu_{0.23}Mg_{2.77}$(Al)O catalyst on activity and reconstitution of LDH (A) and Cu leaching (B). Catalyst, 0.4 g; oxalic acid, 3.2 mmol, water, 400 mL; reaction temperature, 20 °C; (A) O_3/O_2 mixed gas, 1.4 vol.% (200 mL h^{-1}); (B) O_2, 200 mL h^{-1}. ●, quasi-first order rate constant of oxalic acid consumption; ■, intensity of diffraction by basal planes (003) of HT reconstituted; ▲, quasi-first order rate constant of Cu leaching (Shiraga et al., 2006, Elsevier).

charged layers, which was observed in the infrared spectra of the material during the reaction. When the $Cu_{0.23}/Mg_{2.77}(Al)O$ catalyst was used in the reaction for 15 min, the bands around 3500 and 1650 cm^{-1} were intensified, suggesting that interlayer space was filled with water molecules and, at the same time, brucite phase was reconstituted. Moreover a new band at 1640 cm^{-1} and a shoulder at 1320 cm^{-1} appeared (Shiraga et al., 2006). It is likely that these absorption bands are ascribed to interlayer oxalate since these bands also appeared when the sample was dipped in aqueous solution of oxalic acid. This intercalation by oxalate anions can also be supported by the XRD observations. Interlayer distance was calculated assuming that the thickness of the brucite-like layer is 0.48 nm (Miyata, 1975). When the $Cu_{0.23}/Mg_{2.77}(Al)O(600)$ was dipped in distilled water, the basal interlayer spacing of LDH reconstituted was calculated as 0.757 nm, which is close to the value reported for Mg/Al LDH carbonate (Khan and O'Hare, 2002). After the reaction for 15 min, the basal spacing slightly increased to 0.778 nm. The sample prepared by being dipped in aqueous solution of oxalic acid as a reference showed the value of 0.782 nm. It was reported that the basal spacing was 0.960 nm for Mg–Al LDH oxalate (Traversa et al., 1992). It is therefore likely that the intercalation by oxalate anions was not completed in the present samples after the reaction or after the dipping in oxalic acid solution. This is partly due to the rapid decomposition of oxalate in interlayer space of the catalysts. Actually both absorption band around 1640 cm^{-1} and shoulder around 1320 cm^{-1} observed in the infrared spectra disappeared after the reaction for 240 min, suggesting that oxalate anions were totally consumed by the mineralization reaction with ozone (Shiraga et al., 2006).

Leaching of Cu, probably due to the chelation of metals by oxalic acid, was significantly observed at the beginning of the reaction. However the Cu leaching disappeared at the end of the reaction possibly due to the entire consumption of oxalic acid during the reaction. The best result of oxalic acid mineralization was observed over Cu/Mg(Al)O catalyst calcined at 600 °C, on which leaching of the metal was detected. Moreover, reconstitution of LDHs accelerated the mineralization of oxalic acid over the Cu/Mg(Al)O catalyst; oxalate anions were captured and decomposed in the reconstituted LDH interlayer space on the surface of the Cu/Mg(Al)O catalyst, resulting in a remarkable enhancement in the ozonation activity.

5.2. Effect of reversible change between Mg(Al)O and Mg-Al LDH

Hydrogen is forecast to become a major source of energy in future. H_2 production for polymer electrolyte fuel cell (PEFC) is a current world topic. Steam reforming of hydrocarbons, especially of CH_4, is the largest and generally the most economical way to make H_2. However, the H_2 production for PEFC requires enormously high efficiency taking into account that the reformer should be as compact as possible in the FC system on-board a vehicle or even in a stationary FC system. Catalytic conversion seems preferable and, moreover, the catalyst must work under extremely high space velocity, i.e., a sufficient amount of H_2 should be continuously produced in a small reformer and fed to the PEFC. For example, a personal car of 100 horse-power consumes 70 kW of electricity, which requires 70 $m^3\ h^{-1}$ of H_2 for driving, if the PEFC in *status quo* consumes 1 $m^3\ h^{-1}$ of H_2 for producing 1 kW. Thus, the catalyst for the on-board reformer should be exceptionally active compared with that for Fischer–Tropsch and methanol synthesis. Even in the stationary FC system for home, hospitals etc., a small reformer will be preferable and therefore the catalyst must be highly active. Recently supported precious metal catalysts have been frequently used to break this bottleneck (Ashcroft et al., 1990; Basile et al., 1998, 2000, 2001a; Tsyganok et al., 2004); the precious metals such as Rh and Ru are highly active and stable for the reforming reactions, although Pd did not show high activity (Basile et al., 2001b). However, the cost for the fabrication of fuel cell systems is also important, since a large amount of precious metals is required not only for the reformer but also for the fuel cell itself. Use of the cheaper metal, i.e., Ni, is desired for the catalyst preparation of the reformer. These restrictions inevitably require a new concept of catalyst preparation and further of its use in the reformer. Recently Basile et al. (2010) reviewed some specific features of Mg-Al LDH-derived Ni catalysts for partial oxidation or steam reforming of CH_4.

Ni/Mg(Al)O catalyst itself exhibited some prominent catalytic properties in the reforming reactions, but was not sustainable enough in the commercial use in the fuel cells. The sustainability as well as the remarkably high activity was required for the Ni catalyst in the reformer of fuel cells. Ni/Mg(Al)O catalyst was modified by doping with various noble metals, and evaluated by testing under the severe conditions such as DSS (daily start-up and shut-down) or steaming conditions.

5.2.1. Sustainability of Ni/Mg(Al)O catalysts

Supported Ni catalysts have been used in the reforming reactions of hydrocarbons and are conventionally prepared by wet impregnation of different supports. This method is not fully reproducible and may give rise to some inhomogeneity in the distribution of the metal on the surface. The fine Ni metal particles tend to sinter at high temperature, resulting in the catalyst deactivation. Use of the precursors containing Ni^{2+} ions in the crystal structure, which on further calcination and reduction, may result in the formation of highly dispersed and stable metal particles on the surface. This method was applied for the preparation of metal-supported catalyst by using $(Ca,Sr)TiO_3$ perovskite (Hayakawa et al., 1996; Takehira et al., 2002) and Mg-Al LDH (Takehira et al., 2002; Shishido et al., 2002a,b; Tsyganok et al., 2003; Takehira et al., 2003, 2005a) as the precursors. Bhattacharyya et al. (1998) reported that LDH-derived Ni catalysts showed better behavior compared to Ni catalyst prepared by impregnation. High surface area Ni/Mg/Al mixed oxides obtained by calcination of LDH precursor exhibit unusual pore size distribution and low reducibility of the Ni^{2+} ions (Fornasari et al., 1995). Ni/Mg(Al)O catalysts prepared by calcination of Mg(Ni)-Al LDH followed by reduction were successfully applied for the partial oxidation (Hayakawa et al., 1996; Shishido et al., 2002a; Takehira et al., 2002,; Tsyganok et al., 2004;), steam reforming (Shishido et al., 2002a; Takehira et al., 2003) and dry reforming (Shishido et al., 2001; Tsyganok et al., 2004) of CH_4. Although Rh can catalyze direct partial oxidation of CH_4 to CO and $2H_2$ under specifically diluted oxygen supplying conditions at relatively low temperature on Rh catalyst (Hayakawa et al., 1994; Sato et al., 1995), generally CH_4 oxidation proceeds via complete oxidation (4), followed by steam reforming (5) and dry reforming (6) to produce CO and H_2 at high temperature (7). Ni/Mg(Al)O catalyst exhibited high and stable activity in all these reactions. Such

$$CH_4 + 2O_2 \rightarrow CO_2 + 2H_2O\ \Delta H^0_{298K} = -801 kJmol^{-1} \quad (4)$$

$$CH_4 + H_2O \rightarrow CO + 3H_2\ \Delta H^0_{298K} = +206 kJmol^{-1} \quad (5)$$

$$CH_4 + CO_2 \rightarrow 2CO + 2H_2\ \Delta H^0_{298K} = +247 kJmol^{-1} \quad (6)$$

$$CH_4 + 1/2O_2 \rightarrow CO + 2H_2\ \Delta H^0_{298K} = -36 kJmol^{-1} \quad (7)$$

high catalytic performance is uniquely due to the stable and highly dispersed Ni metal particles on the catalysts (Takehira, 2002, Takehira et al., 2004b; Ohi et al., 2006). The Ni catalysts, with varying (Mg + Ni)/Al atomic ratio and constant Ni loading, were prepared from LDH precursors and the properties are listed in Table 8 together with those prepared by impregnation method as references (Takehira et al., 2004b). Both the BET surface areas and the Ni dispersions were higher for the LDH-derived catalysts compared with all *imp*-catalysts and were the highest on $Ni_{0.5}/Mg_{2.5}(Al)O$. The order of the Ni dispersion determined by H_2 pulse method well coresponded to those of Ni metal particle size observed by both XRD and TEM except the case of *imp*-Ni/MgO, in wnich Ni was soluble in MgO lattice to form solid solutions (Parmaliana et al., 1990).

Table 8
Metal composition, surface area, and Ni dispersion of the catalysts (Takehira et al., 2004b, Elsevier).

Catalyst[a]	Atomic ratio (Ni + Mg)/Al	Ni-loading/wt%[b]	BET surface[c] area/m^2 g_{cat}^{-1}	H_2 consumption[d]/μmol g_{cat}^{-1}	Ni dispersion[e]/%	Ni particle size/nm	
						XRD	TEM
Ni0.26/Mg0.74(Al)O	1	16.7	124.6	253.5	17.8	7.8	7.0
Ni0.50/Mg2.50(Al)O	3	15.8	178.6	265.1	19.7	7.0	6.1
Ni0.73/Mg4.27(Al)O	5	17.8	125.1	203.5	13.4	8.2	12.1
imp-Ni0.5/Mg3(Al)O		16.3	95.4	221.5	16.0	8.5	9.8
imp-Ni/α-Al2O3		16.3	8.2	48.6	3.5	31.1	35.5
imp-Ni/γ-Al2O3		16.3	106.3	122.9	8.9	11.4	13.0
imp-Ni/MgO		16.3	17.2	13.8	1.0	–	8.2

[a] Reduced at 800 °C for 0.5 h in H_2/N_2 (5/20 mL min^{-1}).
[b] Determined by ICP analysis for the catalysts after calcination at 850 °C for 5 h and calculated for *imp*-catalysts.
[c] Calcined at 650 °C for 14 h and at 850 °C for 5 h.
[d] Determined by H_2 pulse method.
[e] Impregnated in acetone solution of Ni^{2+} nitrate.

Aiming at the commercial use, a catalyst-life test was carried out for the $Ni_{0.5}/Mg_{2.5}(Al)O$ (Fig. 11) (Takehira et al., 2003). A commercial catalyst FCR (12 wt% Ni/α-Al_2O_3) supplied from Süd Chemie Japan Inc. was used as a reference. $Ni_{0.5}/Mg_{2.5}(Al)O$ was pressed at 22 MPa cm^{-2} and sieved to particles of size 0.71–1.0 mm, while FCR was used as particles of size 2.0–4.0 mm in diameter. The steam reforming reactions over both catalysts were carried out at 800 °C and 0.3 MPa with a mixture of CH_4 and H_2O (1/1.6 vol. ratio) using 20 cm^3 of the catalysts at a space velocity of 2500 h^{-1}. During the life-test, the activity was checked by increasing the space velocity to 10,000 h^{-1} in order to detect any small decline in the activity. The reaction temperature was controlled at the outer wall of the reactor at 800 °C, but that at catalyst bed decreased to 740 and 660 °C at space velocities of 2500 and 10,000 h^{-1}, respectively, due to the endothermic reaction (5). Both at 660 and at 740 °C, i.e., both at space velocities of 10,000 and 2500 h^{-1}, $Ni_{0.5}/Mg_{2.5}(Al)O$ showed high CH_4 conversions following thermodynamic equilibrium, while FCR showed low CH_4 conversions as well as slow decline in the activity.

The sustainability of $Ni_{0.5}/Mg_{2.5}(Al)O$ catalyst was also confirmed under severe oxidative conditions, i.e., in partial oxidation of CH_4 in a mixed gas flow of CH_4, O_2, and N_2 (1/2/1 vol. ratio) (Takehira et al., 2004b), at 800 °C. $Ni_{0.5}/Mg_{2.5}(Al)O$ catalyst exhibited enough high CH_4 conversion even at the high space velocity (9×10^5 mL h^{-1} g_{cat}^{-1}), exceeding the value obtained over 1 wt% Rh/MgO (Ruckenstein and Wang, 2000). Ni species on $Ni_{0.5}/Mg_{2.5}(Al)O$ catalyst were stable even under the presence of O_2, while other Ni catalysts prepared by the impregnation, including FCR, quickly lost activity due to the surface oxidation of Ni particles. Moreover, a heat accumulation during the CH_4 oxidation was the lowest over the $Ni_{0.5}/Mg_{2.5}(Al)O$ catalyst among the catalysts tested. This clearly suggests that the heat of exothermic CH_4 combustion (4) could be quickly consumed by the following endothermic CH_4 reforming by H_2O (5) and CO_2 (6) over the $Ni_{0.5}/Mg_{2.5}(Al)O$ catalyst. Actually $Ni_{0.5}/Mg_{2.5}(Al)O$ also showed a high and stable activity for the autothermal reforming of CH_4 under the copresence of O_2 and H_2O (Takehira et al., 2004b). Thus, $Ni_{0.5}/Mg_{2.5}(Al)O$ catalyst is a hopeful candidate for the reforming of CH_4 which can feed H_2 to fuel cell economically, since the actual reformer is frequently suffering from severe oxidative conditions. The high and sustainable activity of $Ni_{0.5}/Mg_{2.5}(Al)O$ is possibly due to regenerative activity, i.e., occurring of redispersion of fine Ni metal particles during these reforming reactions as explained in the next section.

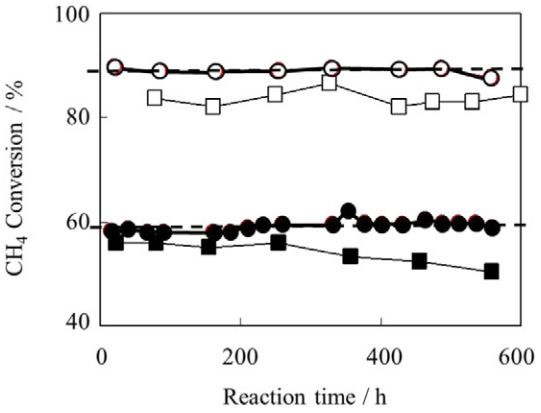

Fig. 11. Catalyst life test in steam reforming of CH_4: ○: $Ni_{0.5}/Mg_{2.5}(Al)O$ and □: FCR (12 wt Ni/α-Al_2O_3) at 740 °C and SV = 2500 h^{-1}; ●: $Ni_{0.5}/Mg_{2.5}(Al)O$ and ■: FCR (12 wt% Ni/α-Al_2O_3) at 660 °C and SV = 10.000 h^{-1}; ▪▪▪▪▪: Thermodynamic equilibrium; CH_4/H_2O = 1/1.6; outer wall temperature, 800 °C; catalyst, 17.3 g (Takehira et al., 2003, the Royal Society of Chemistry).

5.2.2. DSS sustainability of noble metal doped Ni/Mg(Al)O catalyst

In Japan, the home-use PEFC is operated in the DSS (daily start-up and shut-down) mode to keep the safety. The reformer is frequently started up (daytime) and shut down (nighttime), and during the shut-down operation the reformer is purged with steam containing gas. Ni/Mg(Al)O catalysts of varying (Mg + Ni)/Al ratios were tested in the DSS operation mode (Fig. 12A) (Ohi et al., 2006). After pre-reduction of catalyst (50 mg) under H_2/N_2 (5/25 mL min^{-1}) mixed gas at 900 °C for 30 min, the reaction was started at 700 °C. After the reaction for 90 min at 700 °C, the reactor was cooled to 200 °C under purging with steam gas: H_2O/N_2 (100/25 ml min^{-1}). After the reactor temperature was maintained at 200 °C for 30 min, the temperature was increased to 700 °C still under purging conditions. The reaction was again started, carried out at 700 °C for 90 min, and followed by the next purging; the cycle reaction was repeated four times to perform the DSS-like operation. Use of air, O_2/N_2 (40/10 mL min^{-1}), as the purge gas resulted in a quick deactivation of all Ni loaded catalysts due to the oxidation of Ni metal on the catalyst surface. Spent gas, $CO_2/H_2O/N_2$ (40/15/25 mL min^{-1}), was the most inert for the DSS operation causing no significant deactivation of Ni loaded catalysts. Typical results of the DSS test operation with $Ni_{0.5}/Mg_{2.5}(Al)O$ and 16.3 wt% Ni/γ-Al_2O_3 catalyst under steam purge are shown in Fig. 12B; the former was deactivated substantially at the first steam purge and totally at the second steam purge, whereas the latter was totally deactivated at the first steam purge. The deactivation took place mainly via the oxidation of Ni metal by steam during the DSS operation, where MgO was hydrated by steam to form $Mg(OH)_2$ on the catalyst surface, which may assist the oxidation of Ni metal on Mg(Al)O periclase (Ohi et al., 2006).

The sustainability of $Ni_{0.5}/Mg_{2.5}(Al)O$ catalyst in DSS operation was remarkably improved by doping small amount of noble metals, Ru (Miyata et al., 2007; Li et al., 2007a), Rh (Miyata et al., 2006; Li et al., 2007c) and Pt (Miyata et al., 2006; Li et al., 2008), by utilizing reconstitution. $Mg_{2.5}(Ni_{0.5})$-Al LDH was prepared by coprecipitation and

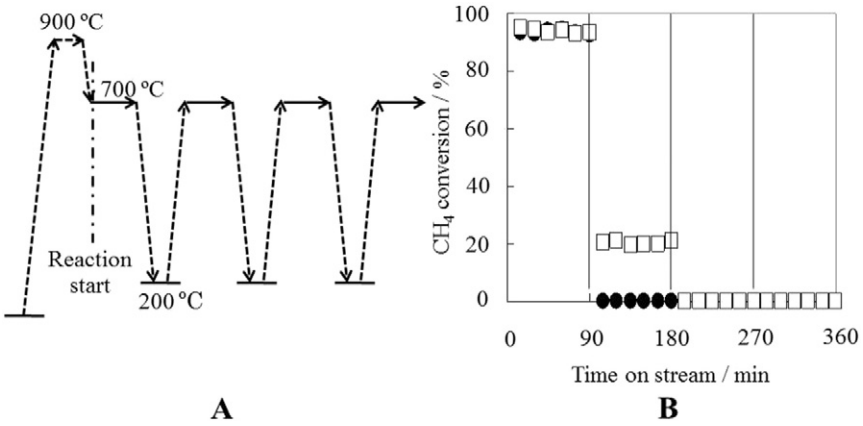

Fig. 12. DSS operation mode (A) and test results (B) with $Ni_{0.5}/Mg_{2.5}(Al)O$ (□) and *imp*-16.3 wt% $Ni/\gamma\text{-}Al_2O_3$ (●) under steam purge (Ohi et al., 2006, Elsevier).

calcined to form $Mg_{2.5}(Al,Ni_{0.5})O$ periclase. When the powders of the periclase were dipped in an aqueous solution of noble metal nitrates, LDH was reconstituted on the surface of $Mg_{2.5}(Al,Ni_{0.5})O$ particles, resulting in the formation of highly dispersed noble metal-Ni supported catalysts after the calcination followed by the reduction. The doping of small amount of noble metal (0.1 wt% of Pt, Rh or Ru) on $Ni_{0.5}/Mg_{2.5}(Al)O$ caused a decrease in the reduction temperature of Ni^{2+} in $Mg_{2.5}(Al,Ni_{0.5})O$ periclase as well as an increase in the amount of H_2 uptake on the Ni^0 over the $Ni/Mg_{2.5}(Al)O$ catalyst, indicating an easy Ni reduction as well as an increase in Ni dispersion (Table 9) (Miyata et al., 2006, 2007; Shiraga et al., 2007; Li et al., 2008).

The LDH reconstitution during the noble metal impregnation was confirmed by the XRD observations (Miyata et al., 2007). Mg(Ni)-Al LDH was reconstituted together with $Mg(OH)_2$ brucite, since MgO reacts very easily even with moisture in the air, especially at low coordination atomic site, to form $Mg(OH)_2$ brucite (Eun et al., 2003). The formation of $Mg(OH)_2$ implies segregation of MgO from periclase, i.e., destruction of original periclase structure. However, the formation of $Mg(OH)_2$ was suppressed by shortening the dipping time or by decreasing the amount of aqueous solution of noble metal. The Mg(Ni,Al)O periclase phase formed together with trace amount of $Mg(Ni)Al_2O_4$ spinel after the calcination at 900 °C for 5 h. The Ni metal reflections appeared after the reduction of the calcined sample at 900 °C for 1 h and very noticeably remained even after the 4th cycle DSS operation.

Temperature Programmed Reduction (TPR) profile of the noble metal, Ru, Rh or Pt, doped Ni/Mg(Al)O catalyst showed a decrease in the reduction temperature of Ni^{2+} with increasing the dope amount (Miyata et al., 2006, 2007; Shiraga et al., 2007; Li et al., 2008). In the absence of noble metal, a single and strong peak appeared at 895 °C for $Ni_{0.5}/Mg_{2.5}(Al)O$ catalyst. This reduction peak shifted toward lower temperature by the doping of noble metal; the shift was the most significant for Ru-doping, followed by Rh- and Pt-doping. The decrease in the reduction temperature of Ni suggests a formation of alloy between noble metals and nickel. The reduction degree of Ni was as follows: $Ni_{0.5}/Mg_{2.5}(Al)O$ (88%) was close to the value (87%) reported for 1.9 wt% Mg(Ni)-Al LDH-derived catalyst (Olafsen et al., 2005) and was lower than those observed for Ni/Al_2O_3 (106%) and Ni/TiO_2 (97%) catalysts prepared by incipient wetness method (Miyazawa et al., 2006). This is certainly due to the fact that a part of Ni was still incorporated as Ni^{2+} in Mg(Al,Ni)O periclase solid solutions even after the reduction (Olafsen et al., 2005). Noble metal doping of even 0.05 wt% induced a significant increase in the H_2 uptake, while a decrease in the reduction degree, on the $Ni_{0.5}/Mg_{2.5}(Al)O$ catalyst; this may be due to an appearance of strong synergy between Ni metal and noble metal.

When Ru-, Rh- or Pt-$Ni_{0.5}/Mg_{2.5}(Al)O$ catalyst was tested for the DSS steam reforming of CH_4 under steam purging, the deactivation due to the Ni metal oxidation by steam was effectively suppressed by hydrogen spillover from noble metal to Ni. In the case of Ru–doping, 0.01 wt% was not sufficient; the activity was quickly lost even after the first steam purging and Ni oxidation simultaneously took place on the catalyst surface (Fig. 13) (Li et al., 2007a). The doping above 0.05 wt% stabilized the catalytic activity. With increasing Ru doping, the activity was more efficiently stabilized; more intensive Ni metal reflections were observed in the XRD patterns of the catalysts after the DSS operation.

All Ru, Rh and Pt were effective for enhancing the stability of the $Ni_{0.5}/Mg_{2.5}(Al)O$ catalyst even with small doping of 0.05 wt% in the DSS steam reforming of CH_4 (Miyata et al., 2006, 2007; Li et al., 2007a, 2008). All Ru, Rh and Pt alone were not active enough even with the loading of 0.1 wt% on $Mg_3(Al)O$, indicating that noble metals worked for stabilizing the activity of the $Ni_{0.5}/Mg_{2.5}(Al)O$ catalyst. It is noteworthy that only 0.05 wt% of all of Ru-, Rh- and Pt-doping was enough to suppress effectively the deactivation of Ni (16.0 wt%) during the DSS steam reforming of CH_4 (Miyata et al., 2006, 2007; Li et al., 2007a, 2008). All Ru-, Rh-, and Pt-$Ni_{0.5}/Mg_{2.5}(Al)O$ catalysts exhibited self-regenerative activity during steam-purged DSS stem reforming of CH_4. On Ru-$Ni_{0.5}/Mg_{2.5}(Al)O$ (Fig. 13), CH_4 conversion decreased slightly just after the steam purge, and, moreover, the decrease was enhanced

Table 9
Surface area, Ni dispersion and Ni particle size of noble metal doped Ni/Mg(Al)O catalysts (Miyata et al., 2006, 2007; Shiraga et al., 2007; Li et al., 2008, Elsevier).

Catalyst	BET surface area/$m^2\ g_{cat}^{-1}$	H_2 uptake[a]/μmol g_{cat}^{-1}	Ni dispersion[a]/%	Ni particle size/nm	
				XRD	H_2 uptake[a]
$Ni_{0.5}/Mg_{2.5}(Al)O$	158.0	120.7	13.1	6.9	7.4
imp-16.3wt%$Ni/\gamma\text{-}Al_2O_3$	106.3	74.4	6.5	10.0	14.9
0.10wt%Ru-$Ni_{0.5}/Mg_{2.5}(Al)O$	146.7	221.9	24.0	5.2	4.0
0.10wt%Rh-$Ni_{0.5}/Mg_{2.5}(Al)O$	148.4	184.0	19.9	5.7	4.9
0.10wt%Pt-$Ni_{0.5}/Mg_{2.5}(Al)O$	134.9	225.3	24.4	5.5	4.0
0.50wt%Ru-$Ni_{0.5}/Mg_{2.5}(Al)O$	148.0	261.4	28.3	5.0	3.4

[a] Reduced at 900 °C for 1 h in H_2/N_2 (5/25 mL min^{-1}) mixed gas and used for the H_2 pulse measurements.

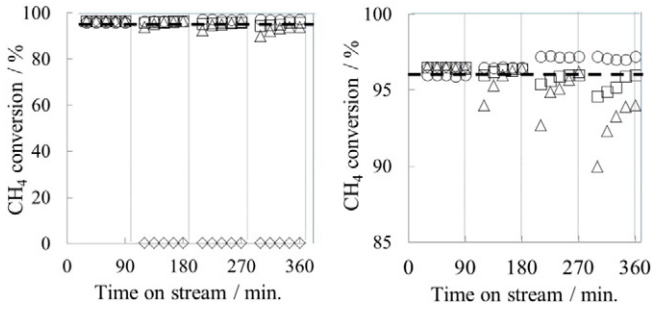

Fig. 13. DSS test results with 0.50 wt% Ru-$Ni_{0.5}/Mg_{2.5}$(Al)O (○), 0.10 wt% Ru—$Ni_{0.5}/Mg_{2.5}$(Al)O (□), 0.05 wt% Ru-$Ni_{0.5}/Mg_{2.5}$(Al)O (△) and 0.01 wt% Ru-$Ni_{0.5}/Mg_{2.5}$(Al)O (◇); ▪▪▪▪▪▪: Thermodynamic equilibrium. $CH_4/H_2O/N_2$ = 50/100/25 mL min^{-1}; 700 °C; catalyst, 50 mg (Li et al., 2007a, Elsevier).

with decreasing Ru doping and was magnified by repeating the steam purge. The decreased CH_4 conversion was due to the oxidation of surface Ni metal into Ni^{2+} in Mg(Ni,Al)O periclase. This indicates that Ni was reversibly reduced and oxidized during the DSS operation; a part of active Ni^0 was oxidized to Ni^{2+} by steam purge, whereas the Ni^{2+} was re-reduced to Ni^0 by hydrogen spillover from Ru or Ni-Ru alloy during the reaction. On the other noble metal-doped Ni/Mg(Al)O catalysts, the same mechanism worked, resulting in the self-regenerative activity (Li et al., 2007a,b,c, 2008).

5.2.3. Self-activation of noble metal doped Ni/Mg(Al)O catalyst

When the supported Ni catalysts are used in the steam reforming of CH_4, Rh- and Pt-doped Ni/Mg(Al)O catalysts were activated without reduction pretreatment (Li et al., 2008). After the catalyst was loaded in the reactor, the temperature was increased under N_2 gas flow from room temperature to 700 °C. When the temperature of the catalyst bed reached 700 °C, the reaction was started by switching the gas flow from N_2 gas to the $CH_4/H_2O/N_2$ mixed gas. In the absence of noble metal, $Ni_{0.5}/Mg_{2.5}$(Al)O catalyst as a control did not show any CH_4 conversion. 0.05 ~ 0.50 wt% Pt- and 0.10 ~ 0.50 wt% Rh-doped $Ni_{0.5}/Mg_{2.5}$(Al)O catalysts exhibited CH_4 conversion at a few min. after starting the reaction, i.e., self-activation occurred without reduction pretreatment, whereas Ru-$Ni_{0.5}/Mg_{2.5}$(Al)O_x catalyst showed no activity even with 0.50 wt% Ru-doping. The activity of Pt-$Ni_{0.5}/Mg_{2.5}$(Al)O catalyst was the highest, followed by Rh-$Ni_{0.5}/Mg_{2.5}$(Al)O catalysts. On all the catalysts, the selectivity to hydrogen was above 95% throughout the reaction, indicating that the steam reforming of CH_4 proceeded.

The ability of noble metals inducing self-activation was in the order of Pt > Rh ≫ Ru, possibly depending on the CH_4 dissociation, or C-H activation, activity of the metal. A theoretical study of the C — H activation was conducted by calculating the total dissociation energy, D_{tot}, for $CH_{4,s}$ $C_s + 4H_s$ as a realistic measure for the activity of the metal in CH_4 dissociation. The total dissociation is shown to be quite exothermic on Rh (−0.7 eV); it is slightly endothermic on Ru (0.01 eV) and Ir (0.3 eV), and it is rather endothermic on Pd and Pt (~1 eV). This indicates that the total dissociation of CH_4 on Rh is thermodynamically the most favorable among the transition metals. The D_{tot} values vary in the order: Rh < Ru < Ir < Pt < Pd (Liao and Zhang, 1998). On the other hand, in the presence of adsorbed oxygen, oxygen promotes CH_4 dissociation on Pt, whereas no such effect is observed on the other transition metals (Au et al., 1999). In the presence of adsorbed oxygen, in addition to the direct dissociation of CH_4 on bare metal surfaces, we may consider the following reactions:

$$CH_{x,s} + O_s \rightarrow CH_{x-1,s} + OH_s \; (x = 4, 3, 2, 1) \quad (8)$$

Because the H atom binds more strongly with O_s than with the bare metal, the CH_4 dissociation reactions in the presence of chemisorbed oxygen, i.e., O_s, have lower reaction energies due to hydroxyl formation (Au and Wang, 1997; Au et al., 1998). The O_s species increases adsorption energies of H on Pt, but decreases those on the other transition metals. Therefore, O_s promotes CH_4 dissociation on Pt, but does not promote it on the other transition metals. In fact, in the partial oxidation of CH_4 over Ru-, Rh-, and Pt-$Ni_{0.5}/Mg_{2.5}$(Al)O, Pt doping was the most effective for self-activation; even the material with 0.05 wt% doping exhibited reforming activity and produced H_2 with high selectivity without induction period (Li et al., 2007c, 2008). The activity order of noble metals for the self-activation was Pt > Rh ≫ Ru; the effect of "adsorbed oxygen species" was clearly confirmed. The same order was obtained also in steam reforming of CH_4 (Li et al., 2007c); steam produced plenty of OH_s on the MgO surface, because $Mg(OH)_2$ is thermodynamically stable compared with MgO under steam atmosphere (Eun et al., 2003). MgO reacted even with moisture in air to form $Mg(OH)_2$ brucite; MgO surface was thus covered by OH_s and further the OH_s species migrated from MgO to Pt metal surface and possibly formed Pt-OH species. One may consider that such OH_s can also promote CH_4 dissociation instead of O_s on Pt. Noble metals as co-catalysts dissociate C — H bond of hydrocarbons to produce H atoms, which in turn migrate to Mg(Ni,Al)O periclase surface by spillover and reduce Ni^{2+} to Ni^0. As a result, metallic Ni species was formed on the catalysts and catalyzed steam reforming of CH_4. Actually all the catalysts self-activated exhibited the diffraction lines of Ni metal in the XRD patterns. Ru containing catalysts such as RUA (commercial catalyst supplied from Süd-Chemie Catalysts Japan Inc., 2 wt% Ru/α-Al_2O_3) and Ru-Ni/Mg(Al)O frequently showed a deactivation during steam- or air-purged DSS steam reforming of CH_4 (Li et al., 2007a), suggesting that the nature of Ru differs from Rh and Pt, and that Ru suffers from the surface deterioration by steam and oxygen.

5.2.4. Surface fine structure of noble metal-doped Ni/Mg(Al)O catalyst

Surface fine structure of the active Ni metal particles investigated by EXAFS and TPR explained the mechanism of self-regeneration of noble metal-doped Ni/Mg(Al)O catalysts (Li et al., 2007a,b, 2008).

The FT k^3-weighted Ru *K*-edge EXAFS spectra of the 0.50 wt% Ru-$Ni_{0.5}/Mg_{2.5}$(Al)O catalyst showed a peak at 0.208 nm after reduction (Li et al., 2007a), that was smaller than the distance of the Ru–Ru bonding (0.226 nm) (Hosokawa et al., 2006), suggesting that the Ru atom bonded mainly to the Ni atom to form Ru-Ni alloy. The 0.50 wt% Rh-$Ni_{0.5}/Mg_{2.5}$(Al)O catalyst after the reduction, showed a peak at 0.220 nm assigned to Rh–Ni bonding, and the absence of Rh–Rh bonding (0.245 nm) (Nagaoka et al., 2005; Mukainakano et al., 2007), indicating the formation of Rh–Ni bonding in Ni-Rh alloy particles. Further, the FT k^3-wighted Pt L_3-edge EXAFS spectra of 0.50 wt% Pt-$Ni_{0.5}/Mg_{2.5}$(Al)O exhibited a peak at 0.225 nm after reduction that was assigned to the Pt–Ni bond.

The curve-fitting results of Ru and Rh *K*-edge and Pt L_3 edge EXAFS for the Ru-Ni, Rh-Ni and the Pt-Ni system, respectively, were discussed (Table 10) (Li et al., 2007a,b, 2008). After the reduction, the total coordination number (C.N.) was much smaller for Ru-Ni ~ 3.5 (Li et al., 2007a), Rh-Ni ~ 5.0 (Li et al., 2007b) and Pt-Ni ~ 6.8 (Li et al., 2008), compared with the values obtained for Ru, Rh and Pt foil (12), respectively, indicating each noble metal was coordinated by Ni. Moreover, the Ru–Ni bonding was more abundant as a main shell compared with that of Ru–Ru bonding, judging from the spectrum after reduction. This strongly indicates that the Ru was located in the surface layer of finely dispersed Ni metal particles after reduction. Similarly, the Rh–Ni and Pt–Ni bondings were also abundant compared with Rh-Rh and Pt-Pt bondings in the spectra, respectively, indicating that Rh and Pt were enriched in the surface layer of the Ni metal particles.

The C.N. was the highest for Pt-Ni, followed by Rh–Ni and Ru-Ni bondings (Table 10). This may be due to the difference in the structure of each ex-catalyst before calcination, i.e., Rh^{3+} (ionic radius: 0.068 nm) can replace the Al^{3+} (ionic radius: 0.051 nm) site (Basile et al., 1998), whereas Ru^{4+}, though its ionic radius is 0.067 nm, cannot replace the

Table 10
Curve fitting results of Ru and Rh *K*-edge and Pt L_3 edge EXAFS after calcination and reduction[a] (Li et al., 2007a, 2007b, 2008, Elsevier).

Sample	Shells	C.N.	*R*/Å	σ/Å	ΔE_0/eV	R_f/%
(0.50wt%Ru-$Ni_{0.5}/Mg_{2.5}$(Al)O) After reduction	Ru–Ni	3.5 ± 0.8	2.46 ± 0.018	0.098 ± 0.022	−9.1 ± 3.3	2.3
(0.50wt%Rh-$Ni_{0.5}/Mg_{2.5}$(Al)O) After reduction	Rh–Ni	5.0 ± 0.4	2.57 ± 0.007	0.072 ± 0.011	3.8 ± 0.9	1.1
(0.50wt%Pt-$Ni_{0.5}/Mg_{2.5}$(Al)O) After reduction	Pt–Ni	6.8 ± 1.1	2.53 ± 0.01	0.074 ± 0.01	9.4 ± 2.2	3.4
After reduction[b]	Pt–Ni	6.7 ± 1.1	2.52 ± 0.01	0.090 ± 0.01	1.9 ± 2.3	19.5
After reduction[c]	Pt–Ni	6.8 ± 1.1	2.53 ± 0.01	0.073 ± 0.01	9.8 ± 2.2	8.5
After reduction[d]	Pt–Ni	7.7 ± 1.2	2.54 ± 0.01	0.081 ± 0.01	9.8 ± 2.2	5.4

[a] C.N., coordination number; *R*, bond length (Å); ΔE_0, difference in the origin of photoelectron energy between the reference and the sample; σ, Debye-Waller factor (Å); R_f, residual factor.
[b] Followed by steaming.
[c] Followed by DSS steam reforming of CH_4.
[d] Followed by steaming and DSS steam reforming of CH_4.

Al^{3+} site (Basile et al., 2000), in the Mg(Ni)-Al LDH. It is likely that Rh^{3+} ions were located more closely to Ni^{2+} in the LDH than Ru^{4+} ions which existed in the amorphous phase separately from the LDH. Such difference in the location between Rh^{3+} and Ru^{4+} ions in the Mg-Al LDH could reasonably provoke the difference in the coordination structure of alloy finally formed on the catalyst particles. Although no information was reported, Pt may be incorporated in Mg(Ni)-Al LDH considering the ionic radius 0.065 nm of Pt^{4+} compared with 0.066 and 0.069 nm of Mg^{2+} and Ni^{2+} (Shannon, 1976), respectively. This indicates that Pt was more deeply incorporated into Ni particles on 0.50 wt% Pt-$Ni_{0.5}/Mg_{2.5}$(Al)O than Ru and Rh on 0.50 wt% Ru- and Rh-$Ni_{0.5}/Mg_{2.5}$(Al)O, respectively.

5.2.5. Mechanism of self-regeneration

The self-regenerative activity was confirmed for 0.50 wt%Pt-$Ni_{0.5}/Mg_{2.5}$(Al)O by EXAFS (Table 10). Shu et al. (2008) reported that the surfaces of Pt–Ni bimetallic catalysts prepared by sequential impregnations of Pt and Ni on γ-Al_2O_3 were always Pt-terminated with the Pt/Ni ratio of 1/1, regardless of the sequential order, i.e., first with Pt and then with Ni, or vice versa. This is due to the segregation of Pt to the surface during the hydrogen reduction, as predicted by means of density functional theory (DFT) modeling and, moreover, verified experimentally by using Auger electron spectroscopy and higher resolution electron energy loss spectroscopy on single crystal Ni/Pt(111) surfaces. Contrarily, B. Li et al. (2007) reported that sequential impregnation, i.e., first Ni followed by Pt, exhibited better catalytic performances than co-impregnation methods in oxidative steam reforming of CH_4. In the present work, Pt-Ni/Mg(Al)O catalysts were prepared by Pt impregnation on Mg(Ni,Al)O periclase, suggesting that Ni particles were originally enriched with Pt in the surface layer. In fact, no significant change was observed in the curve fitting results of Pt L_3-edge EXAFS of 0.50 wt% Pt-$Ni_{0.5}/Mg_{2.5}$(Al)O during the reaction, i.e., reduced, reduced-steamed, reduced-DSS and reduced-steamed-DSS. Only the sample after reduction followed by steaming exhibited a little smaller coordination number, a smaller ΔE_0 and a greater R_f value compared with the other samples (Table 10), suggesting that the Pt–Ni bimetallic structure was slightly distorted due to heavy Ni sintering after steaming. One should notice that the original Pt–Ni bimetallic structure was recovered by DSS steam reforming of CH_4 even after such heavy sintering (vide infra).

Pt-doping was the most effective for the self-activation and both Rh- and Pt-doping was effective for the self-regeneration on noble metal-doped Ni/Mg(Al)O catalyst in CH_4 reforming. Pt may be the best candidate as the noble metal for the commercial use of the present catalyst system, since Rh is still expensive compared with Pt. It must be emphasized that trace Pt-doped Ni/Mg(Al)O exhibited sustainable activity under oxidative conditions, i.e., not only in steam-oxygen mixed purging DSS steam reforming of CH_4 but also in autothermal steam reforming of CH_4. Moreover this catalyst was self-activated and exhibited self-regenerative activity as well as high TOF values in DSS steam reforming of CH_4 (vide infra). The self-activation was performed by hydrogen spillover from Pt and, moreover, the self-regeneration was achieved by the continuous rebirth of finely dispersed active Ni metal particles, which is assisted by reversible oxidation-reduction between Ni^0 and Ni^{2+} on/in Mg(Ni,Al)O periclase (Fig. 14). In this process, sintered Ni metal particles was oxidatively incorporated into Mg(Al)O periclase in the presence of steam, while Ni^{2+} in Mg(Ni^{2+},Al)O was reduced by H spilt over to form fine Ni metal particles. It must be noticed that an oxidative incorporation of Ni^0 into Mg(Ni^{2+},Al)O may proceed via Mg(Ni^{2+})-Al LDH intermediate by rehydration on the surface of Mg(Al)O periclase. MgO reacted even with moisture in air, especially at low coordination atomic sites, to form $Mg(OH)_2$ brucite; MgO surface was covered by adsorbed OH_s and further the OH_s species migrated from MgO to sintered Ni metal particles. The Ni metal particle may be oxidized from the periphery by OH_s migrated from MgO surface to form $Ni^{2+}(OH)_2$ species, followed by incorporation into Mg(Ni^{2+})-Al LDH assisted by rehydration of Mg(Al)O. It is likely that self-regenerative activity is assisted by rehydration or reconstitution.

5.2.6. Self-regenerative activity of passivated Pt-Ni/Mg(Al)O catalyst by steaming

The catalyst life, i.e., the sustainability of the catalyst, is important for the commercial reforming catalysts in the PEFC and seems mainly owing to *anti*-sintering property. The catalyst life tests have been frequently performed with a commercial reformer for several months or years. A steaming treatment of the catalyst under rigorous conditions can be performed in a labo-scale to simulate the catalyst life test in a commercial reformer. Such steaming treatment under high-temperatures, humid and reducing atmospheres causes a severe sintering of supported metal catalysts. Here steaming of catalyst was carried out in a $H_2/H_2O/N_2$ (20/100/25 mL min^{-1}) for 10 h at 900 °C. It is said that

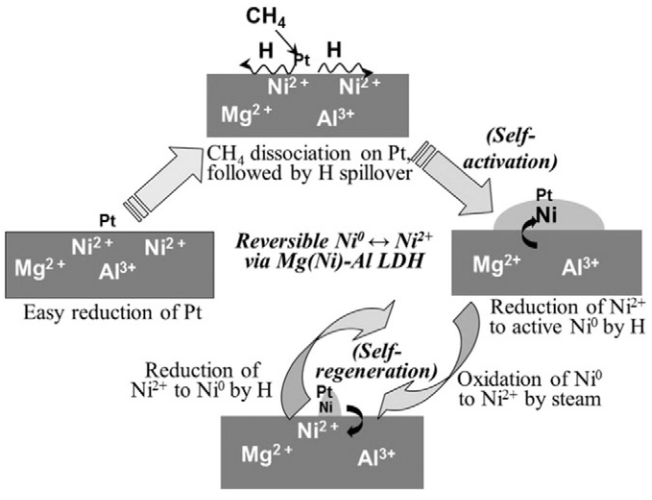

Fig. 14. Plausible mechanism of self-activation and self-regeneration of Pt-Ni/Mg(Al)O catalysts.

Table 11
Turnover frequency of supported Ni catalysts before and after steaming[a] (Li et al., 2007a, 2007b, 2008, Elsevier).

	CH_4 conversion /%		H_2 uptake /μmol g_{cat}^{-1}		TOF[b] /s^{-1}	
Catalyst	Before	After	Before	After	Before	After
$Ni_{0.5}/Mg_{2.5}(Al)O$	14.6	5.42	163.2	26.6	0.35	0.13
0.10wt%Ru-$Ni_{0.5}/Mg_{2.5}(Al)O$	12.8	10.3	213.4	55.3	0.31	0.25
0.10 wt%Rh-$Ni_{0.5}/Mg_{2.5}(Al)O$	12.4	8.95	189.1	55.3	0.30	0.22
0.10 wt%Pt-$Ni_{0.5}/Mg_{2.5}(Al)O$	13.7	7.43	205.0	52.3	0.33	0.18

[a] Steaming was carried out at 900 °C for 10 h in a $H_2/H_2O/N_2$ (20/100/25 mL min^{-1}). The catalysts were used as powders of 0.075–0.180 mm in diameter. Then, SR of CH_4 was carried out at 500 °C in $CH_4/H_2O/N_2$ (88.8/177.6/44.4 mL min^{-1}) at the GHSV of 1.6×10^6 mL g_{cat}^{-1} h^{-1} after pre-reduction at 900 °C for 0.5 h.
[b] TOF value was calculated based on total Ni amount.

such steaming conditions correspond to catalyst testing for ca. 5000 h in the commercial reformer (Li et al., 2008).

DSS steam reforming of CH_4 was carried out between 200 and 700 °C under steam purging over the catalysts after the steaming treatment at 900 °C. The activity was compared by CH_4 conversion. After steaming, commercial FCR and RUA, $Ni_{0.5}/Mg_{2.5}(Al)O$ and 13.5 wt% Ni/γ-Al_2O_3 showed a complete deactivation just after the first steam purging (Li et al., 2007b, 2008). 0.10 wt% Pt-$Ni_{0.5}/Mg_{2.5}(Al)O$ showed a stable activity during the DSS steam reforming of CH_4, followed by 0.1 wt% Rh-$Ni_{0.5}/Mg_{2.5}(Al)O$ (Li et al., 2007a,b, 2008), indicating that noble metal doping was effective for the catalyst sustainability even after steaming. However, 0.1 wt% Ru-$Ni_{0.5}/Mg_{2.5}(Al)O$ was deactivated after steaming probably due to the surface passivation of Ru metal by steam, indicating that Ru is not as tolerable as Pt and Rh. It must be emphasized that, even after steaming, 0.1 wt% Pt-$Ni_{0.5}/Mg_{2.5}(Al)O$ alone showed a high and stable activity not only in stationary operation but also in DSS operation.

A more precise evaluation of catalytic activity has been done based on the TOF of the catalyst for the $Ni_{0.5}/Mg_{2.5}(Al)O$, 0.10 wt% Ru-, Rh- and Pt-$Ni_{0.5}/Mg_{2.5}(Al)O$ catalysts (Table 11) (Li et al., 2007a, b, 2008). TOF values based on total Ni amounts seem more practically reliable compared with those based on surface Ni amounts, since the latter values were severely affected by the sintering of Ni particles. $Ni_{0.5}/Mg_{2.5}(Al)O$ was most severely deactivated, followed by 0.10 wt% Pt-, Ru- and Rh-$Ni_{0.5}/Mg_{2.5}(Al)O$. A decline in TOF value after steaming was more significant on 0.10 wt% Pt-$Ni_{0.5}/Mg_{2.5}(Al)O$ than on 0.10 wt% Ru- and Rh-$Ni_{0.5}/Mg_{2.5}(Al)O$, probably due to a smaller molar amount of Pt than of Ru and Rh at the same mass loading of 0.10 wt%. The TOF values of both FCR and RUA were one digit smaller than those of $Ni_{0.5}/Mg_{2.5}(Al)O$-based catalysts; moreover, heavy deactivation occurred on both commercial catalysts after steaming (Li et al., 2007a). One must notice that TOF values of 0.10 wt% Pt-, Rh- and Ru-$Ni_{0.5}/Mg_{2.5}(Al)O$ showed no remarkable decrease even after steaming, indicating that noble metal doping on $Ni_{0.5}/Mg_{2.5}(Al)O_x$ was quite effective for suppressing the deactivation due to sintering (Li et al., 2007a, b, 2008).

The regeneration of 0.50 wt% Pt-$Ni_{0.5}/Mg_{2.5}(Al)O$ during steaming and further followed by DSS steam reforming of CH_4 was pursued by FT k^3-wighted Pt L_3-edge EXAFS spectra (Fig. 15) (Li et al., 2008). Pt foil exhibited a peak corresponding to Pt–Pt bond with a distance 0.264 nm (Fig. 15f) and PtO_2 showed several peaks, among which a peak due to Pt–O bond appeared at 0.168 nm (Fig. 13g) (Hamada et al., 2007; Basile et al., 1998). The 0.50 wt% Pt-$Ni_{0.5}/Mg_{2.5}(Al)O$ exhibited two peaks at 0.168 and 0.298 nm after calcination (Fig. 15a); the former is assigned to the Pt–O bond. No peak of Pt–Pt bond suggests that Pt species was highly dispersed on the catalyst surface. The peak that appeared at 0.225 nm after reduction (Fig. 15b) can be assigned to the Pt–Ni bond. This peak was observed also after reduction-DSS steam reforming (Fig. 15c). Although this peak was weakened and shifted slightly toward a shorter bond length after steaming (Fig. 15d), it again came back to the original bond length (0.225 nm) as well as the original shape after steaming-DSS steam reforming (Fig. 15e). This clearly indicates that the Pt-Ni species was regenerated during DSS steam reforming of CH_4, although a little affected by steaming treatment.

The sizes of Ni particles on the supported Ni catalysts were calculated based on XRD and H_2 pulse measurements. After the passivation by steaming treatment, the sizes of Ni metal particles on all catalysts significantly increased from 5.0 ~ 7.0 nm to 15 ~ 26 nm, indicating clearly an occurring of sintering of Ni metal particles. The H_2 pulse method gave a larger Ni metal particle size than the XRD method, suggesting a formation of multi-crystalline Ni metal particles. $Ni_{0.5}/Mg_{2.5}(Al)O$ exhibited neither Ni metal nor NiO reflection in the XRD, and no H_2 uptake in the pulse measurements after steaming-DSS steam reforming. Only reflections of periclase were observed. These indicate that Ni was totally oxidized to Ni^{2+} and incorporated into Mg(Ni^{2+},Al)O periclase during DSS steam reforming. In fact, passivated $Ni_{0.5}/Mg_{2.5}(Al)O$ was perfectly deactivated after the first steam purging in DSS steam reforming due to the Ni oxidation. One must notice that, on 0.10 wt% noble metal-$Ni_{0.5}/Mg_{2.5}(Al)O$ catalysts, the increased sizes of sintered Ni metal particles after the steaming substantially decreased after DSS steam reforming (8.0 ~ 16 nm), and closed to the original value. All these catalysts exhibited sustainable activity during the DSS steam reforming of CH_4 even after steaming treatment (Li et al., 2007a, b, 2008). The size decrease, i.e., re-dispersion, of the sintered Ni particles during DSS steam reforming was clearly observed also in TEM images; 0.10 wt% Pt-$Ni_{0.5}/Mg_{2.5}(Al)O$ passivated by steaming exhibited the maximum Ni metal particle size of ca. 36 nm, whereas the maximum size decreased to ca. 15 nm after followed by DSS steam reforming of CH_4 (Li et al., 2008).

The self-regeneration of Pt-Ni/Mg(Al)O catalyst was observed also in TPR curves (Li et al., 2008). TPR of 0.10 wt% Pt-$Ni_{0.5}/Mg_{2.5}(Al)O$ after reduction exhibited a single peak of the $Ni^{2+} \rightarrow Ni^0$ reduction at 850 °C (Li et al., 2008). After steaming at 900 °C, the reduction peak was separated into two peaks, one at 918 °C and another at 267 °C, suggesting that Mg(Ni,Al)O periclase was reductively decomposed to large-sized Ni metal particles and Mg(Ni,Al)O of lower Ni content. The peak at 267 °C can be assigned to the isolated Ni metal particles, whereas the peak at 918 °C to the hard-to-reduce Ni^{2+} in the sintered Mg(Ni,Al)O. At low temperature, some other peaks also appeared at 121 and 200 °C after steaming, indicating a phase separation of Ni-Pt alloy; Pt exhibited reduction peaks at 100–200 °C, whereas Ni was reduced at 250-400 °C in the TPR of supported Pt-Ni bimetallic catalysts (Pawelec et al., 2007). When 0.10 wt% Pt-$Ni_{0.5}/Mg_{2.5}(Al)O$ after steaming was exposed to DSS steam reforming of CH_4, the peak at 200 °C disappeared, whereas the peak at 918 °C completely shifted toward a lower temperature of 830 °C. These results suggest that the separated species, i.e., Pt and Ni, were again combined and reconstituted to the original bimetallic phase on the catalyst; Ni metal particles were covered by Ni-Pt alloy on the surface as well as Ni^{2+} in the Mg(Al)O periclase phase.

Moreover, these noble metal-doped Ni/Mg(Al)O catalysts were enough active for the oxidative reforming of propane, where the most active catalyst was Ru-Ni/Mg(Al)O (Li et al., 2007c; Shiraga et al.,

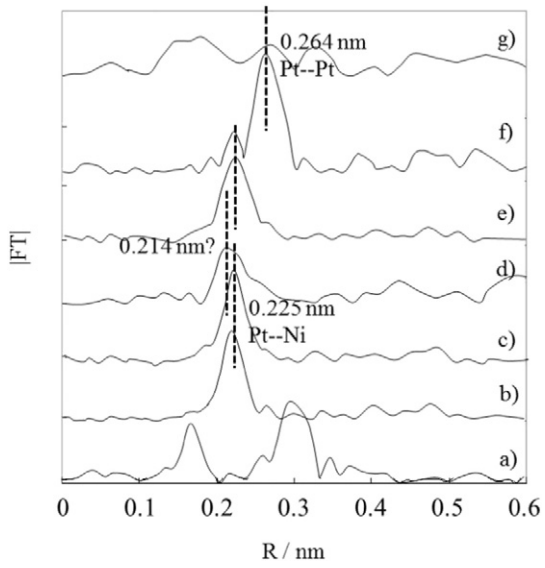

Fig. 15. Fourier transforms of k^3-weighted Pt L_3-edge EXAFS of 0.50 wt% Pt-$Ni_{0.5}$/$Mg_{2.5}$(Al)O during preparation, before and after steaming and further followed by DSS steam reforming of CH_4. (*a*) after calcination; (*b*) after reduction; (*c*) after reduction followed by DSS steam reforming of CH_4; (*d*) after steaming at 900 °C; (*e*) after steaming followed by DSS steam reforming of CH_4; (*f*) Pt foil; (*g*) PtO_2 (Li et al., 2008, Elsevier).

2007). Citrate method was reported to be effective for the preparation of homogeneous and highly dispersed metal supported catalyst, however the present LDH-derived noble metal-doped Ni/Mg(Al)O catalyst was more active and stable than citrate-derived catalyst (Zhan et al., 2009a). The Pt-Ni/Mg(Al)O catalyst prepared by using commercial Mg-Al LDH as the support showed also high activity in steam reforming of CH_4 (Li et al., 2009a; Zhan et al., 2009b).

Finally, one must know that the 0.10 wt% Pt-$Ni_{0.5}$/$Mg_{2.5}$(Al)O catalyst was successfully applied in a prototype test in steam reforming of CH_4 using a commercial reformer for PEFC: the catalyst survived more than 650 times of the DSS operation at GHSV = 650 h^{-1}, in which the initial activity was ca. 20 % higher than the commercial FCR catalyst. This catalyst was further developed by the research group of New Energy Development Organization (NEDO), Japan, and finally the effective catalyst life was estimated as ca. 40,000 h judging from the results obtained by life test: the catalyst survived for longer than 3000 DSS times. This work was completed under collaboration between Hiroshima University, Nikki-Universal Co., Ltd. and Fuji Electric Co., Ltd. financially supported by NEDO

6. Conclusions

LDH possesses several interesting properties, i.e., inclusion of various elements in the structure, homogenous distributions of the elements, rehydration of calcined LDH or reconstitution of LDH, thermostability, porous structure, etc. These characteristics rationally lead to the possible use of LDH as the heterogeneous catalysts. However, the detrimental drawback of LDH comes from the lack of mechanical strength, therefore calcination to mixed oxides or supporting on appropriate carrier, etc., have been tried to improve it. The recent developments of the research aiming at the commercial use of LDH derived materials as the heterogeneous catalysts were reviewed specifically focusing on the catalyst preparations and their uses by adopting reconstitution, or rehydration of LDH, and by loading metal on LDH derived oxide or by loading LDH itself on appropriate supports.

The surface of Mg(Al)O periclace was rehydrated to form base catalysts by generating Brønsted base, OH^-, as active species. These catalysts were effective for various base catalyzed reactions, such as condensation, transesterification, isomerization, cyanoethylation, etc. Unfortunately, however, in all these cases, the catalyst life was very short due to quick deactivation of OH^- by CO_2 in air. It is inevitable to find the other base catalyst possessing the other types of active species tolerant against CO_2.

The rehydration of LDH derived oxide in metal containing aqueous solution caused surface inclusion of active metals, resulting in the formation of novel active site on the catalyst. The rehydration produced highly dispersed surface metal species active for the various reactions, such as oxidation and dehydrogenation. By controlling the rehydration conditions, egg-shell type metal loading was achieved by surface enriching active metal species as observed on Ni/Mg(Al)O catalyst. Bimetallic active species, Pt- or Mg-Cu and Pt-Sn, were supported on Zn(Al)O or Mg(Al)O to produce active catalysts for WGS and propane dehydrogenation reactions, respectively.

Al_2O_3, SiO_2 or carbon nanofibers supported Mg-Al LDH catalysts exhibited high activity for the base catalyzed reactions, such as acetone condensation and transesterification of glycerol carbonate. When magnetic ferrite, such as Fe_3O_4, $MgFe_2O_4$ or $CoFe_2O_4$, was used as the support, the Mg-Al LDH catalyst obtained became magnetically separable, leading to the recyclable use of the catalyst. Moreover, finely tuned core-shell structured magnetic LDH catalyst, Au/Mg-Al LDH/Fe_3O_4, was recently prepared and exhibited magnetically separable and highly active characteristics in the oxidation reaction. Another recent topic is paper structured catalysts prepared by molding or immobilizing the LDH catalyst powders with ceramic fibers; the monolithic catalysts were active for reforming reaction in fuel cell system.

The reconstitution of LDH exhibited dynamic effect on the catalytic behaviors. Nitrate removal in natural water is critical issue, whereas the removal of oxalate, refractory compounds, in water is also challenging task. Pd-Cu/Mg(Al)O completely reduced nitrate to N_2, whereas Cu/Mg(Al)O totally oxidized oxalate to CO_2, by entrapping both nitrate and oxalate as anions in the interlayer space of Mg-Al LDH reconstituted. In the reforming catalysts for fuel cells, enormously high and stable activity was required. When Ni was combined with trace amount of noble metals, self-regenerative activity appeared as observed on Pt-Ni/Mg(Al)O catalysts for the reforming of hydrocarbons. Even under rigorous conditions, i.e., daily start-up and shut-down operation, the Pt-Ni/Mg(Al)O catalyst was active and sustainable for long term even in the catalyst-life test with a commercial reformer.

Acknowledgement

A part of this work has been done during my stay in Hiroshima University. The author would like to thank Prof. Tetsuya Shishido of Tokyo Metropolitan University, Japan, for the XAFS analyses and acknowledge Dr. Dalin Li as Postdoctoral Research Fellows, Hiroshima University, Japan (present address; D. Li: Fuzou University, China), for their excellent experimental works. This work was partly supported by the New Energy and Industrial Technology Development Organization (NEDO) (P05011), Japan.

References

Abelló, S., Medina, F., Tichit, D., Perez-Ramirez, J., Cesteros, Y., Salagre, P., Sueiras, J.E., 2005a. Nanoplatelet-based reconstructed hydrotalcites: towards more efficient solid base catalysts in aldol condensations. Chem. Commun. 1453–1455.

Abelló, S., Medina, F., Tichit, D., Pérez-Ramírez, J., Groen, J.C., Sueiras, J.E., Salagre, P., Cesteros, Y., 2005b. Aldol condensations over reconstructed Mg–Al hydrotalcites: structure–activity relationships related to the rehydration method. Chem. Eur. J. 11, 728–739.

Abelló, S., Medina, F., Tichit, D., Pérez-Ramírez, J., Rodríguez, X., Sueiras, J.E., Salagre, P., Cesteros, Y., 2005c. Study of alkaline-doping agents on the performance of reconstructed Mg–Al hydrotalcites in aldol condensations. Appl. Catal. A: General 281, 191–198.

Abelló, S., Medina, F., Tichit, D., Pérez-Ramírez, J., Sueiras, J.E., Salagre, P., Cesteros, Y., 2007. Aldol condensation of campholenic aldehyde and MEK over activated hydrotalcites. Appl. Catal. B Environ. 70, 577–584.

Abelló, S., Vijaya-Shankar, D., Pérez-Ramírez, J., 2008. Stability, reutilization, and scalability of activated hydrotalcites in aldol condensation. Appl. Catal. A: General 342, 119–125.

Abrevaya, H., Imai, T., 1986. UOP. U.S. Patent 4. 608, p. 360.

Aguilar-Ríos, G., Salas, P., Valenzuela, M.A., Armendáriz, H., Wang, J.A., Salmones, J., 1999. Propane dehydrogenation activity of Pt and Pt–Sn catalysts supported on magnesium aluminate: influence of steam and hydrogen. Catal. Lett. 60, 21–25.

Akporiaye, D., Roennekleiv, M., Hasselgaard, P., 2000. NO Patent 308989 (to Den Norske Stats Oljeselskap AS).

Akporiaye, D., Jensen, S.F., Olsbye, U., Rohr, F., Rytter, E., Rønnekleiv, M., Spjelkavik, A.I., 2001. A novel, highly efficient catalyst for propane dehydrogenation. Ind. Eng. Chem. Res. 40, 4741–4748.

Allada, R.K., Pless, J.D., Nenoff, T.M., Navrotsky, A., 2005. Thermochemistry of hydrotalcite-like phases intercalated with CO_3^{2-}, NO_3^-, Cl^-, I^-, and ReO_4^-. Chem. Mater. 17, 2455–2459.

Álvarez, M.G., Segarra, A.M., Contreras, S., Sueiras, J.E., Medina, F., Figueras, F., 2010. Enhanced use of renewable resources: transesterification of glycerol catalyzed by hydrotalcite-like compounds. Chem. Eng. J. 161, 340–345.

Álvarez, M.G., Chimentão, R.J., Figueras, F., Medina, F., 2012a. Tunable basic and textural properties of hydrotalcite derived materials for transesterification of glycerol. Appl. Clay Sci. 58, 16–24.

Álvarez, M.G., Plíšková, M., Segarra, A.M., Medina, F., Figueras, F., 2012b. Synthesis of glycerol carbonates by transesterification of glycerol in a continuous system using supported hydrotalcites as catalysts. Appl. Catal. B Environ. 113–114, 212–220.

Álvarez, M.G., Chimentão, R.J., Barrabés, N., Föttinger, K., Gispert-Guirado, F., Kleymenove, E., Tichit, D., Medina, F., 2013a. Structure evolution of layered double hydroxides activated by ultrasound induced reconstruction. Appl. Clay Sci. 83–84, 1–11.

Alvarez, M.G., Frey, A.M., Bitter, J.H., Segarra, A.M., De Jong, K.P., Medina, F., 2013b. On the role of the activation procedure of supported hydrotalcites for base catalyzed reactions: glycerol to glycerol carbonate and self-condensation of acetone. Appl. Catal. B Environ. 134–135, 231–237.

Armendáriz, H., Guzmán, A., Toledo, J.A., Llanos, M.E., Vázquez, A., Aguilar-Ríos, G., 2001. Isopentane dehydrogenation on Pt-Sn catalysts supported on Al-Mg-O mixed oxides: effect of Al/Mg atomic ratio. Appl. Catal. A: General 211, 69–80.

Ashcroft, T., Cheetham, A.K., Foord, J.S., Green, M.L.H., Grey, C.P., Murrell, A.J., Vernon, P.D.F., 1990. Selective oxidation of methane to synthesis gas using transition metal catalysts. Nature 344, 319–321.

Atanda, L.A., Balasamy, R.J., Khurshid, A., Al-Ali, A.A.S., Sagata, K., Asamoto, M., Yahiro, H., Nomura, K., Sano, T., Takehira, K., Al-Khattaf, S.S., 2011. Ethylbenzene dehydrogenation over $Mg_3Fe_{0.5-x}Co_xAl_{0.5}$ catalysts derived from hydrotalcites: comparison with $Mg_3Fe_{0.5-y}Ni_yAl_{0.5}$ catalysts. Appl. Catal. A: General 396, 107–115.

Au, C.T., Liao, M.S., Ng, C.F., 1998. A detailed theoretical treatment of the partial oxidation of methane to syngas on transition and coinage metal (M) catalysts (M═Ni, Pd, Pt, Cu). J. Phys. Chem. A 102, 3959–3969.

Au, C.T., Ng, C.F., Liao, M.S., 1999. Methane dissociation and syngas formation on Ru, Os, Rh, Ir, Pd, Pt, Cu, Ag, and Au: a theoretical study. J. Catal. 185, 12–22.

Au, C.T., Wang, H.Y., 1997. Mechanistic studies of methane partial oxidation to syngas over SiO_2-supported rhodium catalysts. J. Catal. 167, 337–345.

Balasamy, R.J., Khurshid, A., Al-Ali, A.A.S., Atanda, L.A., Sagata, K., Asamoto, M., Yahiro, H., Nomura, K., Sano, T., Takehira, K., Al-Khattaf, S.S., 2010. Ethylbenzene dehydrogenation over binary FeO_x–MeO_y/Mg(Al)O catalysts derived from hydrotalcites. Appl. Catal. A: General 390, 225–234.

Balasamy, R.J., Tope, B.B., Khurshid, A., Al-Ali, A.A.S., Atanda, L.A., Sagata, K., Asamoto, M., Yahiro, H., Nomura, K., Sano, T., Takehira, K., Al-Khattaf, S.S., 2011. Ethylbenzene dehydrogenation over FeO_x/(Mg,Zn)(Al)O catalysts derived from hydrotalcites: role of MgO as basic sites. Appl. Catal. A: General 398, 113–122.

Bariás, O.A., Holmen, A., Blekkan, E.A., 1996. Propane dehydrogenation over supported Pt and Pt–Sn catalysts: catalyst preparation, characterization, and activity measurements. J. Catal. 158, 1–12.

Barrabés, N., Just, J., Dafinov, A., Medina, F., Fierro, J.L.G., Sueiras, J.E., Salagre, P., Cesteros, Y., 2006. Catalytic reduction of nitrate on Pt-Cu and Pd-Cu on active carbon using continuous reactor. The effect of copper nanoparticles. Appl. Catal. B Environ. 62, 77–85.

Basile, F., Fornasari, G., Poluzzi, E., Vaccari, A., 1998. Catalytic partial oxidation and CO_2-reforming on Rh- and Ni-based catalysts obtained from hydrotalcite-type precursors. Appl. Clay Sci. 13, 329–345.

Basile, F., Fornasari, G., Gazzano, M., Vaccari, A., 2000. Synthesis and thermal evolution of hydrotalcite-type compounds containing noble metals. Appl. Clay Sci. 16, 185–200.

Basile, F., Fornasari, G., Trifiro, F., Vaccari, A., 2001a. Partial oxidation of methane effect of reaction parameters and catalyst composition on the thermal profile and heat distribution. Catal. Today 64, 21–30.

Basile, F., Fornasari, G., Gazzano, M., Vaccari, A., 2001b. Thermal evolution and catalytic activity of Pd/Mg/Al mixed oxides obtained from a hydrotalcite-type precursor. Appl. Clay Sci. 18, 51–57.

Basile, F., Benito, P., Fornasari, G., Vaccari, A., 2010. Hydrotalcite-type precursors of active catalysts for hydrogen production. Appl. Clay Sci. 48, 250–259.

Baskaran, T., Christpher, J., Sakthivel, A., 2015. Progress on layered hydrotalcite (HT) materials as potential support and catalytic materials. RSC Adv. 5, 98853–98875.

Bhattacharyya, A., Chang, V.W., Schumacher, D.J., 1998. CO_2 reforming of methane to syngas I: evaluation of hydrotalcite clay-derived catalysts. Appl. Clay Sci. 13, 317–328.

Carja, G., Kameshima, Y., Okada, K., 2008. Nanoparticles of iron and vanadium oxides supported on iron substituted LDHs: synthesis, textural characterization and their catalytic behavior in ethylbenzene dehydrogenation. Microporous Mesoporous Mater. 115 (541–547), 110.

Cavani, F., Trifirò, F., Vaccari, A., 1991. Hydrotalcite-type anionic clays: preparation, properties and apllications. Catal. Today 11, 173–301.

Chen, B., Goodwin Jr., J.G., 1995. Isotopic transient kinetic analysis of ethane hydrogenolysis on Ru/SiO_2. J. Catal. 154, 1–10.

Chimentão, R.J., Abelló, S., Medina, F., Llorca, J., Sueiras, J.E., Cesteros, Y., Salagre, P., 2007. Defect-induced strategies for the creation of highly active hydrotalcites in base-catalyzed reactions. J. Catal. 252, 249–257.

Climent, M.J., Corma, A., Iborra, S., Epping, K., Velty, A., 2004a. Increasing the basicity and catalytic activity of hydrotalcites by different synthesis procedures. J. Catal. 225, 316–326.

Climent, M.J., Corma, A., Iborra, S., Velty, A., 2004b. Activated hydrotalcites as catalysts for the synthesis of chalcones of pharmaceutical interest. J. Catal. 221, 474–482.

Corma, A., 1997. From microporous to mesoporous molecular sieve materials and their use in catalysis. Chem. Rev. 97, 2373–2420.

Corma, A., Iborra, S., Velty, A., 2007. Chemical routes for the transformation of biomass into chemicals. Chem. Rev. 107 (2007), 2411–2502.

Cortright, R.D., Dumesic, J.A., 1994. Microcalorimetric, spectroscopic, and kinetic studies of silica-supported pt and pt/sn catalysts for isobutane dehydrogenation. J. Catal. 148, 771–778.

Cortright, R.D., Dumesic, J.A., 1995. Effect of potassium on silica-supported Pt and Pt/Sn catalysts for isobutane dehydrogenation. J. Catal. 157, 576–583.

Cortright, R.D., Hill, J.M., Dumesic, J.A., 2000a. Selective dehydrogenation of isobutane over supported Pt/Sn catalysts. Catal. Today 55, 213–223.

Cortright, R.D.; Watwe, R.M.; Dumesic, J.A, 2000b. Ethane hydrogenolysis over platinum selection and estimation of kinetic parameters. J. Mol. Catal. A: Chemical 163, 91–103.

Davis, R.J., Derouane, E.G., 1991. A non-porous supported-platinum catalyst for aromatization of n-hexane. Nature 349, 313–315.

Delorme, F., Seron, A., Bizi, M., Jean-Prost, V., Martineau, D., 2006. Effect of time on the reconstruction of the $Mg_4Al_2(OH)_{12}CO_3{\cdot}3H_2O$ layered double hydroxide in a Na_2CO_3 solution. J. Mater. Sci. 41, 4876–4882.

De Souza Ramos, M., De Santana Santos, M., Pacheco Gomes, L., Albornoz, A., Do Carmo Rangel, M., 2008. The influence of dopants on the catalytic activity of hematite in the ethylbenzene dehydrogenation. Appl. Catal. A: General 341, 12–17.

Di Cosimo, J.I., Díez, V.K., Apesteguía, C.R., 1998a. Synthesis of α, β-unsaturated ketones over thermally activated Mg–Al hydrotalcites. Appl. Clay Sci. 13, 433–449.

Di Cosimo, J.I., Díez, V.K., Xu, M., Iglesia, E., Apesteguía, C.R., 1998b. Structure and surface and catalytic properties of Mg-Al basic oxides. J. Catal. 178, 499–510.

Eun, J.H., Lee, J.H., Kim, S.G., Um, M.Y., Park, S.Y., Kim, H.J., 2003. The protection of MgO film against hydration by using Al2O3 capping layer deposited by magnetron sputtering method. Thin Solid Films 435, 199–204.

Fang, W.H., Chen, J., Zhang, Q.H., Deng, W.P., Wang, Y., 2011. Hydrotalcite-supported gold catalyst for the oxidant-free dehydrogenation of benzyl alcohol: studies on support and gold size effects. Chem. Eur. J. 17 (2011), 1247–1256.

Feng, J., He, Y., Liu, Y., Du, Y., Li, D., 2015. Supported catalysts based on layered double hydroxides for catalytic oxidation and hydrogenation: general functionality and promising application prospects. Chem. Soc. Rev. 44, 5291–5391.

Fornasari, G., Gazzano, M., Matteuzzi, D., Trifirò, F., Vaccari, A., 1995. Structure and reactivity of high-surface-area Ni/Mg/A1 mixed oxides. Appl. Clay Sci. 10, 69–82.

Fukahori, S., Kitaoka, T., Tomoda, A., Suzuki, R., Wariishi, H., 2006a. Methanol steam reforming over paper-like composites of Cu/ZnO catalyst and ceramic fiber. Appl. Catal. A: General 300, 155–161.

Fukahori, S., Koga, H., Kitaoka, T., Tomoda, A., Suzuki, R., Wariishi, H., 2006b. Hydrogen production from methanol using a SiC fiber-containing paper composite impregnated with Cu/ZnO catalyst. Appl. Catal. A: General 310, 138–144.

Fukahori, S., Koga, H., Kitaoka, T., Nakamura, M., Wariishi, H., 2008. Steam reforming behavior of methanol using paper-structured catalysts: experimental and computational fluid dynamic analysis. Int. J. Hydrog. Energy 33, 1661–1670.

Gauthard, F., Epron, F., Barbier, J., 2003. Palladium and platinum-based catalysts in the catalytic reduction of nitrate in water: effect of copper, silver, or gold addition. J. Catal. 220, 182–191.

Guth, U., Brosda, S., Schomburg, J., 1996. Applications of clay minerals in sensor techniques. Appl. Clay Sci. 11, 229–236.

Hamada, S., Ikeue, K., Machida, M., 2007. Catalytic NO–H_2–O_2 reaction over Pt/Mg–Al–O prepared from $PtCl_6^{2-}$- and $Pt(NO_2)_4^{2-}$-exchanged hydrotalcites. Appl. Catal. B Environ. 71, 1–6.

Hansen, H.C.B., Koch, C.B., 1995. Synthesis and characterization of pyroaurite. Appl. Clay Sci. 10, 5–19.

Hayakawa, T., Sato, K., Tsunoda, T., Hamakawa, S., Suzuki, K., Nakamura, J., Takehira, K., Uchijima, T., 1994. Partial oxidation of methane: continuous production of synthesis gas over Rh/YSZ/Ag under oxygen supply. J. Chem. Soc. Chem. Commun. 1899–1990.

Hayakawa, T., Harihara, H., Andersen, A.G., York, A.P.E., Suzuki, K., Yasuda, H., Takehira, K., 1996. A sustainable catalyst for the partial oxidation of methane to syngas: $Ni/Ca_{1-x}Sr_xTiO_3$, prepared in situ from perovskite precursors. Angew. Chem. Int. Ed. Eng. 35, 192–195.

Hibino, T., Tsunashima, A., 1998. Characterization of repeatedly reconstructed Mg-Al hydrotalcite-like compounds: gradual segregation of aluminum from the structure. Chem. Mater. 10, 4055–4061.

Hora, L., Kelbichova, V., Kikhtyanin, O., Bortnovskiy, O., Kubička, D., 2014. Aldol condensation of furfural and acetone over Mg Al layered double hydroxides and mixed oxides. Catal. Today 223, 138–147.

Hora, L., Kikhtyanin, O., Čapek, L., Bortnovskiy, O., Kubička, D., 2015. Comparative study of physico-chemical properties of laboratory and industrially prepared layered double hydroxides and their behavior in aldol condensation of furfural and acetone. Catal. Today 241, 221–230.

Hosokawa, S., Nogawa, S., Taniguchi, M., Utani, K., Kanai, H., Imamura, S., 2006. Oxidation characteristics of Ru/CeO_2 catalyst. Appl. Catal. A: General 288, 67–73.

Humblot, F., Candy, J.P., Le Peltier, F., Didillon, B., Basset, J.M., 1998. Surface organometallic chemistry on metals: selective dehydrogenation of isobutane into isobutene on bimetallic catalysts prepared by reaction of tetra n-butyltin on silica-supported platinum Catalyst. J. Catal. 179 (459–468), 210.

Imai, T., 1987. UOP. U.S. Patent 4,716,143.

Imai, T., 1988a. UOP. U.S. Patent 4,762,960.

Imai, T., Abrevaya, H., Bricker, J.C., Jan, D.-Y., 1988b. UOP. U.S. Patent 4,786,625.

Imai, T., Jan, D.Y., 1988c. UOP. U.S. Patent 4,788,371.

Iyi, N., Fujii, K., Okamoto, K., Sasaki, T., 2007. Factors influencing the hydration of layered double hydroxides (LDHs) and the appearance of an intermediate second staging phase. Appl. Clay Sci. 35, 218–227.

Jana, S.K., Kubota, Y., Tatsumi, T., 2007. High activity of Mn-MgAl hydrotalcite in heterogeneously catalyzed liquid-phase selective oxidation of alkylaromatics to benzylic ketones with 1 atm. of molecular oxygen. J. Catal. 247, 214–222.

Jin, L.Y., 1991. Platinum-tin complexing and its application to catalysis. Appl. Catal. 72, 33–38.

Kagunya, W., Jones, W., 1995. Aldol condensation of acetaldehyde using calcined layered double hydroxides. Appl. Clay Sci. 10, 95–102.

Kasprzyk-Hordern, B., Ziółek, M., Nawrocki, J., 2003. Catalytic ozonation and methods of enhancing molecular ozone reactions in water treatment. Appl. Catal. B Environ. 46, 639–669.

Khan, A.I., O'Hare, D., 2002. Intercalation chemistry of layered double hydroxides: recent developments and applications. J. Mater. Chem. 12, 3191–3198.

Koga, H., Fukahori, S., Kitaoka, T., Tomoda, A., Suzuki, R., Wariishi, H., 2006. Autothermal reforming of methanol using paper-like Cu/ZnO catalyst composites prepared by a papermaking technique. Appl. Catal. A Gen. 309, 263–269.

Koga, H., Fukahori, S., Kitaoka, T., Nakamura, M., Wariishi, H., 2008. Paper-structured catalyst with porous fiber-network microstructure for autothermal hydrogen production. Chem. Eng. J. 139, 408–415.

Kooli, F., Depège, C., Ennaqadi, A., De Roy, A., Besse, J.P., 1997. Rehydration of Zn-Al layered double hydroxides. Clay Clay Miner. 45, 92–98.

Lee, G., Jeong, Y., Takagaki, A., Jung, J.C., 2014. Sonication assisted rehydration of hydrotalcite catalyst for isomerization of glucose to fructose. J. Mol. Catal. A: Chemical 393, 289–295.

Lemaignen, L., Tong, C., Bergon, V., Burch, R., Chadwick, D., 2002. Catalytic denitrification of water with palladium-based catalysts supported on activated carbons. Catal. Today 75, 43–48.

Li, B., Kado, S., Mukainakano, K., Miyazawa, T., Miyao, T., Naito, S., Okumura, K., Kunimori, K., Tomishige, K., 2007. Surface modification of Ni catalysts with trace Pt for oxidative steam reforming of methane. J. Catal. 245, 144–155.

Li, D., Atake, I., Shishido, T., Oumi, Y., Sano, T., Takehira, K., 2007a. Self-regenerative activity of Ni/Mg(Al)O catalysts with trace Ru during daily start-up and shut-down operation of CH_4 steam reforming. J. Catal. 250, 299–312.

Li, D., Shishido, T., Oumi, Y., Sano, T., Takehira, K., 2007b. Self-activation and self-regenerative activity of trace Rh-doped Ni/Mg(Al)O catalysts in steam reforming of methane. Appl. Catal. A: General 332, 98–109.

Li, D., Shiraga, M., Atake, I., Shishido, T., T., Oumi, Y., Sano, T., Takehira, K., 2007c. Partial oxidation of propane over Ru promoted Ni/Mg(Al)O catalysts Self-activation and prominent effect of reduction–oxidation treatment of the catalyst. Appl. Catal. A: General 321, 155–164.

Li, D., Nishida, K., Zhan, Y., Shishido, T., T., Oumi, Y., Sano, T., Takehira, K., 2008. Superior catalytic behavior of trace Pt-doped Ni/Mg(Al)O in methane reforming under daily start-up and shut-down operation. Appl. Catal. A Gen. 350, 225–236.

Li, D., Zhan, Y., Nishida, K., T., Oumi, Y., Sano, T., Shishido, T., Takehira, K., 2009a. "Green" preparation of "intelligent" Pt-doped Ni/Mg(Al)O catalysts for daily start-up and shut-down CH4 steam reforming. Appl. Catal. A: General 363, 169–179.

Li, L., Feng, Y.J., Li, Y.S., Zhao, W.R., Shi, J.L., 2009b. Fe_3O_4 core/layered double hydroxide shell nanocomposite: versatile magnetic matrix for anionic functional materials. Angew. Chem. Int. Ed. 48 (2009), 5888–5892.

Liao, M.S., Zhang, Q.E., 1998. Dissociation of methane on different transition metals. J. Mol. Catal. A Chem. 136, 185–194.

Liu, P., Degirmenci, V., Hensen, E.J.M., 2014a. Unraveling the synergy between gold nanoparticles and chromium-hydrotalcites in aerobic oxidation of alcohols. J. Catal. 313, 80–91.

Liu, P., Derchi, M., Hensen, E.J.M., 2014b. Promotional effect of transition metal doping on the basicity and activity of calcined hydrotalcite catalysts for glycerol carbonate synthesis. Appl. Catal. B Environ. 144, 135–143.

Liu, S.; Jiang, X.; G. Zhuo, G. 2008. Heck reaction catalyzed by colloid of delaminated Pd-containing layered double hydroxide. J. Mol. Catal. A Chem. 290, 72–78.

Maeda, T., Pee, A.K., Haa, D., 1995. JP 07196573.

Marchi, A.J., Apesteguía, C.R., 1998. Impregnation-induced memory effect of thermally activated layered double hydroxides. Appl. Clay Sci. 13, 35–48.

Meitzner, G., Via, G.H., Lytle, F.W., Fung, S.C., Sinfelt, H., 1988. Extended X-ray absorption fine structure studies of platinum-tin catalysts. J. Phys. Chem. 92, 2925–2932.

Merlen, E., Gueroult, P., d'Espinose de la Caillerie, J.-B., Rebours, B., Bobin, C., Clause, O., 1995. Hydrotalcite formation at the alumina/water interface during impregnation with Ni(II) aqueous solutions at neutral pH. Appl. Clay Sci. 10, 45–56.

Meyn, M., Beneke, K., Lagaly, G., 1990. Anion-exchange reactions of layered double hydroxides. Inorg. Chem. 29, 5201–5207.

Mi, F., Chen, X., Ma, Y., Yin, S., Yuan, F., Zhang, H., 2011. Facile synthesis of hierarchical core–shell Fe_3O_4@MgAl–LDH@Au as magnetically recyclable catalysts for catalytic oxidation of alcohols. Chem. Commun. 47, 12804–12806.

Millange, F., Walton, R.I., O'Hare, D., 2000. Time-resolved in situ X-ray diffraction study of the liquid-phase reconstruction of Mg-Al-carbonate hydrotalcite-like compounds. J. Mater. Chem. 10, 1713–1720.

Mitsudome, T., Noujima, A., Mizugaki, T., Jitsukawa, K., Kaneda, K., 2009. Efficient aerobic oxidation of alcohols using a hydrotalcite-supported gold nanoparticle catalyst. Adv. Synth. Catal. 351, 1890–1896.

Miura, S., Umemura, Y., Shiratori, Y., Kitaoka, T., 2013. In situ synthesis of Ni/MgO catalysts on inorganic paper-like matrix for methane steam reforming. Chem. Eng. J. 229, 515–521.

Miyata, S., 1975. The synthesis of hydrotalcite-like compounds and their structures and physico-chemical properties, the systems $MgAlNO_3$, MgAlCl, $MgAlClO_4$, NiAlCl, ZnAlCl. Clay Clay Miner. 31, 305–311.

Miyata, S., 1980. Physico-chemical properties of synthetic hydrotalcites in relation to composition. Clay Clay Miner. 28, 50–56.

Miyata, T., Li, D., Shiraga, M., Shishido, T., T., Oumi, Y., Sano, T., Takehira, K., 2006. Promoting effect of Rh, Pd and Pt noble metals to the Ni/Mg(Al)O catalysts for the DSS-like operation in CH_4 steam reforming. Appl. Catal. A: General 310, 97–104.

Miyata, T., Shiraga, M., Li, D., Atake, I., Shishido, T., Oumi, Y., Sano, T., Takehira, K., 2007. Promoting effect of Ru on Ni/Mg(Al)O catalysts in DSS-like operation of CH_4 steam reforming. Catal. Commun. 8, 447–451.

Miyazawa, T., Kimurea, T., Nishikawa, J., Kado, S., Kunimori, K., Tomishige, K., 2006. Catalytic performance of supported Ni catalysts in partial oxidation and steam reforming of tar derived from the pyrolysis of wood biomass. Catal. Today 115, 254–262.

Mokhtar, M., Inayat, A., Ofili, J., Schwieger, W., 2010. Thermal decomposition, gas phase hydration and liquid phase reconstruction in the system Mg/Al hydrotalcite/mixed oxide: a comparative study. Appl. Clay Sci. 50, 176–181.

Moneyron, J.E., de Roy, A., Forano, C., Besse, J.P., 1995. Realization of humidity sensors based on a screen-printed anionic clay. Appl. Clay Sci. l0, 163–175.

Moulijn, J.A., Makkee, M., Van Diepen, A., 2001. Chemical Process Technology. John Wiley & Sons, Chichester.

Mukainakano, Y., Li, B., Kado, S., Miyazawa, T., Okumura, K., Miyao, T., Naito, S., Kunimori, K., Tomishige, K., 2007. Surface modification of Ni catalysts with trace Pd and Rh for oxidative steam reforming of methane. Appl. Catal. A General 318, 252–264.

Myers, V.S., Weir, M.G., Carino, E.V., Yancey, D.F., Pande, S., Crooks, R.M., 2011. Dendrimer-encapsulated nanoparticles: new synthetic and characterization methods and catalytic applications. Chem. Sci. 2, 1632–1646.

Nagaoka, K., Jentys, A., Lercher, J.A., 2005. Methane autothermal reforming with and without ethane over mono- and bimetal catalysts prepared from hydrotalcite precursors. J. Catal. 229, 185–196.

Nagendrappa, G., 2011. Organic synthesis using clay and clay-supported catalysts. Appl. Clay Sci. 53, 106–138.

Nishida, K., Atake, I., Li, D., Shishido, T., Oumi, Y., Sano, T., Takehira, K., 2008. Effects of noble metal-doping on $Cu/ZnO/Al_2O_3$ catalysts for water–gas shift reaction catalyst preparation by adopting "memory effect" of hydrotalcite. Appl. Catal. A: General 337, 48–57.

Nishida, K., Li, D., Zhan, Y., Shishido, T., Oumi, Y., Sano, T., Takehira, K., 2009. Effective MgO surface doping of Cu/Zn/Al oxides as water–gas shift catalysts. Appl. Clay Sci. 44, 211–217.

Nishimura, S., Takagaki, A., Ebitani, K., 2010. Monodisperse iron oxide nanoparticles embedded in mgal hydrotalcite as a highly active, magnetically separable, and recyclable solid base catalyst. Bull. Chem. Soc. Jpn. 83, 846–851.

Nishimura, S., Takagaki, A., Ebitani, K., 2013. Characterization, synthesis and catalysis of hydrotalcite-related materials for highly efficient materials transformations. Green Chem. 15, 2026–2042.

Ohi, T., Miyata, T., Li, D., Shishido, T., Kawabata, T., Sano, T., Takehira, K., 2006. Sustainability of Ni loaded Mg–Al mixed oxide catalyst in daily startup and shutdown operations of CH_4 steam reforming. Appl. Catal. A: General 308, 194–203.

Ohishi, Y., Kawabata, T., Shishido, T., Takaki, K., Zhang, Q., Wang, Y., Nomura, K., Takehira, K., 2005. Mg–Fe–Al mixed oxides with mesoporous properties prepared from hydrotalcite as precursors: catalytic behavior in ethylbenzene dehydrogenation. Appl. Catal. A: General 288, 220–231.

Olafsen, A., Slagtern, Å., Dahl, I.M., Olsbye, U., Schuurman, Y., Mirodatos, C., 2005. Mechanistic features for propane reforming by carbon dioxide over a Ni/Mg(Al)O hydrotalcite-derived catalyst. J. Catal. 229, 163–175.

Olsbye, U., Akporiaye, D., Rytter, E., Ronnekleiv, M., Tangstad, E., 2002. On the stability of mixed M^{2+}/M^{3+} oxides. Appl. Catal., A 224, 39–49.

Palomares, A.E., Prato, J.G., Márquez, F., Corma, A., 2003. Denitrification of natural water on supported Pd/Cu catalysts. Appl. Catal. B Environ. 41, 3–13.

Palomares, A.E., Prato, J.G., Rey, F., Corma, A., 2004. Using the "memory effect" of hydrotalcites for improving the catalytic reduction of nitrates in water. J. Catal. 221, 62–66.

Parmaliana, A., Arena, F., Frusteri, F., Giordano, N., 1990. Temperature-programmed reduction study of NiO–MgO interactions in magnesia-supported Ni catalysts and NiO–MgO physical mixture. J. Chem. Soc. Faraday Trans. 1 (86), 2663–2669.

Passos, F.B., Schmal, M., Vannice, M.A., 1996. Effect of In and Sn on the adsorption behavior and hydrogenolysis activity of Pt/Al_2O_3 catalysts. J. Catal. 160, 106–117.

Pavel, O.D., Bîrjega, R., Che, M., Costentin, G., Angelescu, E., Şerban, S., 2008. The activity of Mg/Al reconstructed hydrotalcites by "memory effect" in the cyanoethylation reaction. Catal. Commun. 9, 1974–1978.

Pavel, O.D., Zăvoianu, R., Bîrjega, R., Angelescu, E., 2011. The effect of ageing step elimination on the memory effect presented by $Mg_{0.75}Al_{0.25}$ hydrotalcites (HT) and their catalytic activity for cyanoethylation reaction. Catal. Commun. 12, 845–850.

Pavel, O.D., Tichit, D., Marcu, I.-C., 2012. Acido-basic and catalytic properties of transition-metal containing Mg–Al hydrotalcites and their corresponding mixed oxides. Appl. Clay Sci. 61, 52–58.

Pawelec, B., Damynova, S., Arishtirova, K., Fierro, J.L.G., Petrov, L., 2007. Structural and surface features of PtNi catalysts for reforming of methane with CO_2. Appl. Catal. A Gen. 323, 188–201.

Pérez-Ramírez, J., Mul, G., Kapteijn, F., Moulijn, J.A., 2001. On the stability of the thermally decomposed Co–Al hydrotalcite against retrotopotactic transformation. Mater. Res. Bull. 36, 1767–1775.

Pérez-Ramírez, J., Abelló, S., Van der Pers, N.M., 2007. Memory effect of activated Mg-Al hydrotalcite: in situ XRD studies during decomposition and gas-phase reconstruction. Chem. Eur. J. 13, 870–878.

Pinnavaia, T.J., Chibwe, M., Constantino, V.R.L., Yun, S.K., 1995. Hydrotalcite-like structures as molecular containers for preparation of microporous carbons. Appl. Clay Sci. 10, 117–186.

Polshettiwar, V., Luque, R., Fihri, A., Zhu, H., Bouhrara, M., Basset, J., 2011. Magnetically recoverable nanocatalysts. Chem. Rev. 111, 3036–3075.

Purnama, H., Ressler, T., Jentoft, R.E., Soerijanto, H., Schlögl, R., Schomäcker, R., 2004. CO formation/selectivity for steam reforming of methanol with a commercial CuO/ZnO/Al_2O_3 catalyst. Appl. Catal. A: General 259, 83–94.

Quang-Tuyen, T., Kaida, T., Sakamoto, M., Sasaki, K., Shiratori, Y., 2015. Effectiveness of paper-structured catalyst for the operation of biodiesel-fueled solid oxide fuel cell. J. Power Sources 283, 320–327.

Rao, K.K., Gravelle, M., Valente, J.S., Figueras, F., 1998. Activation of Mg–Al hydrotalcite catalysts for aldol condensation reactions. J. Catal. 173, 115–121.

Rives, V., Ulibarri, M.A., 1999. Layered double hydroxides (LDH) intercalated with metal coordination compounds and oxometalates. Coord. Chem. Rev. 181, 61–120.

Rocha, J., del Arco, M., Rives, V., Ulibarri, M.A., 1999. Reconstruction of layered double hydroxides from calcined precursors: a powder XRD and ^{27}Al MAS NMR study. J. Mater. Chem. 9, 2499.

Roelofs, J.C.A.A., Van Dillen, A.J., De Jong, K.P., 2000. Base-catalyzed condensation of citral and acetone at low temperature using modified hydrotalcite catalysts. Catal. Today 60, 297–303.

Roelofs, J.C.A.A., Lensveld, D.J., Van Dillen, A.J., De Jong, K.P., 2001. On the structure of activated hydrotalcites as solid base catalysts for liquid-phase aldol condensation. J. Catal. 203, 184–191.

Roelofs, J.C.A.A., Van Bockhoven, J.A., Van Dillen, A.J., Geus, J.W., De Jong, K.P., 2002. The thermal decomposition of Mg–Al hydrotalcites: effects of interlayer anions and characteristics of the final structure. Chem. Eur. J. 8, 5571–5579.

Ruckenstein, E., Wang, H.Y., 2000. Partial oxidation of methane to synthesis gas over MgO-supported Rh catalysts: the effect of precursor of MgO. Appl. Catal. A General 198, 33–41.

Rytter, E., Akporiaye, D., Olsbye, U., 2000. Statoil. Norwegian Patent NO 307,639.

Salmones, J., Wang, J.-A., Galicia, J.A., Aguilar-Rios, G., 2002. H_2 reduction behaviors and catalytic performance of bimetallic tin-modified platinum catalysts for propane dehydrogenation. J. Mol. Catal. A: Chemical 184, 203–213.

Sato, T., Wakabayashi, T., Shimada, M., 1986. Adsorption of various anions by magnesium aluminum oxide of ($Mg_{0.7}Al_{0.3}O_{1.15}$). Ind. Eng. Chem. Prod. Res. Dev. 25, 89–92.

Sato, T., Fujita, H., Endo, T., Shimada, M., Tsunashima, A., 1988. Synthesis of hydrotalcite-like compounds and their physico-chemical properties. React. Solid 5, 219–228.

Sato, K., Nakamura, J., Uchijima, T., Hayakawa, T., Hamakawa, S., Tsunoda, T., Takehira, K., 1995. Partial oxidation of CH, to synthesis gas using an Rh|YSZ|Ag electrochemical membrane reactor. J. Chem. Soc. Faraday Trans. 91, 1655–1661.

Shannon, R.D., 1976. Revised effective ionic radii and systematic studies of interatomic distances in halides and chalcogenides. Acta Crystallogr. A 32, 751–767.

Sharma, S.K., Parikh, P.A., Jasra, R.V., 2008. Eco-friendly synthesis of jasminaldehyde by condensation of 1-heptanal with benzaldehyde using hydrotalcite as a solid base catalyst. J. Mol. Catal. A: Chemical 286, 55–62.

Sharma, S.K., Parikh, P.A., Jasra, R.V., 2010. Reconstructed Mg/Al hydrotalcite as a solid base catalyst for synthesis of jasminaldehyde. Appl. Catal. A: General 386, 34–42.

Shiraga, M., Kawabata, T., Li, D., Shishido, T., Komaguchi, K., Sano, T., Takehira, K., 2006. Memory effect-enhanced catalytic ozonation of aqueous phenol and oxalic acid over supported Cu catalysts derived from hydrotalcite. Appl. Clay Sci. 33, 247–259.

Shiraga, M., Li, D., Atake, I., Shishido, T., T., Oumi, Y., Sano, T., Takehira, K., 2007. Partial oxidation of propane to synthesis gas over noble metals-promoted Ni/Mg(Al)O catalysts—high activity of Ru–Ni/Mg(Al)O catalyst. Appl. Catal. A: General 318, 143–154.

Shiratori, Y., Sakamoto, M., Uchida, T., Le, H., Quang-Tuyen, T., Sasaki, K., 2015. Hydrotalcite-dispersed paper-structured catalyst for the dry reforming of methane. Int. J. Hydrog. Energy 40, 10807–10815.

Shishido, T., Sukenobu, M., Morioka, H., Furukawa, R., Shirahase, H., Takehira, K., 2001. CO_2 reforming of CH_4 over Ni/Mg–Al oxide catalysts prepared by solid phase crystallization method from Mg–Al hydrotalcite-like precursors. Catal. Lett. 73, 21–26.

Shishido, T., Sukenobu, M., Morioka, H., Kondo, M., Wang, Y., Takaki, K., Takehira, K., 2002a. Partial oxidation of methane over Ni/Mg-Al oxide catalysts prepared by solid phase crystallization method from Mg-Al hydrotalcite-like precursors. Appl. Catal. A: General 223, 35–42.

Shishido, T., Wang, P., Kosaka, T., Takehira, K., 2002b. Steam reforming of CH_4 over Ni/Mg-Al catalyst prepared by *spc*-method from hydrotalcite. Chem. Lett. 752–753.

Shu, Y., Murillo, L.E., Bosco, J.P., Hang, W., Frenkel, A.I., Chen, J.G., 2008. The effect of impregnation sequence on the hydrogenation activity and selectivity of supported Pt/Ni bimetallic catalysts. Appl. Catal. A Gen. 339, 169–179.

Sinfelt, J.H., 1972. Kinetics of Ethane Hydrogenolysis. J. Catal. 27, 468–471.

Stanimirova, T.S., Vergilov, I., Kirov, G., Petrova, N., 1999. Thermal decomposition products of hydrotalcite-like compounds: low-temperature metaphases. J. Mater. Sci. 34, 4153–4161.

Stanimirova, T.S., Kirov, G., Dinolova, E., 2001. Mechanism of hydrotalcite regeneration. J. Mater. Sci. Lett. 20, 453–455.

Stanimirova, T.S., Kirov, G., 2003. Cation composition during recrystallization of layered double hydroxides from mixed (Mg, Al) oxides. Appl. Clay Sci. 22, 295–301.

Stobbe, D.E., van Buren, F.R., Stobbe-Kreemers, A.W., Van Dillen, A.J., Geus, J.W., 1991. Iron oxide dehydrogenation catalysts supported on magnesium oxide. Part 2.-Reduction behaviour. J. Chem. Soc. Faraday Trans. 87, 1631–1637.

Stoica, G., Santiago, M., Abelló, S., Pérez-Ramírez, J., 2010. Reactivity of Mg-Al hydrotalcites in solid and delaminated forms in ammonium carbonate solutions. Solid State Sci. 12, 1822–1830.

Takehira, K., 2002. Highly dispersed and stable supported metal catalysts prepared by solid phase crystallization method. Catal. Surv. Jpn. 6, 19–32.

Takehira, K., Shishido, T., Kondo, M., 2002. Partial oxidation of CH_4 over Ni/$SrTiO_3$ catalysts prepared by a solid-phase crystallization method. J. Catal. 207, 307–316.

Takehira, K., Shishido, T., Wang, P., Kosaka, T., Takaki, K., 2003. Steam reforming of CH_4 over supported Ni catalysts prepared from a Mg–Al hydrotalcite-like anionic clay. Phys. Chem. Chem. Phys. 5, 3801–3810.

Takehira, K., Shishido, T., Shoro, D., Murakami, K., Honda, M., Kawabata, T., Takaki, K., 2004a. Preparation of egg-shell type Ni-loaded catalyst by adopting "Memory Effect" of Mg–Al hydrotalcite and its application for CH_4 reforming. Catal. Commun. 5, 209–213.

Takehira, K., Shishido, T., Wang, P., Kosaka, T., Takaki, K., 2004b. Autothermal reforming of CH_4 over supported Ni catalysts prepared from Mg–Al hydrotalcite-like anionic clay. J. Catal. 221, 43–54.

Takehira, K., Kawabata, T., Shishido, T., Murakami, K., Ohi, T., Shoro, D., Honda, M., Takaki, K., 2005a. Mechanism of reconstitution of hydrotalcite leading to eggshell-type Ni loading on Mg–Al mixed oxide. J. Catal. 231, 92–104.

Takehira, K., Shishido, T., Shoro, D., Murakami, K., Honda, M., Kawabata, T., Takaki, K., 2005b. Novel and effective surface enrichment of active species in Ni-loaded catalyst prepared from Mg–Al hydrotalcite-type anionic clay. Appl. Catal. A: General 279, 41–51.

Teodorescu, F., Pălăduță, A.-M., Pavel, O.D., 2013. Memory effect of hydrotalcites and its impact on cyanoethylation reaction. Mater. Res. Bull. 48, 2055–2059.

Therias, S., Mousty, C., 1995. Electrodes modified with synthetic anionic clays. Appl. Clay Sci. 10, 147–162.

Thomas, C.L., 1970. Catalytic Processes and Proven Catalysts. Academic Press, New York.

Tichit, D., Vaccari, A., 1998. Editorial. Appl. Clay Sci. 13, 311–315.

Tichit, D., Bennani, M.N., Figueras, F., Tessier, R., Kervennal, J., 1998. Aldol condensation of acetone over layered double hydroxides of the meixnerite type. Appl. Clay Sci. 13, 401–415.

Tichit, D., Coq, B., Cerneaux, S., Durand, R., 2002. Condensation of aldehydes for environmentally friendly synthesis of 2-methyl-3-phenyl-propanal by heterogeneous catalysis. Catal. Today 75, 197–202.

Tichit, D., Coq, B., 2003. Catalysis by hydrotalcites and related materials. Cat Tech 7, 206–217.

Tichit, D., Lutic, D., Coq, B., Durand, R., Teissier, R., 2003. The aldol condensation of acetaldehyde and heptanal on hydrotalcite-type catalysts. J. Catal. 219, 167–175.

Tope, B.B., Balasamy, R.J., Khurshid, A., Atanda, L.A., Yahiro, H., Shishido, T., Takehira, K., Al-Khattaf, S.S., 2011. Catalytic mechanism of the dehydrogenation of ethylbenzene over Fe–Co/Mg(Al)O derived from hydrotalcites. Appl. Catal. A: General 407, 118–126.

Traversa, E., Nunziante, P., Chiozzini, G., 1992. Thermal decomposition of Mg–Al hydroxides coprecipitated in the presence of oxalate ions. Thermochim. Acta 199, 25–33.

Tsyganok, A.I., Tsunoda, T., Suzuki, K., Hamakawa, S., Takehira, K., Hayakawa, T., 2003. Dry reforming of methane over catalysts derived from nickel-containing Mg-Al layered double hydroxides. J. Catal. 213, 191–203.

Tsyganok, A.I., Inaba, M., Tsunoda, T., Suzuki, K., Takehira, K., Hayakawa, T., 2004. Combined partial oxidation and dry reforming of methane to synthesis gas over noble metals supported on Mg–Al mixed oxide. Appl. Catal. A: General 275, 149–155.

Ulibarri, M.A., Pavlovic, I., Barriga, C., Hermosín, M.C., Cornejo, J., 2001. Adsorption of anionic species on hydrotalcite-like compounds: effect of interlayer anion and crystallinity. Appl. Clay Sci. 18, 17–27.

Vaccari, A., 1999. Clays and catalysis: a promising future. Appl. Clay Sci. 14, 161–198.

Virnovskaia, A., Jorgensen, S., Hafizovic, J., Prytz, O., Kleimenov, E., Hävecker, M., Bluhm, H., Knop-Gericke, A., Schlögl, R., Olsbye, U., 2007a. In situ XPS investigation of Pt(Sn)/Mg(Al)O catalysts during ethane dehydrogenation experiments. Surf. Sci. 601, 30–43.

Virnovskaia, A., Morandi, S., Rytter, E., Ghiotti, G., Olsbye, U., 2007b. Characterization of Pt,Sn/Mg(Al)O catalysts for light alkane dehydrogenation by FT-IR spectroscopy and catalytic measurements. J. Phys. Chem. C 111, 14732–14742.

Wang, Q., O'Hare, D., 2012. Recent advances in the synthesis and application of layered double hydroxide (LDH) nanosheets. Chem. Rev. 4124–4155.

Wang, Q., Tay, H.H., Guo, Z., Chen, L., Liu, Y., Chang, J., Zhong, Z., Luo, J., Borgna, A., 2012. Morphology and composition controllable synthesis of Mg–Al–CO_3 hydrotalcites by tuning the synthesis pH and the CO_2 capture capacity. Appl. Clay Sci. 55, 18–26.

Weckhuysen, B.M., Schoonheydt, R.A., 1999. Alkane dehydrogenation over supported chromium oxide catalysts. Catal. Today 51, 223–232.

Winter, F., Van Dillen, A.J., De Jong, K.P., 2004. Single-stage liquid-phase synthesis of methyl isobutyl ketone under mild conditions. J. Mol. Catal. A Chem. 219, 273–281.

Winter, F., Koot, V., Van Dillen, A.J., Geus, J.W., De Jong, K.P., 2005. Hydrotalcites supported on carbon nanofibers as solid base catalysts for the synthesis of MIBK. J. Catal. 236, 91–100.

Winter, F., Wolters, M., Jos van Dillen, A., De Jong, K.P., 2006. A hydrotalcite-based catalyst system for the single-stage liquid-phase synthesis of MIBK. Appl. Catal. A: General 307, 231–238.

Xu, Z.P., Zeng, H.C., 2001. Decomposition pathways of hydrotalcite-like compounds $Mg_{1-x}Al_x(OH)_2(NO_3)_x \cdot nH_2O$ as a continuous function of nitrate anions. Chem. Mater. 13, 4564–4572.
Xu, Y., Zhang, H., Duan, X., Ding, Y., 2009. Preparation and investigation on a novel nano-structured magnetic base catalyst MgAl–OH-LDH/$CoFe_2O_4$. Mater. Chem. Phys. 114, 795–801.
Xu, Z.P., Zhang, J., Adebajo, M.O., Zhang, H., Zhou, C., 2011. Catalytic applications of layered double hydroxides and derivatives. Appl. Clay Sci. 53, 139–150.
Xu, S., Liao, M.-C., Zeng, H.-Y., Chen, C.-R., Duan, H.-Z., Liu, X.-J., Du, J.-Z., 2015. Magnetic hydrotalcites as solid basic catalysts for cellulose hydrolysis. Appl. Clay Sci. 115, 124–131.
Yu, S., Kim, E., Park, S., Song, I.K., Jung, J.C., 2012. Isomerization of glucose into fructose over Mg–Al hydrotalcite catalysts. Catal. Commun. 29, 63–67.
Zhan, Y., Li, D., Nishida, K., Shishido, T., T., Oumi, Y., Sano, T., Takehira, K., 2009b. Citrate or hydrotalcite? As the precursor of Pt or Ru-doped Ni/Mg(Al)O catalyst for propane oxidative reforming. Appl. Catal. A: General 356, 231–242.
Zhan, Y., Li, D., Nishida, K., Shishido, T., Oumi, Y., Sano, T., Takehira, K., 2009a. Preparation of "intelligent" Pt/Ni/Mg(Al)O catalysts starting from commercial Mg–Al LDHs for daily start-up and shut-down steam reforming of methane. Appl. Clay Sci. 45, 147–154.
Zhang, H., Qi, R., Evans, D.G., Duan, X., 2004. Synthesis and characterization of a novel nano-scale magnetic solid base catalyst involving layered double hydroxide supported on a ferrite core. J. Solid State Chem. 177, 772–780.
Zhou, C.H., 2011a. Clay mineral-based catalysts and catalysis. Appl. Clay Sci. 53, 85–86.
Zhou, C.H., 2011b. An overview on strategies towards clay-based designer catalysts for green and sustainable catalysis. Appl. Clay Sci. 53, 87–96.

Dr. Katsuomi Takehira was born in 1942. He received the M. Eng. and the D. Eng. degrees in chemical engineering from the Hiroshima University and the Tokyo Institute of Technology, Japan in 1967 and 1981, respectively. He worked for 10 years as a Researcher in the National Chemical Laboratory for Industry (NCLI) in Tokyo, Ministry International Trade and Industry (MITI), Japan, and studied in the Institut Français du Pétrole in Rueil Malmaison, France for one and a half year. He became a Director of the Department of Surface Chemistry, NCLI in Tsukuba, Japan in 1993 and moved to Hiroshima University as a Professor of the Department of Chemistry and Chemical Engineering in 1997. After retiring from Hiroshima University in 2006, he became a Professor Emeritus of the University. In the same year, he was request ed to stay in the University as a Specially Appointed Professor and engaged in Project Research for 4 years on reforming catalysts for PEFC supported by New Energy and Industrial Technology Development Organization (NEDO), Japan. From 2010 to 2013, he continued the catalyst research for 3 years in King Fahd University of Petroleum and Minerals, Saudi Arabia, as a Visiting Research Professor. During his stay in Tokyo, Rueil Malmaison, Tsukuba and Hiroshima, he mainly explored various types of catalytic system for the oxidative conversion of hydrocarbons. Since 1995 he has been engaged in the research work of reforming catalysts for the hydrogen production for PEFCs and now focused on the nano-sized supported metal catalysts derived from LDH materials. He published more that 200 papers, 30 reviews and claimed 60 patents.